DIPLOMARBEIT

Impact of Waveguide Input Coupling on Vertical Cavity Surface Emitting Laser Diodes

ausgeführt am
Institut für Nachrichtentechnik und Hochfrequenztechnik
der Technischen Universität Wien

von

Stefan Schwarz

Olbersdorf 138
2842 Thomasberg

Matrikelnr.: 0425136

Wien, im September 2009

Supervisors:
Univ. Prof. Dr. Walter R. Leeb
Dipl. Ing. Gerhard Schmid

Abstract

This diploma thesis deals with physical effects in the light output of a vertical cavity surface emitting laser (VCSEL) diode caused by external optical feedback. Such feedback might be induced by reflections from the beginning of a optical waveguide due to a connected refractive index step. The thesis also investigates the influence on waveguide coupled power on opto-electronic waveguide boards due to external feedback caused variations in the laser output.

The work was initiated by measurements on opto-electronic waveguide boards, carried out at the institute, showing strong waveguide output power oscillations over board temperature. These measurements are reported in Chapter 1. Chapter 3 shows that such oscillatory behavior cannot be attributed to the laser diode as an intrinsic property, but must be the result of an interaction with the environment. A literature search showed that external optical feedback can be the source of oscillations in the laser output, if the feedback is coherent to the laser internal light and the relative phase between the two varies. The theoretical results found in literature are summarized in Chapter 2. This Chapter also provides a short introduction into the theory of VCSELs.

Chapter 3 investigates the laser diode in detail. Results of static as well as dynamic measurements are reported showing changes in VCSEL output spectrum with drive current and modulation frequency. A connection between spectral lines and transversal VCSEL internal cavity modes is established in this Chapter, showing that every spectral line corresponds to a different mode. Therefore changes in the spectrum are equivalent to variations in the transversal modal power distribution or equivalently in the transversal beam intensity distribution. It is also looked into the temperature behavior of the device, showing variations in the laser spectrum and total power with temperature, but no oscillatory behavior.

All external optical feedback measurement results are reported in Chapter 4. It is first shown that incoherent feedback has a strong influence on the laser output spectrum and power, but without any oscillations when varying the feedback phase or strength. Therefore coherent feedback is investigated afterwards, showing oscillatory variations in the laser spectrum with feedback phase, but no change in total output power. That leads to the assumption that a modal filtering element is necessary to translate the variations in the VCSEL transversal intensity distribution into corresponding total power variations after the filter. It is shown that a fiber and therefore also the waveguide in the opto-electronic waveguide boards can act as such an element and explain the power oscillations of the waveguide output light reported in Chapter 1.

Finally Chapter 5 concludes the results and casts a light onto questions that could not be answered and would need further investigation.

Kurzfassung

Diese Diplomarbeit beschäftigt sich mit physikalischen Effekten zu Folge externer, optischer Rückkopplung, die sich auf den Ausgangsstrahl eines Vertical-Cavity Surface-Emitting Lasers (VCSEL) auswirken. Eine derartige Rückkopplung kann beispielsweise durch Reflexionen am Beginn eines optischen Wellenleiters (durch Änderungen des optischen Brechungsindex) hervorgerufen werden. Weiters wird im Zuge der Arbeit untersucht welchen Einfluss derartige Effekte auf die Wellenleiter-koppelbare Lichtleistung, auf optoelektronischen Leiterplatten, haben.

Den Ausschlag für diese Arbeit gaben Messungen, die am Institut auf solchen optoelektronischen Leiterplatten durchgeführt wurden und starke Oszillationen der Ausgangsleistung des Wellenleiters über der Temperatur gezeigt haben. Diese Messungen werden in Kapitel 1 näher beschrieben. Kapitel 3 zeigt, dass solche Oszillationen über der Temperatur nicht von der Laser Diode selbst erzeugt werden, sondern durch eine Interaktion mit der Umgebung hervorgerufen werden. In der entsprechenden Literatur gibt es klare Hinweise, dass optische Rückkopplung zu oszillatorischem Ausgangsverhalten des Lasers führen kann, sofern das rückgekoppelte Licht kohärent zum Licht innerhalb der Laser Diode ist und sich die gegenseitige Phasenlage der beiden ändert. Theoretische Ergebnisse aus unterschiedlichen Literaturstellen sind in Kapitel 2 zusammengefasst. In diesem Kapitel wird auch näher auf die theoretische, mathematische Beschreibung von VCSELn eingegangen.

In Kapitel 3 findet eine messtechnische Charakterisierung der Oberflächen-emitierenden Laser Diode statt. Messergebnisse sowohl statischer als auch dynamischer Messungen werden präsentiert, die klare Veränderungen im Ausgang des VCSELs mit der Stärke des injizierten Stromes und der Modulationsfrequenz zeigen. Weiters wird gezeigt, dass es eine Entsprechung zwischen den einzelnen Spektrallinien im Ausgang des Lasers und Laser-internen, transversalen optischen Moden gibt. Daraus folgt, dass Veränderungen im Spektrum der Laser Diode äquivalent sind zu Veränderungen in der Leistungsverteilung der transversalen Moden und auch zu entsprechenden Variationen des transversalen Strahlprofils des Lasers. Auch das thermische Verhalten der Laser Diode wird in diesem Kapitel untersucht, mit dem Ergebnis, dass sich zwar das Spektrum des Lasers mit der Temperatur verändert, dieses Verhalten jedoch nicht oszillatorischer Natur ist.

Kapitel 4 beschreibt alle Messungen, die zur Untersuchung des Einflusses von externer, optischer Rückkopplung durchgeführt wurden. Zunächst wird beschrieben welche Auswirkungen inkohärente Rückkopplung zeigt, wobei sich herausstellt, dass keine Oszillationen der Leistung oder des Spektrums des VCSEL Ausgangs, weder mit der Stärke noch mit der Phase des rückgekoppelten Lichts, erzeugt werden können. Deshalb wird danach der Einfluss von kohärenter, externer Rückkopplung untersucht. Hier zeigt sich ein periodisches Verhalten des Ausgangsspektrums (und damit der modalen Leistungen) der Laser Diode mit der Phase des extern rückgekoppelten Lichts, jedoch nur eine vernachlässigbare Beeinflussung der gesamten Ausgangsleistung. Das führt zu der Annahme, dass ein Moden filterndes Element nötig ist, welches Veränderungen in der modalen Leistungsverteilung in entsprechende Variationen der Gesamtleistung umsetzt. Es wird gezeigt dass Glasfasern diese Aufgabe übernehmen können, woraus geschlossen wird, dass auch die Wellenleiterstrukturen auf den optoelektronischen Leiterplatten als Modenfilter fungieren können und somit, in Verbindung mit externer Rückkopplung, Grund für die in Kaptiel 1 beschriebenen Leistungsoszillationen sein können.

Kapitel 5 letztlich fasst die Ergebnisse noch einmal zusammen und wirft ein Licht auf noch offene Fragen.

Acknowledgments

To Prof. Walter R. Leeb,

for supportive weakly discussions
and asking the necessary promoting questions
as well as giving the right hints

To Gerhard Schmid,

for sharing his profound lab experience
and his help in giving this thesis its final touch

To my parents,

for endless patience, supply and confidence
and giving me the possibility of studying
the amazing field of electrical engineering

To my brother and sister,

for helping me finding again my motivation
whenever frustration and exhaustion tried to gain the upper hand

Contents

List of Figures

List of Tables

Glossary

α_i	internal losses
α_m	mirror losses
β_z	propagation constant along the optical axis
Γ	optical confinement factor
Γ_t	transversal optical confinement factor
Γ_z	longitudinal optical confinement factor
$\Delta\Phi$	phase shift of external reflections due to the distance to the external reflector
$\Delta\Phi_r$	change in feedback phase of the external reflections due to change in positon of the external reflector Δz_r
Δr	change in VCSEL mirror reflectivity due to external feedback
Δz_r	change in position of the external reflector alonge the optical axis
η_i	current injection efficiency
η_o	optical efficiency
η_p	power conversion efficiency
η_s	slope efficiency
θ_0	angle of beam divergence
ω	angular frequency
B	bimolecular recombination coefficient
c_0	vacuum speed of light, $2.998 \cdot 10^{-8}\,m/s$
CCD	charge coupled device
d_a	thickness of separate confinement structure
d_{qw}	thickness of quantum wells
d_R	Rayleigh distance
D	VCSEL total diameter
D_N	diffusion coefficient
DBR	distributed Bragg reflector
DFB	distributed feedback
DUT	device under test
f_r	frequency of the laser turn on transients
F_b	fraction of power coupled out with the bottom DBR
F_t	fraction of power coupled out with the top DBR
FPR	feedback power ratio
g_0	logarithmic gain coefficient
$g(\tau)$	normalized autocorrelation function of the light field
$\hbar$	reduced Planck constant
I	VCSEL current
I_{th}	threshold current
L_{coh}	coherence length
L_{eff}	effective cavity length

MMF	multi mode fiber
n_c	refractive index of the VCSEL equivalent waveguide cladding
n_g	refractive index of the VCSEL equivalent waveguide core
n_{qw}	number of quantum wells
n_r	refractive index of the reflector glass plate
n_s	refractive index of the surrounding medium
N_{tr}	transparency carrier density
OSA	optical spectrum analyzer
P	VCSEL output power
PAC	pyroelectric array camera
PR	logarithmic power ratio of minimum and maximum fiber output power
PZT	piezo electric element
q	electron charge, $1.602 \cdot 10^{-19}\,C$
r_b	bottom DBR field reflectivity
r_{eff}	equivalent two mirror cavity field reflectivity
r_{ext}	external reflector field reflectivity
r_s	current spreading coefficient
r_t	top DBR field reflectivity
R_b	bottom DBR power reflectivity
R_{ext}	external reflector power reflectivity
R_{ox}	oxide aperture radius
R_t	top DBR power reflectivity
RF	radio frequency
SMF	single mode fiber
t_d	turn on delay of the laser
TPA	two photon absorption
U	VCSEL voltage
U_{th}	threshold voltage
V_a	active volume
VCSEL	vertical cavity surface emitting laser
VISTAS	VCSEL integrated spatio temporal device simulator
z	longitudinal coordinate/coordinate of the optical axis
z_{0r}	position of the external reflector alonge the optical axis

Chapter 1

Motivation

This diploma thesis was initiated by measurements carried out at the Institute of Communications and Radio-Frequency Engineering at the Vienna University of Technology on opto-electronic printed circuit boards developed at a styrian company. The boards are intended for high data rate applications where the advantages of optical data transmission, namely high bandwidth, low crosstalk and inherent immunity to electro-magnetic interference, are beneficial.

The present chapter is intended to give a short overview about the technology used to produce the opto-electronic printed circuit boards in Section 1.1. Afterwards in Section 1.2 the measurement results mentioned above will be presented and the ambiguities which necessitate further investigation will be pointed out clearly.

1.1   Opto-Electronic Printed Circuit Boards

Figure 1.1 shows a schematic of the opto-electronic printed circuit boards under investigation. The board mainly consists of a standard FR4 substrate which carries a light source, the vertical cavity surface emitting laser (VCSEL) diode, an optical waveguide and a light sink, the photo diode. The electro-optical elements are electrically connected to copper lines by bond wires, which can be fed over coaxial connectors.
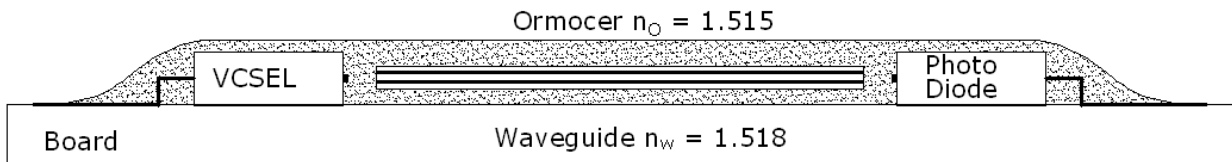
Figure 1.1: Schematic of an opto-electronic printed circuit board

The whole board is covered with a polymer coating from the ORMOCER® material system ([1]) developed at Frauenhofer-ISC in Germany. The waveguide is directly laser-written into the polymer by exploiting the so called two-photon absorption (TPA) process (see [2]). TPA is a high intensity process that necessitates using a pulsed femtosecond laser with a focus of about $30\,\mu m$ diameter in order to achieve the high intensities necessary. The process increases the refractive index of the ORMOCER® in the volume of the laser focus

from about $n_O = 1.515$ to $n_W = 1.518$. By running the focus through the material it is possible to write waveguides with any desired three dimensional form.

The distance between the beginning and end of the waveguide and the laser and photo diode respectively is about $10\,\mu m$. It is not possible to get closer to the two devices, which would be beneficial in terms of losses, because then the waveguide writing laser beam could harm the diodes. To guide as much light power as possible it is advantageous to have a waveguide with a large core diameter. A large diameter would call for a laser with a large focus but still high intensity which means that a femtosecond laser with very large output power would be necessary. Such a device is not available at time. The overall waveguide is therefore made of a bundle of seven waveguides which are written with seven lasers simultaneously. The cross section of the resulting waveguide structure is shown in Figure 1.2.
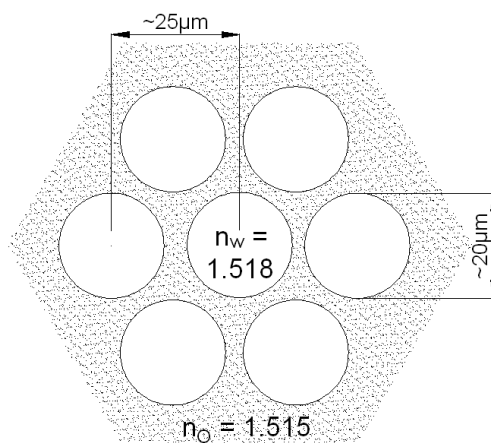
Figure 1.2: Cross section through the waveguide

The refractive index does not change abruptly between waveguide core and the surrounding ORMOCER® medium, but it changes gradually with a Gaussian like shape. The reason for this is the divergence of the writing laser beam which decreases the local laser intensity. Decreasing the distance between the waveguides is not possible because bringing the writing laser beams closer to each other would cause so high intensities in the overlapping region that the polymer material could be harmed.

1.2 Previous Measurements necessitating further Investigation

During the measurement of the photocurrent versus temperature on the opto-electronic boards described above, some boards showed pronounced current oscillations over temperature. Figure 1.3 shows the measurement result for a specific board. Other similar boards did not show such behavior.

In this measurement the board temperature was linearly increased from 0 to $80\,°C$ in about 8 and a half hour and afterwards decreased again to $0\,°C$ (dashed line). The VCSEL was driven at a constant current of $6\,mA$ and the current produced by the photo diode was measured (solid line). This current is directly proportional to the incident light power. There was no explanation at hand for this behavior, therefore it was decided to further investigate it, which initiated this Diploma thesis. Following observations and statements can be made from this measurement:

- Until about $50\,°C$ the optical power measured at the photo diode increases when just looking at the envelope and ignoring the oscillations. The reason may be found in an increase in the numerical

aperture of the waveguide due to increasing refractive index difference between waveguide core and surrounding material. This allows the waveguide to guide the light more efficiently (this behavior was observed in all waveguide boards).

- Above $50\,^{\circ}C$ the optical power starts to decrease. This behavior is due to a decrease in VCSEL output power with temperature (see Chapter 3 for details).

- The maximum ratio of the peak to peak current oscillations[1] equals about 5 in the observed temperature regime. This corresponds to a ratio of almost $7\,dB$ in the received optical power.

- The period of the current oscillation is about $10\,^{\circ}C$, but it varies slightly over temperature.
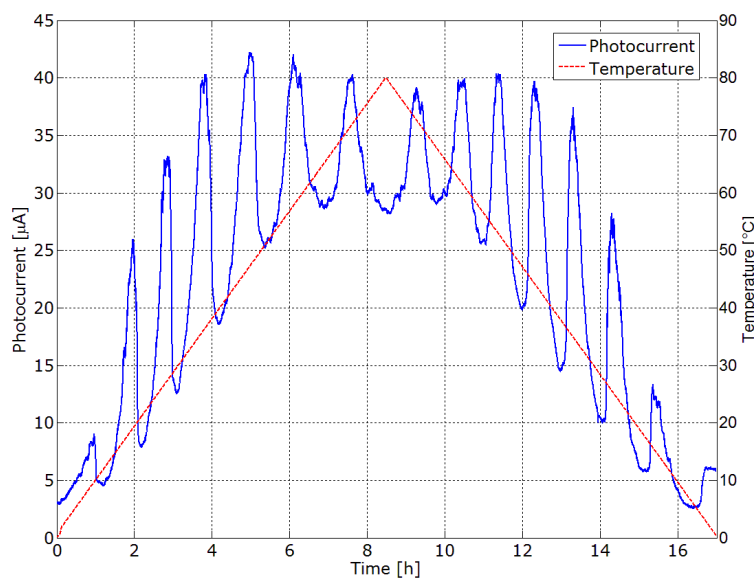
Figure 1.3: Temperature behavior of a waveguide board

The same measurement was also carried out at a much shorter time scale, the temperature was increased in $90\,min$. It showed in principle the same result, the magnitude and period of the current oscillations over temperature did not change.

Further measurements were already carried out to find out where along the waveguide the power gets lost. Therefore he cut back the board to lengths of $12\,cm$, $9\,cm$, $6\,cm$, $3\,cm$ and $1\,mm$ measured from the laser diode on and observed the total light power at that lengths together with the optical intensity distribution over temperature. Figure 1.4 shows an example of two intensity distributions measured at the cut $1\,mm$ off the laser at two different temperatures. Figure (a) corresponds to a temperature where the output power is minimum (at about $5\,^{\circ}C$) and in (b) the power is at a neighboring maximum (at about $10\,^{\circ}C$). In the figures the seven core waveguide can be identified. For clarity the waveguide is marked with seven white circles. But also a large stray light ring can be seen. This light is not guided through the ORMOCER$^{\circledR}$ layer. The cut-off in the luminous distribution marks the polymer - air border.

Comparing figures a) and b) clearly shows that the power in the two left waveguide cores varies very strong with temperature. The transversal alignment between laser diode and seven core waveguide seems not to be ideal, as the other five waveguides are hardly involved in the guiding process. This is possible because the transversal tolerances in the fabrication process are in the order of $15\,\mu m$ (according to the manufacturer).

---

[1]the maximum ratio of a current maximum and neighboring minimum

Observations of these measurements are:

- The oscillatory behavior does not change when cutting back the board (neither the period nor the magnitude) → the reason may be found at the beginning of the waveguide.

- The transversal alignment between laser diode and waveguide is not ideal. The VCSEL does not irradiate the waveguide centrally. Most of the power is guided in only two waveguide cores.
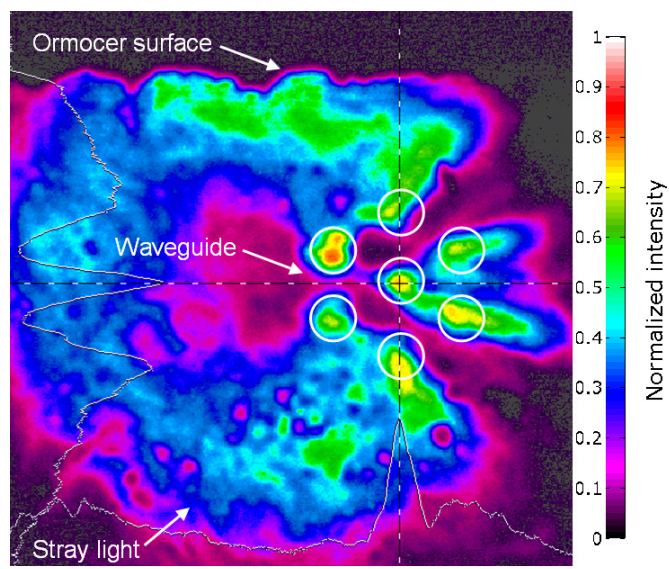
(a) Distribution at a power minimum
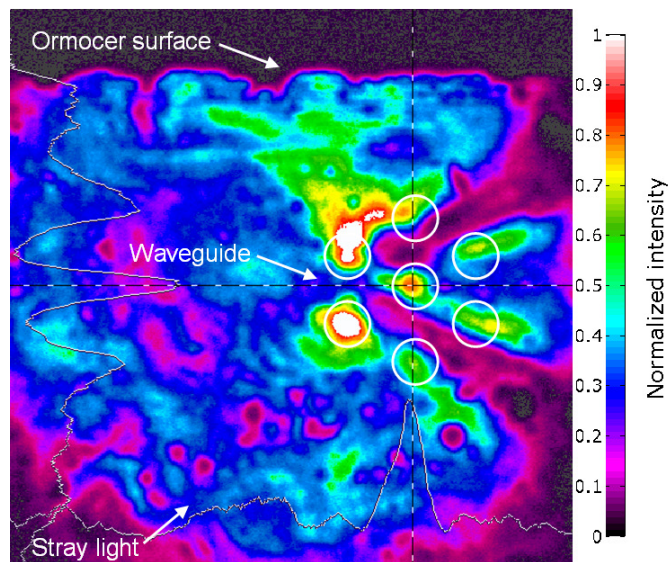
(b) Distribution at a power maximum

Figure 1.4: Normalized intensity distributions at waveguide cut $1\,mm$

Taking these results as a prerequisite the task is to identify possible reasons for the oscillatory behavior and try to confirm or refute them with the help of measurements.

Chapter 2

Theoretical Basics

This chapter is intended to introduce the basics of vertical cavity surface emitting laser (VCSEL) diodes and the mathematical treatment of laser external feedback effects. Therefore in Section 2.1 an overview about the design and structure of VCSELs is given (which differentiates them from classical edge emitting lasers) and also about important physical effects that are necessary for interpreting the measurement results of later sections. Basic knowledge about laser principals is presupposed (cf. [3]).

Section 2.2 deals with physical effects that occur when part of the laser output light is reflected back into the laser cavity from somewhere outside. The fundamental mathematics are described and an overview about different effects, that are mentioned in literature, is given. Those effects are principally the same for all kind of laser diodes but whether they are observable or not depends strongly on the laser structure and the optical modes that are related with it.

2.1 Vertical Cavity Surface Emitting Laser

The most promising type of laser diode today for data com applications is the VCSEL. This is due to various reasons. First it allows cheap and easy production by using just standard micro electronic fabrication steps. It is not necessary to cleave the wafer to get access to the light output because light is emitted directly out of the top surface. This also allows to produce laser arrays of almost arbitrary size (just limited by the wafer size) which is important for highly parallel interconnects. Furthermore the vertical constructions enables on wafer testing. The second beneficial characteristics of VCSELs is their small active volume which allows even sub μA threshold currents at a high yield and large modulation bandwidth. Another advantageous characteristics is their circular shape. Due to this shape also the output beam is circular and has low divergence compared to edge emitting laser diodes, which allows easy and efficient fiber coupling.

All these beneficial properties are achieved by the unique structure of the VCSEL diode which is described in some detail in the following section (see also [4], [5]).

2.1.1 Design and Structure

Figure 2.1 shows the basic structure of a so called oxide confined vertical cavity surface emitting laser diode. There also exist a lot of other structures like etched mesa, proton implanted or buried heterostructure but those are of little importance today. This is because the oxide aperture, which gives this structure its name, allows easy current and optical confinement. The structure shown in the figure is circularly symmetric. The light as well as the current travel through the device along the longitudinal coordinate z.

2.1.1.1 Threshold current

The active region of the device is longitudinally defined by the three quantum wells (QWs), which are shown in brown in the center region of Figure 2.1. In order to achieve very low threshold currents, which is beneficial

in terms of power dissipation, one needs to keep the active volume as small as possible. The longitudinal extent is already very small ($\sim 30\,nm$) due to the usage of quantum wells. To keep the transversal extent small the pumped area is confined by the oxide aperture which acts as a highly resistive layer that inhibits current flowing through it. Therefore the current and with it the active layer is confined like shown in the figure.
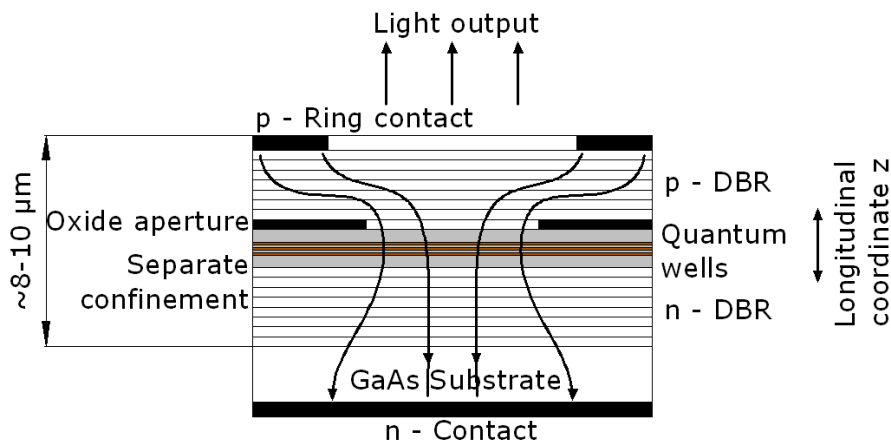
Figure 2.1: Oxide confined VCSEL

But to keep the threshold current low it is also necessary to confine the optical wave to the active region where it experiences gain. This too is achieved with the oxide aperture because it causes a negative step in refractive index. This step effectively produces a circular optical step index waveguide that confines the light to the active region (see Section 2.1.2 for more details). Making the oxide aperture smaller leads at the beginning to smaller threshold currents, but this process does not carry on at aperture diameters smaller than about $1\,\mu m$ because then ohmic losses and weak guiding of the optical wave begin to dominate, which counteract the decrease in threshold current (see [4], [5], [6]).

2.1.1.2 Distributed Bragg Reflectors

The effective length of the VCSEL laser cavity is just in the order of a single wavelength. Therefore the light experiences only little gain during one round trip and it is necessary to compensate for this by the use of highly reflective mirrors. This is in contrast to edge emitting lasers, where the light travels along the active layer and therefore experiences much more gain. In VCSELs reflectivities in the order of 99.95% and more are necessary to keep the threshold current at reasonable values. These can only be achieved by the use of distributed bragg reflectors (DBRs) as shown in the figure. Typically the top mirror (p-DBR) has a slightly lower reflectivity in order to couple as much light as possible out of the useful upper surface. Some formulas quantifying this are given in Section 2.1.3.

2.1.1.3 Band Structure

Figure 2.2 shows the band structure of the VCSEL conduction band along the longitudinal coordinate together with the optical standing wave pattern that is a consequence of the usage of DBRs. The figure shows that the cavity is typically designed such, that the three quantum wells fall approximately into a maximum of the standing wave pattern. In this figure the conduction band edge lies at a energy of $0\,meV$.

The energy values given in the figure are approximately valid for a gallium arsenide (GaAs) device, which is the material typically used for $850\,nm$ VCSELs. Of course they depend on the exact material composition of the device. The total maximum of the field can be found at the beginning of the two DBR mirrors.
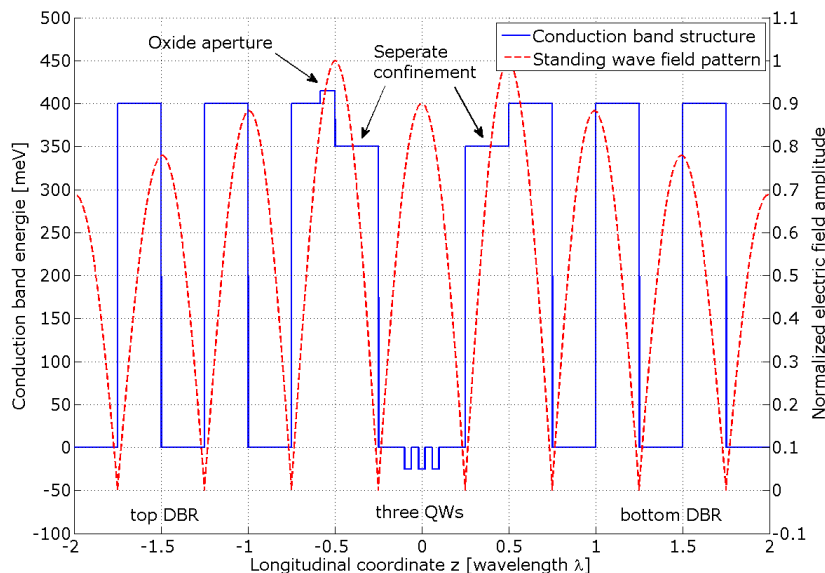
Figure 2.2: VCSEL conduction band structure

Inside the mirrors the envelope of the electric field falls of exponentially. The mirrors themselves consist of quarter wavelength thick stacks of dielectric material with different refractive index. In the gallium arsenide - aluminum gallium arsenide (GaAs-AlGaAs) material system this can be achieved by varying the material composition (varying the proportions of Ga and Al used).

The separate confinement structure, also shown in the figure, acts as a electronic confinement. It is necessary to keep the electrons in the proximity of the quantum wells, so that they are available for stimulated emission. If this structure would not exist the device would be much slower, because electrons would need more time to diffuse to the QWs.

More details about the design and structure of VCSELs and also the mathematical description can be found in [4] and [5].

2.1.2 Optical Modes

Due to their small effective cavity length of just about a wavelength VCSELs in general just support one longitudinal optical mode. The standing wave pattern of this mode is also shown in Figure 2.2. Other optical modes with a multiple of the wavelength of this mode would also be possible, but those are already outside the gain bandwidth of the device.

Still in general there are several transversal modes, belonging to the same longitudinal mode, that are able to oscillate. Pure single mode operation (which is defined to have a side-mode suppression ratio of more than $30\,dB$) can be achieved by reducing the oxide aperture diameter. In literature typical $850\,nm$ single mode devices have a oxide aperture diameter of about $3.5\,\mu m$ (see [4] Chapter 3).

As already mentioned in Section 2.1.1 the oxide aperture introduces a refractive index step that creates a waveguide like structure inside the laser cavity. This is schematically depicted in Figure 2.3. Due to this refractive index step oxide confined VCSELs can be classified as index guided (in contrast to gain guided).

2.1.2.1 Mathematical Description

The transversal modes are not described uniquely in literature. Marc Jungo uses in his description in [6] the same modes that are used to describe the passive, weakly-guiding, step-index, cylindrical waveguide namely
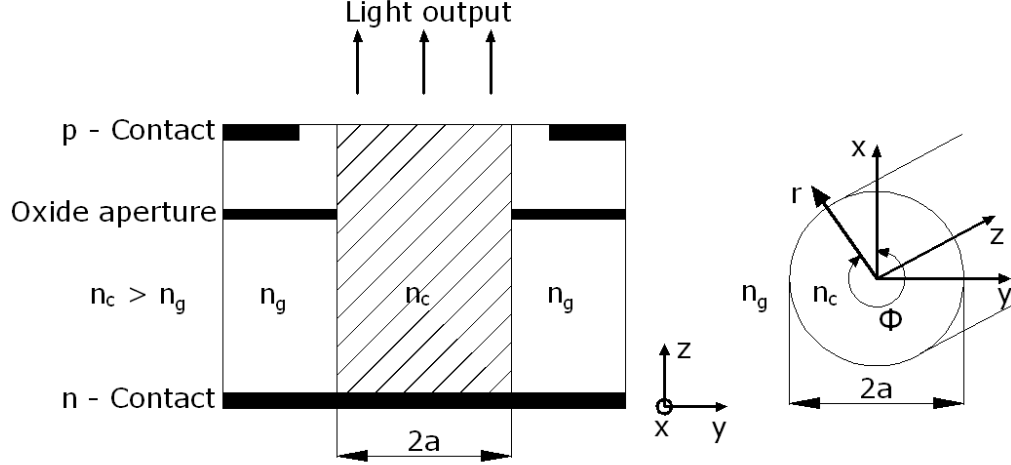
Figure 2.3: Schematic of the VCSEL waveguide

the **Bessel modes**. The intensity distribution inside the VCSEL cavity is given by

$$S_{lp}(r,\phi,t) = S_p^{(c)}(t)|\Psi_p(r)|^2\cos^2(l\phi) + S_p^{(s)}(t)|\Psi_p(r)|^2\sin^2(l\phi). \tag{2.1}$$

Index p represents the radial and l the azimuthal mode order (corresponding to the number of zeros in $0 \leq r < \infty$ and $0 \leq \phi < 180°$), $S_p^{(c)}$ and $S_p^{(s)}$ represent the total intensity in the two helical polarities and Ψ_p is the radial field profile given by

$$\Psi_p = \begin{Bmatrix} J_p(k_t r)/J_p(k_t a) & r \leq a \\ K_p(\gamma_t r)/K_p(\gamma_t a) & r > a \end{Bmatrix}. \tag{2.2}$$

Here J_p and K_p are the Bessel function and modified Bessel function of order p. k_t, γ_t are the transversal component of the wave vector and the transversal decay component respectively given by

$$k_t^2 = n_c^2\left(\frac{2\pi}{\lambda}\right)^2 - \beta_z^2 \tag{2.3}$$

$$\gamma_t^2 = \beta_z^2 - n_g^2\left(\frac{2\pi}{\lambda}\right)^2, \tag{2.4}$$

with λ the wavelength of the mode. λ and β_z are the only two unknown left. They are related via a dispersion relation, that can be obtained by considering boundary conditions for the electro-magnetic field components at $r = a$ (e.g. [6]). β_z is given by the resonance condition (see 2.1.3) inside the laser cavity. Jungo uses these modes for his VCSEL device simulator VISTAS (VCSEL integrated spatio temporal advanced simulator).

Other authors like [4] or [7] use **Laguerre Gaussian modes** to describe the laser field. These modes are generally used to describe graded index circularly symmetric waveguide structures with a parabolic refractive index profile. The authors argue that this better matches the reality due to thermally induced refractive index variations. The corresponding intensity distribution inside the laser cavity is given by

$$S_{lp}(r,\phi,t) = S_p^{(c)}(t)\left(\frac{2r^2}{w_0^2}\right)^l|L_{p-1}^{(l)}(\frac{2r^2}{w_0^2})|^2\cos^2(l\phi)e^{-\frac{2r^2}{w_0^2}} + S_p^{(s)}(t)\left(\frac{2r^2}{w_0^2}\right)^l|L_{p-1}^{(l)}(\frac{2r^2}{w_0^2})|^2\sin^2(l\phi)e^{-\frac{2r^2}{w_0^2}}. \tag{2.5}$$

Here $L_{p-1}^{(l)}$ is the generalized Laguerre polynomial of kind l and order $p-1$.

The fundamental mode ($l = 0, p = 1$) is just a Gaussian beam and correspondingly w_0 is the radius of the beam waist. The great advantage of these modes is that the far field distribution is readily available in closed form. For more details on this see Appendix B.4. Figures of far field intensity distributions of different modes can be found in later chapters (e.g. 3.1.4).

Irrespective of which mathematical description is used for the transversal modes, the nomenclature follows always the same rule. The modes are named according to their mode numbers l and p as LP_{lp}, where LP stands for "linearly polarized".

2.1.2.2 Emission Wavelength

The structure and material of the device solely determine the emission wavelength. The material defines the gain bandwidth and thereby the longitudinal mode that experiences gain (this delivers β_z). The material composition (refractive index) together with the structure determine the waveguide and with it the possible transversal modes. All these modes have slightly different wavelength. The wavelength difference is just in the order of a few tens of picometers. The wavelength is given via the dispersion relation (with constant β_z).

In many devices there is a further splitting of the spectral line corresponding to one transversal mode due to anisotropies in the cavity. This can lead to a splitting of different polarizations and also of the two helical polarities. So the four fold degeneracy of higher order modes (the fundamental mode is only two fold degenerate) can be lifted (see [18]).

The wavelength shows a shift towards larger values with temperature of typically $\frac{\partial \lambda}{\partial T} = 0.07 \, nm/K$. This also translates into a corresponding shift with current due to internal heating effects (typically $\frac{\partial \lambda}{\partial I} = 0.2 \, nm/mA$). The shift is a combination of two effects, firstly the peak material gain in the quantum wells shifts due to band gap shrinkage and secondly the cavity resonance shifts because of changes in the average refractive index and thermal expansion(see [4], [5]).

2.1.2.3 Coupling between Modes

The different transversal modes of a VCSEL can not be considered as being independent from each other. There are three different effects that lead to mutual coupling between the modes.

- Gain competition

  The optical modes are competing for the total gain that is available in the laser cavity. This leads to cross gain saturation effects which means that stimulated emission by one mode causes gain saturation not only for itself (self-saturation), but also for the other modes.

- Spatial hole burning

  This effect weakens gain competition and can lead to coexistence of spatially weak overlapping modes. A mode mainly saturates the gain at those areas where its intensity is high. If intensity maxima of two modes do not overlap then both may experience enough gain. The strength of the influence of spatial hole burning depends strongly on the diffusion coefficient. If the diffusion coefficient is large differences in the spatial gain distribution are equalized fast and vice versa.

- Spectral hole burning

  Another effect that promotes coexistence of different modes. Every mode has a slightly different wavelength and therefore different modes need carriers at different energy levels for stimulated emission.

These effects lead to complicated turn on behavior where the power shifts dynamically between the different modes. Which modes coexist after the transients and how the total power is distributed between the different modes can only be calculated by taking into account the full rate equations for the photons and carriers and the coupling between them like it is done in [6] (also more details can be found there).

2.1.3   Basic Relations

This section gives the definitions of some basic and important parameters characterizing and describing the VCSEL. Most of these parameters will be used in Chapter 3 to characterize a certain VCSEL. Constants used in the formulas are defined in the glossary.

- Threshold current

  This is the current at which the gain in the cavity exceeds the losses and the device starts to oscillate. It marks the point in the output power versus current characteristics at which the power starts to increase significantly (see for example Figure 3.2).

$$I_{th} = \frac{q V_a B N_{tr}^2}{\eta_i} e^{2\frac{(\alpha_i + \alpha_m)}{\Gamma g_0}} \tag{2.6}$$

  Active volume: $V_a = \pi R_{ox}^2 n_{qw} d_{qw}$

- Differential quantum efficiency

  Describes the slope of the power versus current characteristics above threshold. It is in general not a constant, as the characteristics is not linear.

$$\eta_d = \frac{q}{\hbar\omega}\frac{\partial P}{\partial I} = \eta_o \cdot \eta_i \tag{2.7}$$

$$\eta_o = F_t \frac{\alpha_m}{\alpha_i + \alpha_m} \tag{2.8}$$

$$F_t = \frac{1 - R_t}{1 - R_t + \sqrt{R_t/R_b}(1 - R_b)} \tag{2.9}$$

  A related value is the slope efficiency given by

$$\eta_s = \frac{\partial P}{\partial I}. \tag{2.10}$$

- Power conversion efficiency

  This value equals the ratio of output to input power

$$\eta_p = \frac{P}{I \cdot U} \tag{2.11}$$

  and is also not a constant.

- Differential series resistance

$$r_s = \frac{\partial U}{\partial I} \tag{2.12}$$

- Mirror losses

  Describe the total losses through the top and bottom DBR.

$$\alpha_m = \frac{1}{2L_{eff}} \ln \frac{1}{R_t R_b} \tag{2.13}$$

- Cavity resonance condition

  For a optical mode to be able to oscillate, the phase must be reproduced after one round trip inside the laser cavity. This means that the total phase shift must be a integer multiple m of 2π.

  $$\beta_z \cdot 2L_{eff} = m \cdot 2\pi \tag{2.14}$$

  As can be seen in Figure 2.2 the design is typically such that $m = 2$. The effective cavity length L_{eff} takes into account the penetration depth of the light into the DBRs and can be calculated from the phase shift encountered (e.g. [4] or [5]).

- Optical confinement factor

  This value equals the ratio of the active volume V_a and the volume occupied by the optical mode V_p. It depends on the mode under investigation. The confinement factor can be split into a longitudinal and a transversal part.

  $$\Gamma = \frac{V_a}{V_p} = \Gamma_z \cdot \Gamma_t \tag{2.15}$$

  $$\Gamma_t = \frac{\int_{\mathcal{A}_a} S_{lp}(r,\phi)dA}{\int_{\mathcal{A}_p} S_{lp}(r,\phi)dA} \tag{2.16}$$

  $$\Gamma_z = \frac{L_a}{L_{eff}}\left[1 + \frac{\sin(\beta_z L_a)}{\beta_z L_a}\right] \tag{2.17}$$

  Here $\mathcal{A}_a$ is the active area and $\mathcal{A}_p$ is the area occupied by the mode (generally an infinite area). The active area is for example influenced by spatial hole burning. L_a is the active length and for the VCSEL it is equal to $L_a = n_{qw}d_{qw}$. The term in brackets in the last equation above is called the enhancement factor, it is typically close to two for VCSELs. Details and derivations can be found in [8].

- Modal threshold gain

  This is the gain that is necessary to compensate for the losses inside the laser cavity. The total losses are composed of laser internal losses, due to light absorption and scattering and external losses, due to mirror coupling losses. It depends on the mode under investigation because the internal losses are mode dependent. Following equation must be satisfied for the gain to compensate for the losses (m indicates the mode under investigation).

  $$e^{2L_{eff}\Gamma_m g_{th,m}} \cdot e^{-2L_{eff}\alpha_{i,m}} \cdot R_t R_b = 1$$
  $$\Gamma_m g_{th,m} = \alpha_{i,m} + \frac{1}{2L_{eff}}\ln\frac{1}{R_t R_b} \tag{2.18}$$

  The optical confinement factor takes into account that the mode volume is larger than the active volume and therefore the mode does not experience gain over its full volume.

2.2 External Feedback Effects

A literature search for possible reasons for the effects observed on the opto-electronic waveguide boards described in Chapter 1 revealed external optical feedback as the only explanation for periodic variations in the laser output beam characteristics (power, spectrum, intensity distribution).

There is a lot of literature available giving different rather complicated mathematical descriptions for effects observed when a laser is exposed to such feedback (e.g. [11], [15], [14], [13], [12]). For special cases like weak, coherent feedback simple intuitive models are available (one of those will be explained in 2.2.3).

2.2.1 Coherent and Incoherent External Feedback

Generally it is necessary to distinguish between the two cases of coherent and incoherent external feedback. In the coherent case the light fed back into the laser cavity through external reflections is coherent to the light inside the cavity, which means that there is a fixed phase relation between the two whereas for incoherent feedback this is not the case.

Coherent reflections produce an interference effect. The optical fields add up on a field basis which enables constructive and destructive interference. In this case, depending on the phase relation, the reflected light can lead to an enhancement or reduction of the laser output power.

Incoherent feedback does not produce any interference effect because in this case the reflected and internal light just add up on a power basis. There is no fixed phase relation and so in the mean any interference effects cancel out. Such external feedback can just lead to an enhancement of laser output power. It can also lead to variations in the power distribution to the individual laser modes (modal power distribution) due to differences in the efficiency with which the reflected light couples back into the laser internal modes (see B.4 for details).

The distinction between the two cases is based on the coherence length L_{coh} of the laser. This is a measure of the degree of temporal coherence quantified as a propagation length over which coherence degrades significantly (see [10]).

$$L_{coh} = \tau_{coh} \cdot c_0 \tag{2.19}$$

The coherence time τ_{coh} is defined over the normalized autocorrelation function $g(\tau)$ of the statistically stationary light field $E(t)$

$$g(\tau) = \frac{< E^*(t)E(t+\tau) >}{< E^*(t)E(t) >} \tag{2.20}$$

$$\tau_{coh} = \int_{-\infty}^{\infty} |g(\tau)|^2 d\tau, \tag{2.21}$$

where $<>$ means the temporal average and * stands for complex conjugation. According to [17] the coherence length of VCSELs typically lies in the order of a few millimeters to centimeters for multi mode devices and tens of centimeters to few meters for single mode devices.

2.2.2 Regimes of Optical Feedback Strength

Experimental investigations on **single mode laser devices** of different kind (DFB lasers, VCSELs, HeNe lasers) lead to the identification of five different feedback regimes depending on the feedback strength (see [11], [8]). In these regimes the laser shows distinct spectral behavior. The strength of feedback is quantified with the so called feedback power ratio (FPR) given by

$$FPR = 10 \log_{10} \frac{P_r}{P_{out}}. \tag{2.22}$$

P_{out} is the VCSEL output power and P_r the reflected power coupled back to the laser (measured at the laser surface over the same area as P_{out}). The regime boundaries given in the following list were reported in [16] for a particular VCSEL.

- Regime I - $FPR < -65\,dB$

  Single mode operation, spectral line narrowing or broadening depending on feedback phase;

- Regime II - $-65\,dB < FPR < -40\,dB$

  Multi mode operation, spectral line splitting and mode hopping occurs;

- Regime III - $-40\,dB < FPR < -35\,dB$

  Single mode operation, spectral line narrowing for all feedback phases;

- Regime IV - $FPR > -35\,dB$

  Multi mode operation with strong spectral line broadening, coherence collapse;

- Regime V

  Single mode operation in a very narrow external cavity mode; can not be observed in VCSELs due to their highly reflective DBR mirrors;

In multi mode laser devices those regimes can not be observed. Theoretically, if the modes were independent from each other, every mode would undergo these regimes, but the mutual coupling between the modes prevents them from doing so.

2.2.3 Weak Coherent Feedback

The situation of interest for the measurements I did during the work on my Diploma thesis is coherent feedback with a relatively weak strength. This means that the external reflections take place at a distance smaller than the coherence length of the multi mode VCSEL and they are so weak that multiple reflections in the external cavity can be ignored, which is facilitated by the beam divergence. Figure 2.4 shows the idealized setup used for the mathematical description.
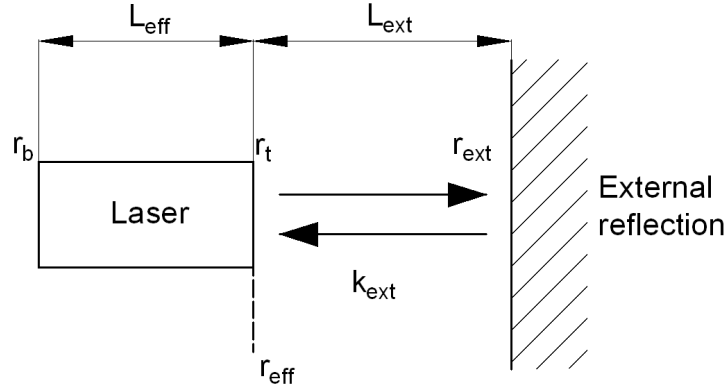
Figure 2.4: Idealized external feedback model

The laser has a effective cavity length of L_{eff} and top and bottom field reflectivities of r_t and r_b respectively. The external cavity is composed of an external reflector at distance L_{ext} with reflectivity r_{ext}. The external propagation constant is given by k_{ext}.

   It is possible to combine the two reflectivities r_t and r_{ext} into a single effective reflectivity r_{eff}. This allows to describe the three mirror cavity as a two mirror cavity with a different reflectivity. The calculation can be carried out easily with the help of scattering theory as described in [8]. Ignoring multiple reflections the result is given by

$$r_{eff} = r_t + \Delta r = |r_{eff}|e^{j\Phi_{eff}} \tag{2.23}$$

$$\Delta r = (1 - r_t)^2 r_{ext}e^{-j\Delta\Phi} \tag{2.24}$$

$$\Delta\Phi = 2k_{ext}L_{ext}. \tag{2.25}$$

The polar plot of the effective reflectivity is shown in Figure 2.5. The top mirror reflectivity r_t and Δr add
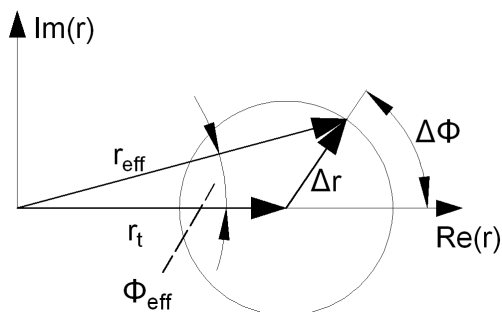
Figure 2.5: Polar plot of equivalent two mirror cavity reflectivity

up vectorial. The circle shown in the figure gives all possible values that r_{eff} can take on depending on the phase $\Delta\phi$. This phase varies periodically with the distance to the external reflector with a period of $\frac{\lambda}{2}$.

The variation in the magnitude of the effective reflectivity translates directly into a corresponding variation in the modal threshold gain according to (2.18) with the top mirror reflectivity replaced by the effective reflectivity

$$\Gamma_m g_{th,m} = \alpha_{i,m} + \frac{1}{L_{eff}} \ln \frac{1}{|r_b r_{eff,m}|}. \tag{2.26}$$

A modal dependence of the effective reflectivity has been taken into account due to two reasons

1. Different transversal modes have different wavelength $\rightarrow$ the phase of the external reflectivity $\Delta\Phi$ is mode dependent

2. The amount of power that couples back into the individual modes is different (see B.4) $\rightarrow$ the magnitude of the external reflectivity Δr is also mode dependent.

Changing the threshold gain of the device, by varying the external feedback phase[1], clearly has an influence on the output power. Decreasing the necessary threshold gain increases the output power at constant drive current and vice versa.

But here again the mutual coupling between the modes comes into play. This coupling can lead to "out of phase" behavior, which means that the modal power does not vary according to the external feedback phase. Suppose a initially strong mode experiences a weak effective reflectivity due to the external reflections. Then the power of this mode will decrease. According to gain competition this leaves more gain for the other modes and their power will increase although they might also experience a weak reflectivity. In this case the effects due to gain competition dominate the variation in the mirror reflectivity.

It has to be mentioned that external feedback can also lead to a slight wavelength shift due to the phase difference between the original reflectivity r_t and the effective reflectivity r_{eff}. This phase change can be taken into account by a corresponding change in the effective cavity length (see [8] for details) which has an influence on the cavity resonance condition according to (2.14).

---

[1]e.g. by changing the distance to the external reflector

Chapter 3

VCSEL Characterization

This chapter describes measurements intended to characterize the static, dynamic and temperature behavior of a vertical cavity surface emitting laser diode. This is important to enable distinguishing between VCSEL intrinsic effects and such that are caused by external optical feedback which is discussed in Chapter 4.

In Section 3.1 therefore the static output attributes of the VCSEL are investigated. The power versus current characteristics of a certain VCSEL type will be presented as well as spectra and far field intensity distributions. Many of the terms defined in Section 2.1.3 will be used for device characterization.

Section 3.2 will take a look at the output characteristics under modulation at different bias levels and data rates. There it will be shown that these attributes do not change drastically under modulation and therefore the results obtained in Chapter 4, where the VCSEL is not modulated, are also valid when considering such a dynamic situation.

Lastly in Section 3.3 the intrinsic temperature behavior of the laser diode will be investigated showing that there are no oscillations in the VCSEL output over temperature.

3.1   Static Behavior

Static characterization of the laser diode means characterizing the input - output behavior of the device under constant bias conditions (constant drive voltage and current). It delivers the typical parameters that are used to describe the laser coarsely and can also be found in the data sheet. The VCSEL under investigation is a ULM Photonics multi mode $5\,Gb/s$ device (ULM 850-05-TN-U46FOP).

In this section the output power versus current characteristics of the device and parameters that can be obtained from it will be presented as well as spectra and far field intensity profiles under different drive current conditions and the dependence of the beam divergence on the current. It will also be shown that different spectral lines in the VCSEL output correspond to different transversal modes. Appendix B.3 shows furthermore that there can be a splitting of those lines due to anisotropies encountered by the two different polarizations of a transversal mode.

3.1.1   Output Power - Current Characteristics

3.1.1.1   Measurement Setup

Figure 3.1 shows the measurement setup used to obtain the power - current characteristics of the VCSEL diode and additionally the voltage - current characteristics. The VCSEL is driven with a DC current, whose magnitude can be adjusted with the current source. The total light output power as well as the laser voltage are observed with the power meter and the voltmeter respectively. Details about the devices used in this and all other measurement setups can be found in Appendix A.1.
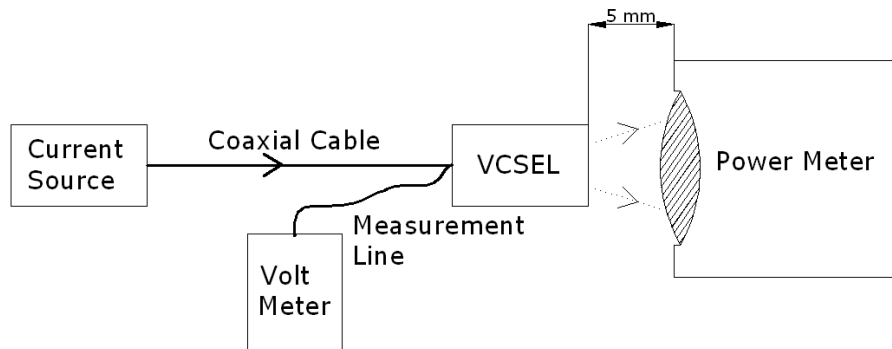
Figure 3.1: Setup to measure the power - current characteristics

3.1.1.2 Measurement Results

The results of this measurement are shown in Figure 3.2. The black dashed curve was not measured, it shows the ideal linear characteristics of the laser if no thermal effects would lead to power saturation. This saturation can be seen in the solid blue curve (labeled VCSEL output power) at high drive currents. It is mainly due to carrier and current leakage effects as well as increased non radiative recombinations. Increasing the current even further than shown in the figure would lead to thermal roll over marked by decreasing output power with increasing current (see [4]).

The black dashed curve also allows the determination of the laser threshold current I_{th}. This is the current where this linear fit equals $0\,W$. The inset shows that it is equal to

$I_{th} = 1.28\,mA.$

The differential quantum efficiency and slope efficiency of the device (according to Section 2.1.3) for operation beyond threshold are not constant due to the nonlinearity of the characteristics, but at the beginning, where linearity is given (the blue line labeled VCSEL output power and black dashed line are equal), they can be found to equal

$\eta_d = 0.255$
$\eta_s = 0.373\,W/A,$

taking into account the emission wavelength of about $847\,nm$.

From the red line labeled VCSEL voltage it is evident that the voltage varies only little due to the small VCSEL series resistance. The voltage at threshold equals $U_{th} = 1.6\,V$. This characteristics allows to determine the differential series resistance r_s of the device. It is shown in Figure 3.3 together with the power conversion efficiency η_p. The series resistance was obtained by interpolating the voltage characteristics and numerically differentiating the curve with respect to the current. It is just meaningful beyond threshold and therefore not given before. All obtained values are in good agreement with the data sheet given by the manufacturer.
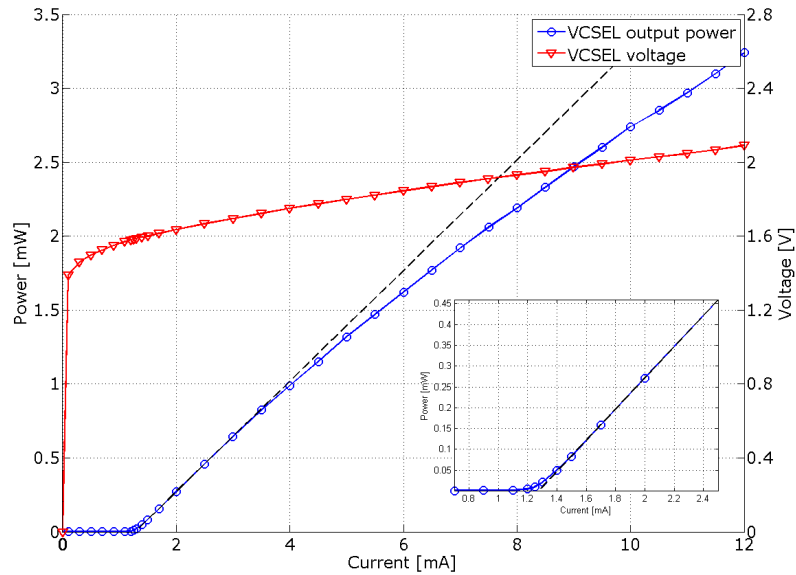
Figure 3.2: Output power - current and voltage - current characteristics
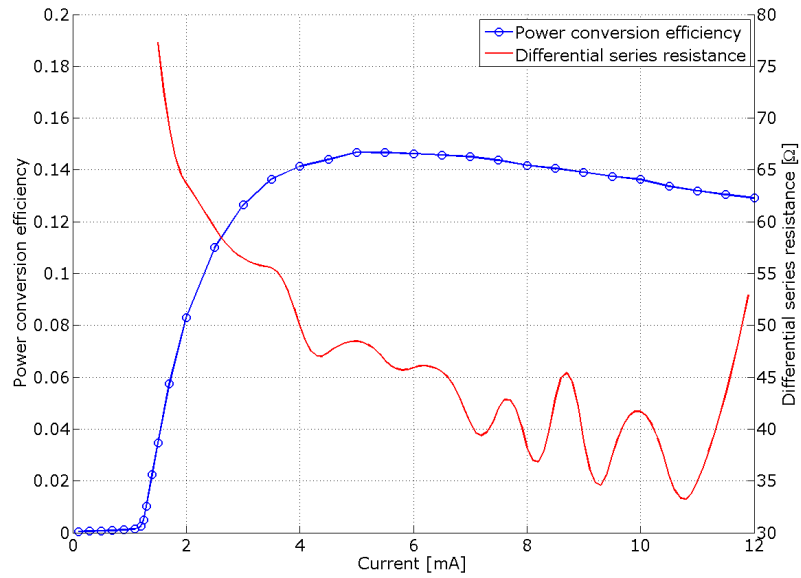
Figure 3.3: Differential series resistance and power conversion efficiency

3.1.2 Dependence of Spectrum on Drive Current

3.1.2.1 Measurement Setup

The setup used to measure spectra is shown in Figure 3.4. It is necessary to couple the light into a multi mode fiber (MMF) in order to feed it to the optical spectrum analyzer (OSA). The setup incorporates a

beam splitter cube (BS1) in order to deflect a part of the beam onto a CCD camera. This camera allows to measure far field intensity distributions with a high resolution. The setup does not allow easy evaluation of the beam divergence due to the objectives (L1, L2) in use which would complicate the calculation. Therefore in Section 3.1.3 another setup is used to determine the divergence.
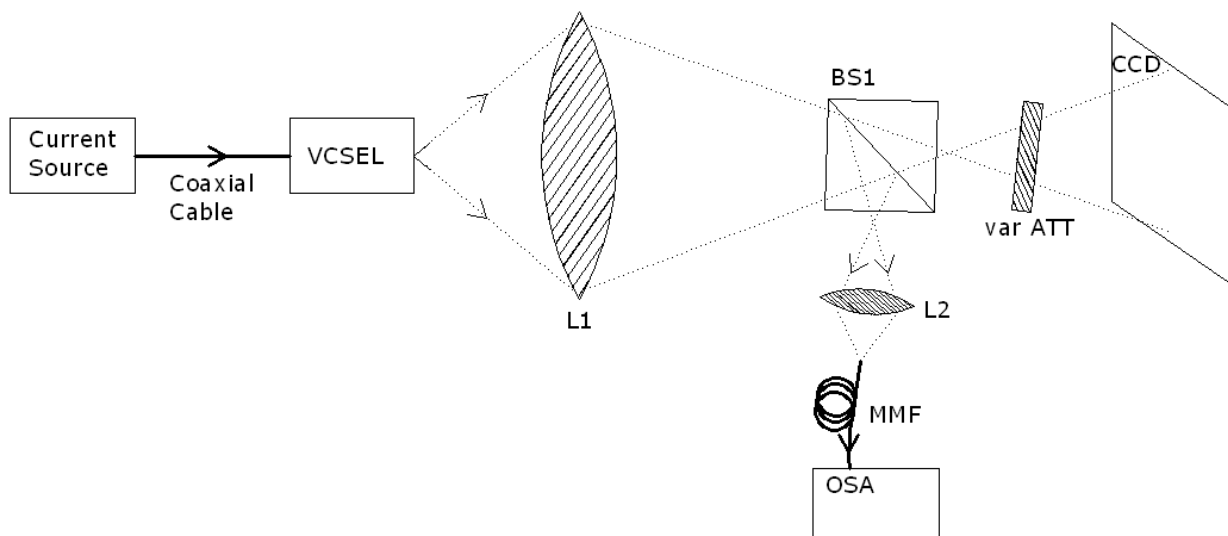
Figure 3.4: Setup to measure spectra and far field intensity distributions

3.1.2.2   Measurement Results

Figure 3.5 shows measured VCSEL output spectra at different drive currents. As can be seen the spectral width increases with current, more spectral lines emerge. Some spectral lines are assigned to the corresponding transversal modes inside the VCSEL cavity (see 2.1.2). This assignment will be justified in Section 3.1.4. The same dependence is shown in Figure 3.6 in a two dimensional way, by putting the information about the magnitude of the power spectral density into the color coding. This figure is something like a spectrogram, with the time dependency replaced by a current dependency. Spectra have been measured in a $0.5\,mA$ grid. The depiction shows clearer how the spectrum changes with current. First at $1\,mA$ the VCSEL is driven below threshold and there is almost no output power in the two visible spectral lines. Increasing the current beyond threshold the output power increases drastically. At $1.5\,mA$ a third spectral line appears additionally and the two original ones have shifted to a slightly larger wavelength. With increasing current this process carries on, new spectral lines emerge and the overall wavelength shifts towards larger values. Above $7\,mA$ the width of the spectrum does not increase anymore. From 7 to $10\,mA$ no new spectral lines appear anymore, just the power distribution among the different spectral lines varies and the overall spectrum shifts further towards larger wavelengths.
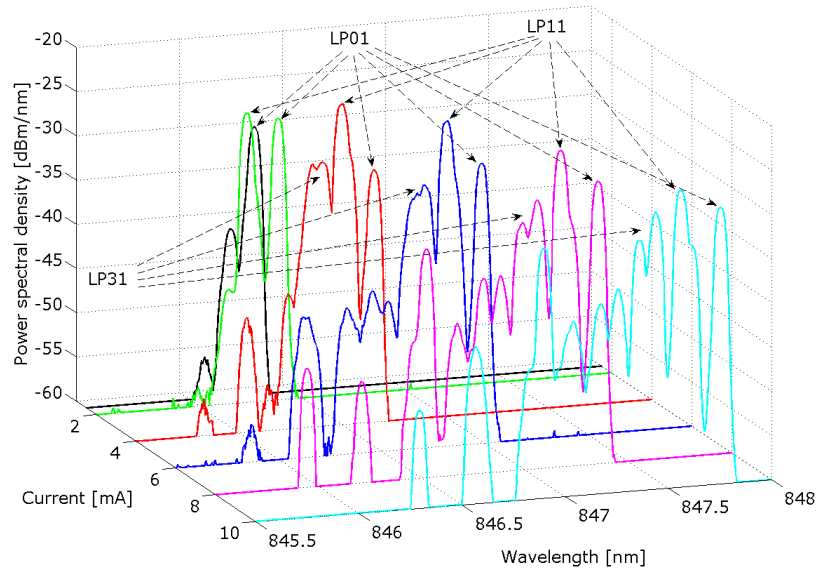
Figure 3.5: Comparison of VCSEL output spectra at different drive currents
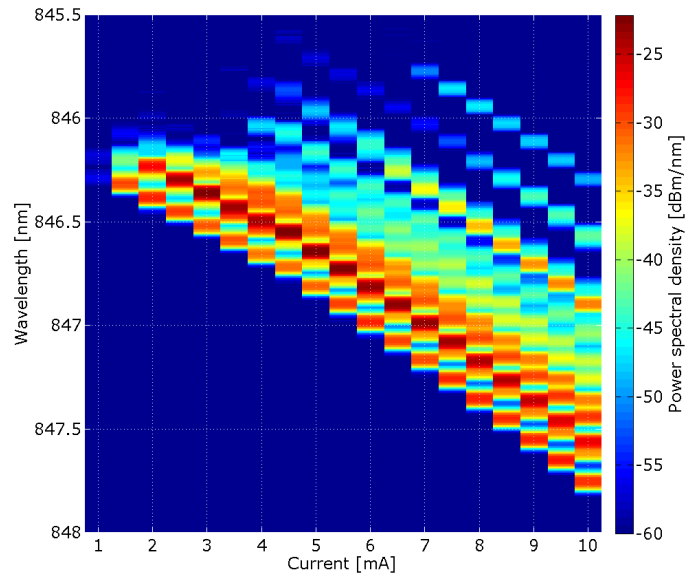
Figure 3.6: "Spectrogram" of the VCSEL output spectrum

Figure 3.6 shows that the shift in VCSEL wavelength is not linear over temperature. Nevertheless it is commonly characterized by just one parameter $\frac{\partial \lambda}{\partial I}$. This value equals

$$\frac{\partial \lambda}{\partial I} = 0.182 \, nm/mA$$

at a drive current of $6\,mA$, which is the typical bias level for the VCSEL under investigation according to

19

the data sheet.

3.1.3   Beam Divergence

For evaluating the beam divergence it is also necessary to measure far field intensity distributions. But, in order to keep the calculation of the divergence angle simple, it is advantageous not to use any optical elements between laser diode and camera. Therefore the same measurement setup as shown in Figure 3.1 is used with the power meter replaced by a pyroelectric array camera (PAC). The PAC was used because it can handle very high light intensities which allows to irradiate the camera directly, without necessity for a optical attenuator. The disadvantage of this device is its rather low resolution (124×124 pixel on an area of $12.4\,mm \times 12.4\,mm$).
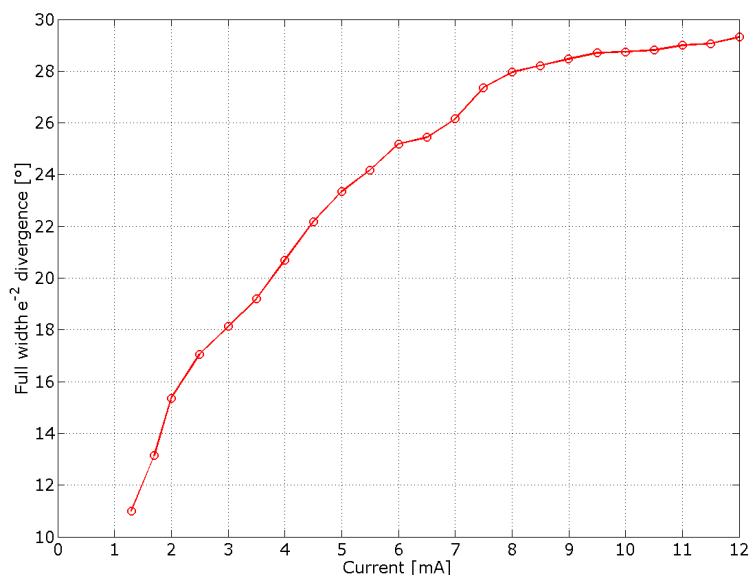
Figure 3.7: Divergence of the VCSEL output beam depending on the drive current

The evaluation of the beam divergence is easily possible by determining the diameter $2w_0$ at which the beam intensity has decreased to $\frac{1}{e^2}$ of its maximum value. Taking into account the distance z_0 to the pyroelectric array the full width $\frac{1}{e^2}$ divergence angle is given by

$$\theta_0 = 2\arctan(\frac{w_0}{z_0}). \tag{3.1}$$

Appendix B.1 shows how the evaluation has been carried out using Matlab. Figure 3.7 shows the result of this procedure. The divergence is increasing with drive current because more and more higher order modes with larger divergence are being excited as will be shown in 3.1.4. At currents larger than about $8\,mA$ the effect starts to saturate due to two effects. First, as Figure 3.6 shows, the spectral growth stops at currents higher than about $7\,mA$ and therefore no new higher order modes are being excited anymore and second also the increase in total output power is getting weaker due to internal heating effects as Figure 3.2 shows.

3.1.4   Matching Transverse Modes with Spectral Lines

As already described in Section 2.1.2 the wavelengths of the individual transversal modes in the VCSEL cavity are slightly different. Higher order modes generally have smaller wavelengths, the exact values can be determined from a dispersion relation.

(a) Measured distribution

(b) Simulated distribution
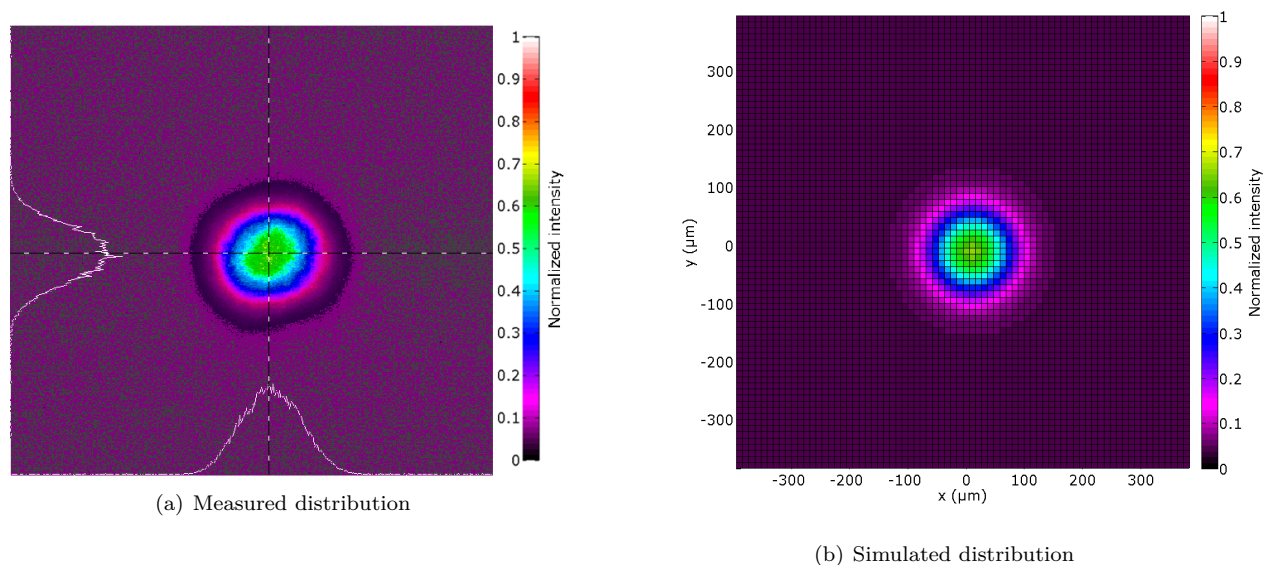
Figure 3.8: Far field distributions at $1.5\,mA$ drive current

As Equation (2.18) indicates the threshold gain is varying for different transversal modes mainly because the spatial overlap between the mode and the active area is changing due to different spatial intensity patterns. This is accounted for by the transversal part of the optical confinement factor given in Equation (2.15). It is calculated from the overlap integral between the transversal intensity distribution and the active area according to Equation (2.16). Due to the mutual coupling effects between transversal modes (gain competition, spatial and spectral hole burning) the active area, a mode experiences, is not constant. Spatial hole burning e.g. weakens the gain for other modes where a dominating mode has its intensity maxima and leaves much gain where it is minimal. Due to these facts it is not possible to calculate analytically which modes radiate at a specific current. This can only be evaluated numerically. Therefore it is difficult to find out which transversal modes correspond to which spectral lines.

Still there is a heuristic possibility to figure out at least the dominating modes. It is a based on the far field intensity distributions at a specific current and the corresponding spectrum. This approach tries to find that modes that best reproduce the measured far field intensity distributions with the help of simulations. Parts of the freely available software tool VISTAS ([23]) are used for that. It allows to assign powers to transversal VCSEL modes (so called modal powers) and calculate the corresponding far field intensity distribution. The modal powers can be estimated by numerically integrating over the corresponding spectral lines in the measured spectra. Still there is the uncertainty of how much power is allocated to the two helical polarities. This can just be found out by trial and error. There is always some asymmetry in the measured far field intensity distribution which allows to estimate this power partitioning.

The procedure was carried out in an iterative way by starting at a simple spectrum with just one dominating mode (at $I = 1.5\,mA$ bias current), trying to find the corresponding transversal VCSEL mode and then carrying on to more difficult spectra. The spectrum is shown in Figure 3.5, clearly the mode at about $846.35\,nm$ is dominating and the VCSEL is almost operating single mode. Figure 3.8 a) shows the measured far field intensity distribution. Clearly the distribution has a Gaussian like shape (a Gaussian fit to this distribution is presented in Appendix B.1) and there is only one mode that reproduces such a distribution which is the LP01 mode. The simulated far field is given in 3.8 b) in a distance to the VCSEL of $1\,mm$. The parameters of VISTAS were adjusted in such a way, that the simulated divergence of the LP01 mode is equal to the measured one which is about $11\,°$ (full width). Details on the parameter extraction procedure can be found in Appendix B.2.

(a) Measured distribution

(b) Simulated distribution
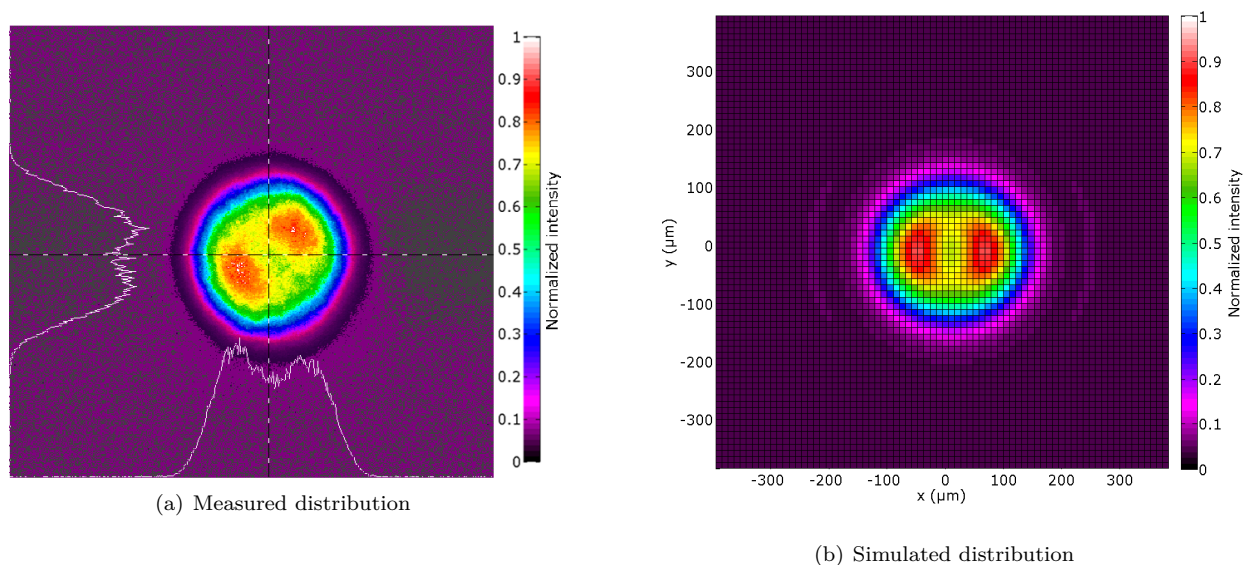
Figure 3.9: Far field distributions at $2\,mA$ drive current

Now that this first mode is identified the next step in the iteration process is going to a bias current where the spectrum is dominated by two modes and trying to identify the next mode. Figure 3.5 shows that this is the case at $2\,mA$. The new mode is even dominating the spectrum, but the difference in total modal power to the original mode is just about $1\,dB$. The measured intensity distribution, shown in Figure 3.9 (a), clearly shows that one helical polarity is dominating, due to the angular asymmetry. The new mode must be ring shaped with just one radial intensity maximum in $0 \leq r < \infty$. This points towards the LP11 mode. The assumption is also confirmed by the facts that lower order modes tendentially have a lower threshold current, because their spatial overlap with the active region is large. Also spatial hole burning of the LP01 mode does not influence the LP11 mode because it is minimal where LP01 has its maximum. The beam divergence is still low too at $2\,mA$, about $15.5\,°$ and modes with higher order (larger mode numbers l and p) would lead to larger values. The power distribution between the two helical polarities was figured out by trial and error, the result is shown in Figure 3.9 (b) and gives a good fit to the measurement. The axes of the two beam profiles are slightly tilted with respect to each other. The simulated beam divergence equals $16\,°$.

In the third step a drive current of $10\,mA$ was chosen as the operating condition. The spectrum shows that here already a lot of modes are radiating, but the three with largest wavelength are dominating. The third spectral line, labeled with LP31 in Figure 3.5, is split into two sub lines, the four fold degeneracy of the mode, due to polarization and the two helical polarities, is partly lifted. It can be stated that it is just one transversal mode by looking at the evolution with drive current. At $4\,mA$ the spectral line is hardly split. $10\,mA$ was chosen as the operating condition because there the third mode is strongest. In this situation the third mode is about $2\,dB$ stronger than LP01, LP11 is about $3\,dB$ stronger than LP01 and there is another quite strong mode at about $846.8\,nm$ which is $3\,dB$ weaker than LP01. This mode together with all other modes, that are even weaker, are being neglected in a first step. Such weak modes do not appreciably influence the far field intensity distribution.

Figure 3.11 a) shows the measured far field distribution. It has a hexagonal like structure (look at the blue ring). This structure must be produced by the sum of LP01, LP11 and another mode. One of the two helical polarities of the new mode must be dominating, otherwise the resulting beam profile would be more symmetric. The measured intensity profile also does not show any additional maxima in radial direction, there is still a ring like shape. This restricts the search to the class of LPl1 modes. Figure 3.10 shows one

(a) LP21

(b) LP31
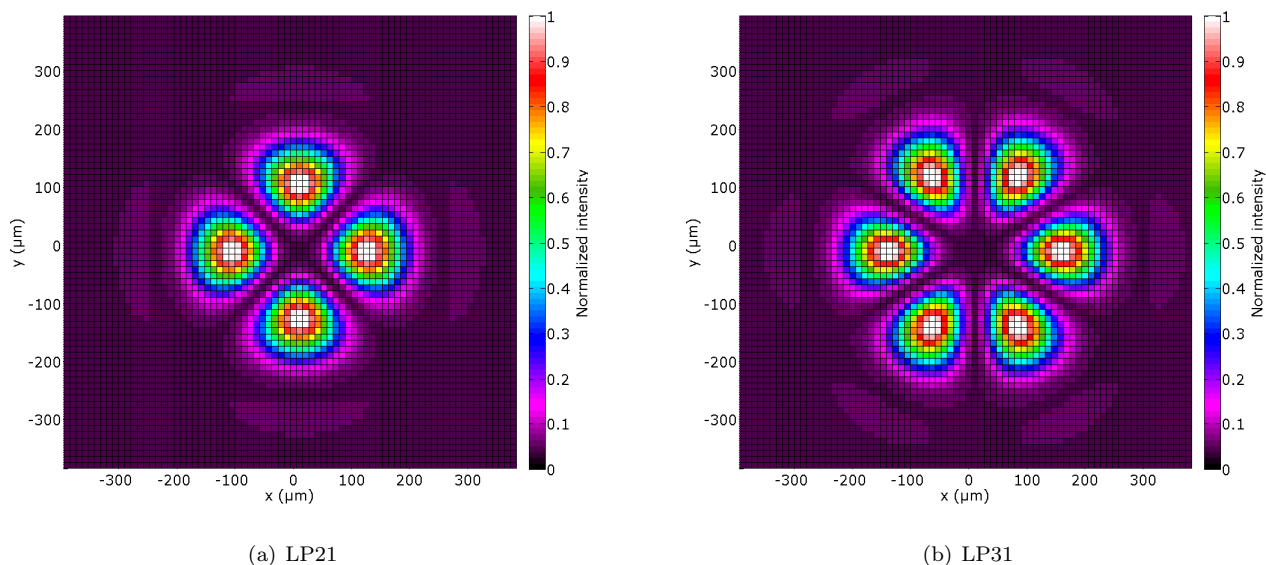
Figure 3.10: Far field distributions of two specific modes

(a) Measured distribution

(b) Simulated distribution
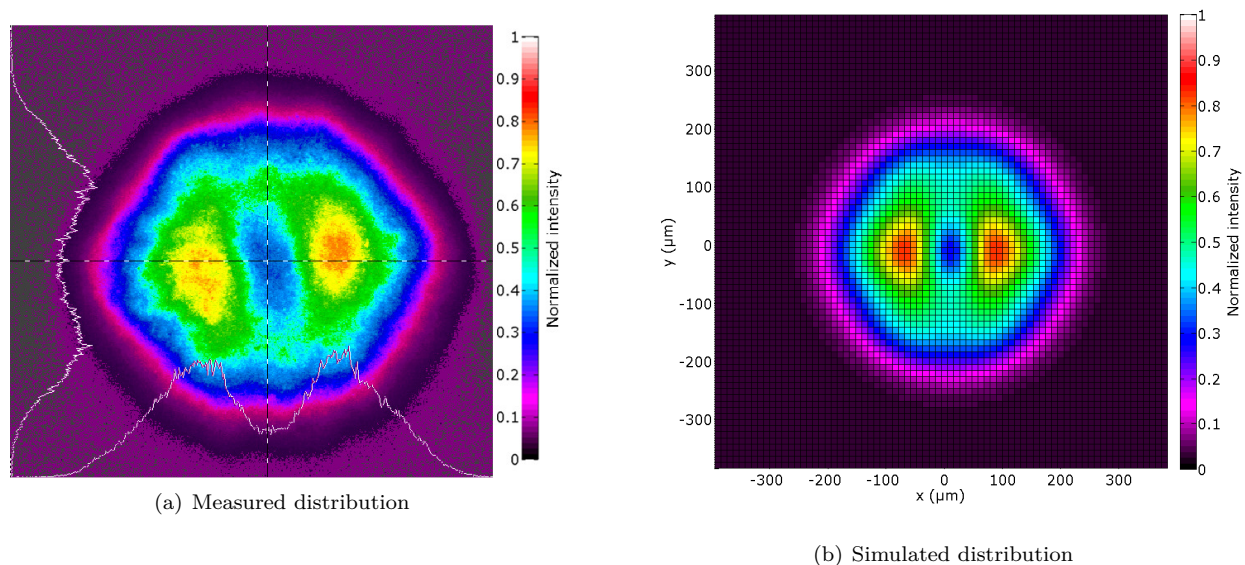
Figure 3.11: Far field distributions at $10\,mA$ drive current

helical polarity of the LP21 and LP31 mode in the far field. Clearly adding LP21 to LP11 and LP01 does not produce a hexagonal structure, but LP31 does. The result, when adjusting the powers of the two helical polarities accordingly, is shown in Figure 3.11 (b). Again a good fit to the measurement can be obtained, but the divergence is too low. The measured divergence equals $28.5\,°$ and the simulated one is just $25.5\,°$. This can be explained by the fact that all the other modes have been ignored. If they have large divergence then this will also have an influence on the total divergence. This shows that it is highly probable that the third spectral line corresponds to LP31, but it can not be stated with complete confidence, as the mode is not dominating the intensity distribution.

It is not possible to identify more modes with this approach because there is no bias condition where one of the other modes would be strong enough to dominate the far field distribution.

3.2 Dynamic Behavior

In this section the operation of the VCSEL under modulation is investigated. The opto-electronic waveguide boards described in Chapter 1 are intended for data transmission and therefore the dynamic behavior of the VCSEL is what influences the performance of the boards. Nevertheless, to keep the measurements as simple as possible and do not artificially complicate the interpretation, the feedback investigation in Chapter 4 is carried out in a static manor. To carry over the results also to dynamic situations it is necessary to show that the output characteristics of the VCSEL do not change remarkably under modulation. The important property for the later reasoning is the intensity distribution of the VCSEL or equivalently the spectrum. It will be shown that modulating the VCSEL does not change the principal output behavior concerning these quantities.

The measurements are not only carried out with a "packaged" ULM VCSEL 850-05-TN-U46FOP but also with a "bonded" Avalon multi mode VCSEL of the type AP-A72-0101-0000. The first laser diode is packaged in a TO46 housing whereas the second one is directly bonded onto a printed circuit board. This allows modulation at higher data rates due to better RF characteristics. Both types of lasers are also used during later measurements. The results are just shown for the ULM VCSEL because they are similar for the other laser diode too.
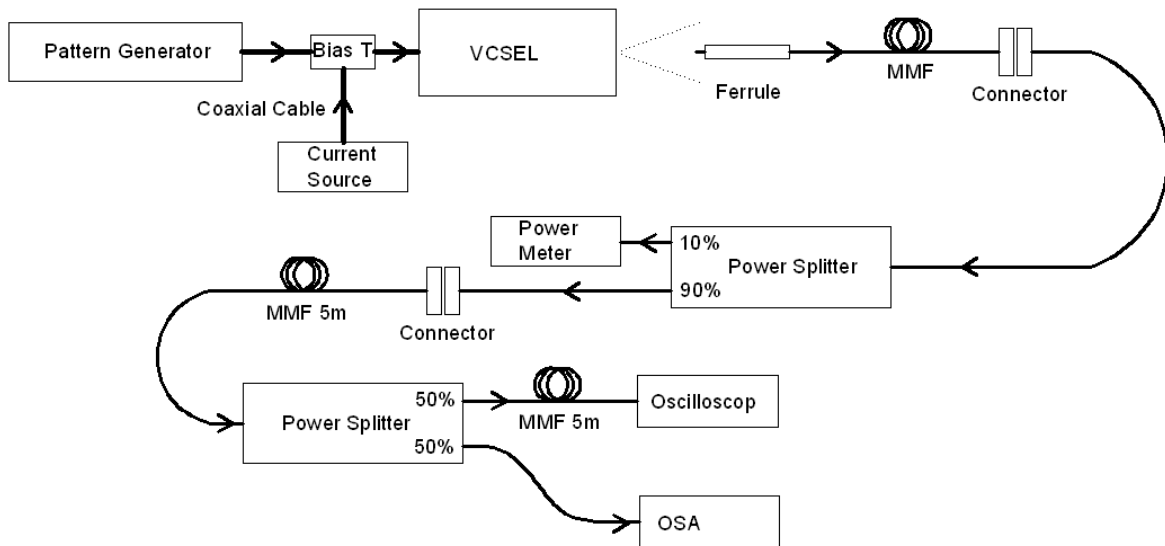
Figure 3.12: Setup to measure the VCSEL spectrum and time response at modulation

3.2.1   Measurement Setup and Conditions

To contemporary measure the VCSEL mean output power, spectrum and the time dependency of the light output power, the measurement setup shown in Figure 3.12 is used. The bias T allows to feed the VCSEL simultaneously with a bias current from the current source and a modulation signal from the pattern generator. The laser output light is fed into a multi mode fiber and from there into the three measurement instruments, the power meter, the oscilloscope and the optical spectrum analyzer. Also the far field intensity distribution is observed, with a measurement setup that is similar to the one shown in Figure 3.4, just without the beam splitter and the spectrum analyzer, but therefore of course with the same electrical supply as the one shown in Figure 3.12.

  The measurements were carried out with a 01 bit sequence at different "data rates"[1] and bias levels. Measurements were also carried out with a pseudo random bit sequencse, but those are not reported as the results are similar. The advantage of the 01 bit sequence is that the position of the zeros and ones are known, which allows easy evaluation of the turn on delay t_d as well as the duty cycle of the device. Figures 3.13 and 3.14 show the two bias and modulation situations under investigation for the ULM VCSEL characteristics with a $1\,Gb/s$ 01 bit sequence.
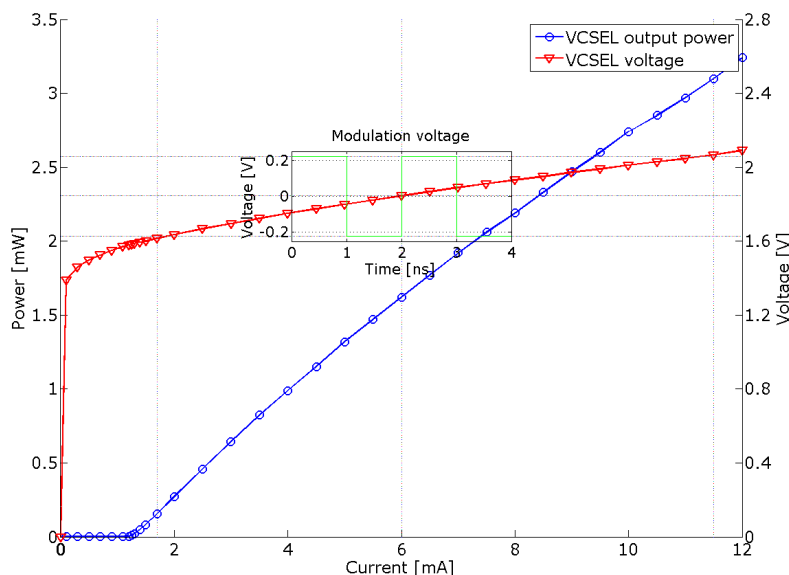
Figure 3.13: Drive condition for the ULM VCSEL at $6\,mA$ bias current and $1\,Gb/s$ bit rate

The situation shown in Figure 3.13 is the typical and important situation that will occur in practice. The VCSEL is driven far beyond threshold and the modulation amplitude is such that the VCSEL does not turn off during a zero, because that would make the operation slow (at every logical one it would be necessary to rebuild a inversion). The bias current is chosen high so that the extinction ratio between a logical zero and a one (logarithmic ratio of the powers of the two states) becomes large. A high current also allows higher bit rates because the necessary carrier densities for the two different bit states are achieved faster. The bias condition shown in Figure 3.14 is not typically used because here the VCSEL turns off during a zero. It was chosen to see whether this influences the VCSEL output behavior or not.

  To see whether the AC electrical signal gets distorted by the cable and bias T, it was measured at the input of the laser diode. The normalized input voltage (normalized with respect to the maximum at $622\,Mb/s$)

---

[1]Although such a deterministic sequence does not carry any information and therefore the information bit rate would be zero, every zero and one is counted as a bit. This terminology is used because it is the one given by the pattern generator.
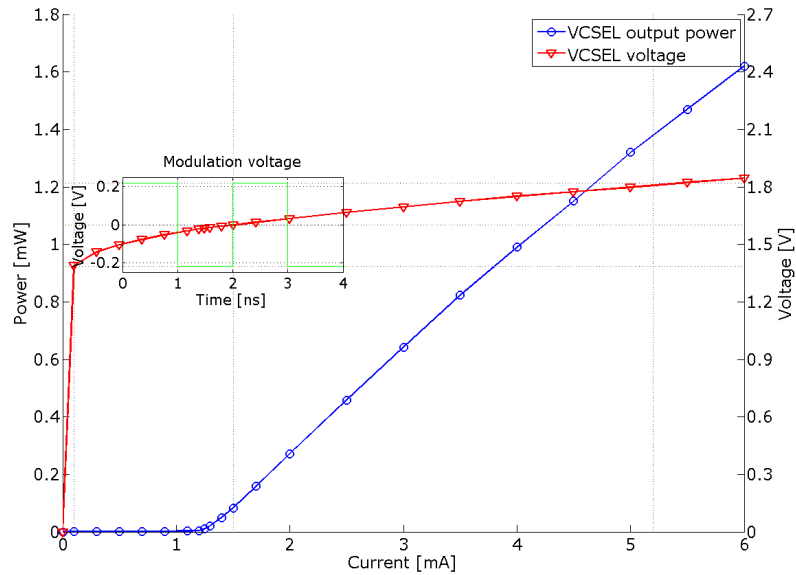
Figure 3.14: Drive condition for the ULM VCSEL at $1.5\,mA$ bias current and $1\,Gb/s$ bit rate
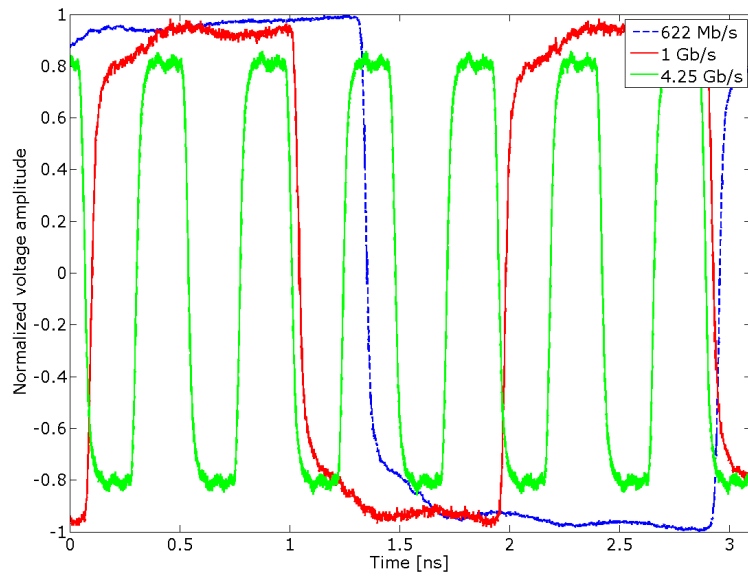
Figure 3.15: Normalized AC VCSEL input voltage

for three different bit rates under investigation is shown in Figure 3.15. For moderate bit rates ($622\,Mb/s$, $1\,Gb/s$) the voltage amplitude is almost not influenced, but at $4.25\,Gb/s$ there is clearly a attenuation noticeable, the amplitude is lower by a factor of 0.8. The long settle time of the signal is a property of the generator itself.

3.2.2 Time Domain Results

This section presents time resolved measurements of the VCSEL output power, when the laser diode is modulated and biased under the conditions described above.

3.2.2.1 Bias Current well above Threshold

Figure 3.16 shows the temporal response to a 01 input sequence at three different bit rates when biasing the VCSEL well above threshold at $I = 6\,mA$ (remember the threshold current of the device equals $I_{th} = 1.28\,mA$).
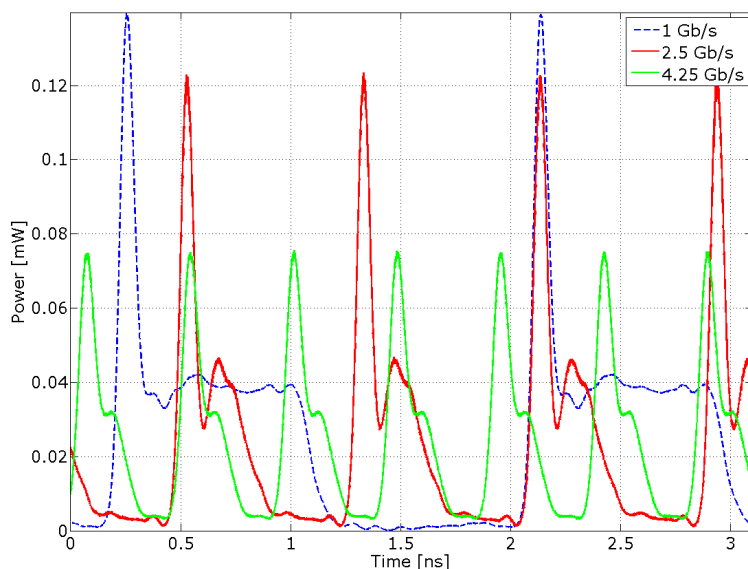
Figure 3.16: Time dependence of the output power of a packaged VCSEL subject to 01 bit sequence modulation at a bias current well above threshold

The laser diode shows a large overshoot at turn on whose magnitude depends on the bit rate. This dependence arises from the fact that the drive voltage amplitude is lower at higher bit rates (due to the attenuation of the cable and bias T). Reducing the voltage amplitude at constant bit rate also reduces the amount of overshoot but the extinction ratio too. The overshoot is not so high for the Avalon VCSEL (not shown here). One reason may be better RF characteristics of the bonded laser compared to the packaged one. At $1\,Gb/s$ the overshoot in terms of maximum power compared to steady state power of the logical one is lower than a factor of 1.5 for the Avalon laser compared to a factor of more than 3 for the ULM VCSEL shown above. The zero level increases with the bit rate which is again due to the smaller drive voltage amplitude.

3.2.2.2 Bias Current slightly above Threshold

In Figure 3.17 the same results are shown for a bias current just slightly above threshold at $I = 1.5\,mA$. At this bias current it was not possible to modulate the laser with data rates higher than $1\,Gb/s$ (at $2.5\,Gb/s$ just the first overshoot is present before the VCSEL turns off again). Compared to the situation at high bias current here the duty cycle between a zero and a one is not 50% anymore because the VCSEL turns off at every logical zero and it takes time to build up the necessary inversion to turn on again at a logical one.

In the figure the turn on delay time t_d is visualized. It is the time between the rising edge of the logical one in the input voltage and the rising edge of the one in the output power. The rising edge of the voltage
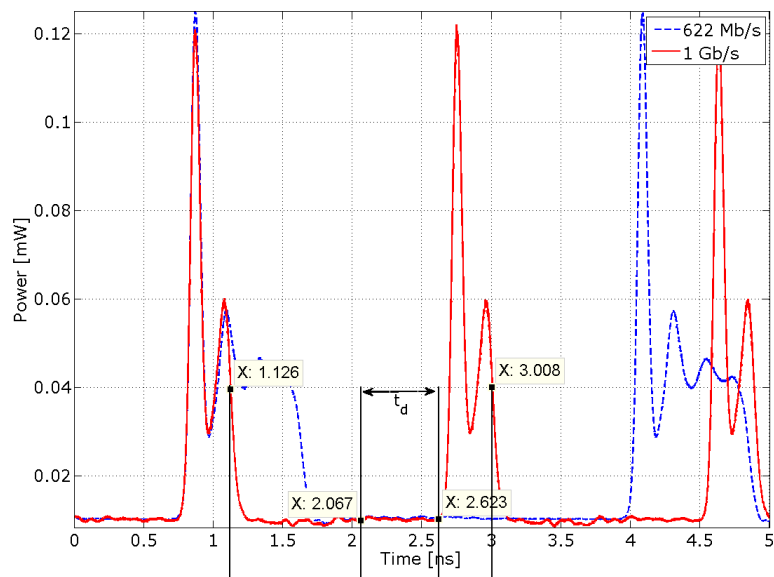
Figure 3.17: Time dependence of the output power of a packaged VCSEL subject to 01 bit sequence modulation at a bias current slightly above threshold

lies exactly midway between the two trailing edges[2]. Of course there is also a turn off delay which has been neglected here because it is much shorter than the turn on delay. It depends just on the photon lifetime (the average time that photons spend in the cavity) which is about two orders of magnitude lower ($\propto ps$) than the turn on delay time. The turn on delay equals about

$$t_d \approx 600\,ps$$

at this driving conditions. Knowing some material parameters like the diffusion coefficient, the auger recombination coefficient and the bimolecular (spontaneous) recombination coefficient it would allow the estimation of the carrier lifetime according to [8].

The transient response shows a constant oscillation frequency f_r that does not depend on the bit rate. It can be estimated to equal about

$$f_r \approx 4\,GHz.$$

This frequency is mainly a property of the laser itself (the relaxation oscillation frequency) influenced by external circuitry parasitics (see [19]).

3.2.3 Spectra and Intensity Distributions under Modulation

The VCSEL spectrum and intensity distribution are the quantities that are of real importance for the argumentation, explaining the oscillatory behavior observed on the waveguide boards, that will be carried out in Chapter 4. This section is intended to show that this reasoning is also valid when the VCSEL is modulated and not just statically driven. Therefore spectra and far field intensity profiles with and without modulation will be compared.

---

[2]The difference between the two trailing edges is not exactly $2\,ns$ because the bit rate is $1.0625\,Gb/s$ and not $1\,Gb/s$

28

3.2.3.1 Bias Current well above Threshold

Spectra corresponding to different bit rates for a VCSEL bias current of $6\,mA$ are shown in Figure 3.18. The spectrum at $0\,Gb/s$ corresponds to the situation of no modulation.
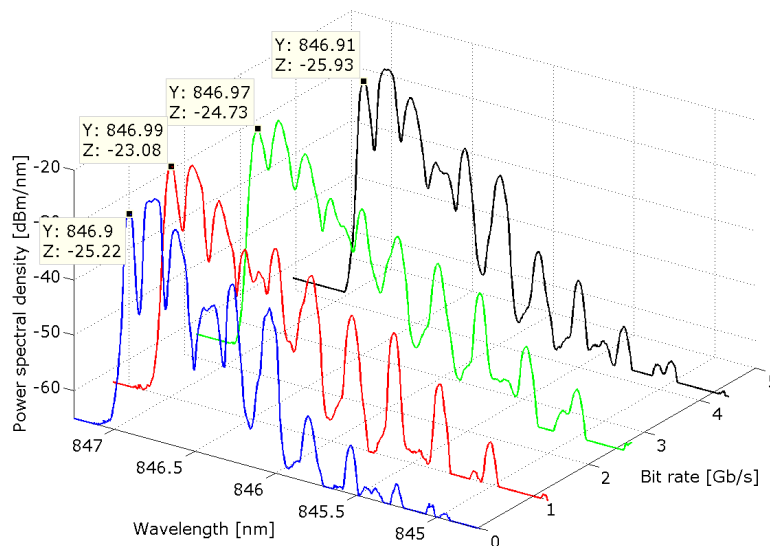
Figure 3.18: Comparison of the output spectra of a VCSEL subject to modulation with a 01 bit sequence at a bias current well above threshold

Following observations can be made from the spectra

- The dominating modes in the VCSEL spectrum stay the same.

- A slight power shift from the dominating modes towards higher order modes at smaller wavelengths occurs. Those spectral lines are increasing but are still weak compared to the dominating ones.

- At bit rates of $1\,Gb/s$ and $2.5\,Gb/s$ the wavelength shifts by about $0.1\,nm$ towards larger wavelengths. At $4.25\,Gb/s$ the wavelength shift is negligible.

- The higher the bit rate the smaller the change in the VCSEL output spectrum compared to the case without modulation.

A possible explanation for the wavelength shift could be that the mean current for modulation at $1\,Gb/s$ increases to $\bar{I} \approx \frac{11.5+1.7}{2}\,mA = 6.6\,mA$ (c.f. Figure 3.13) compared to $6\,mA$ if there is no modulation. This corresponds to a wavelength shift of

$$\Delta\lambda = \Delta I \cdot \tfrac{\partial\lambda}{\partial I} = 0.6\,mA \cdot 0.182\,nm/mA = 0.109\,nm.$$

The increase of power in the higher order modes can be explained by assuming that the spectrum is just a mean of the two spectra corresponding to a bias current of $1.7\,mA$ for the logical zero and about $11.5\,mA$ for the logical one. The overall spectrum will be dominated by the one at larger current and there higher order modes are stronger according to Figure 3.6. Both explanations can also describe the behavior at $4.25\,Gb/s$. There the input voltage amplitude is lower and therefore also the variations in the spectrum decrease.

Figure 3.19 shows a comparison of transversal far field intensity distributions at different bit rates. In accordance with the spectrum the intensity distribution gets weaker in the central region (which is dominated

by the modes at largest wavelengths - compare figure (a) and (b)) but therefore the spot size increases slightly because of the increase in power of modes at smaller wavelength. Those modes have a high mode order and also a high divergence. At $4.25\,Gb\,s$ the far field intensity distribution as well as the spectrum stay almost the same.

(a) No modulation

(b) $1\,Gb/s$

(c) $4.25\,Gb/s$
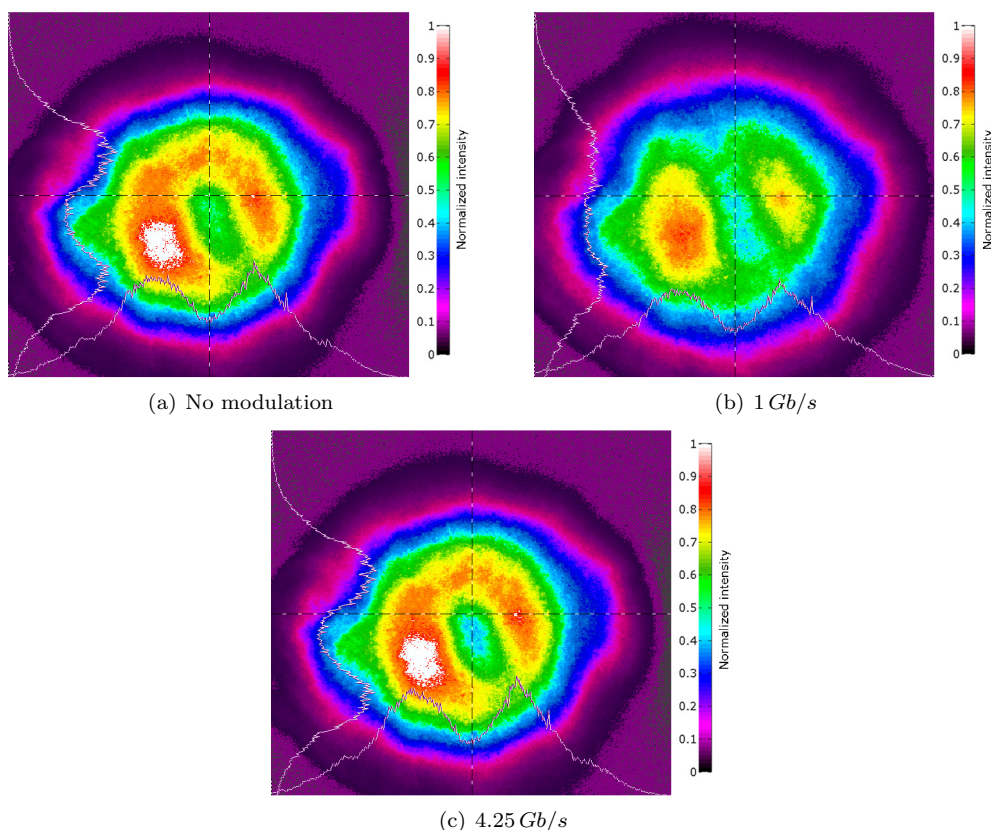
Figure 3.19: Measured far field intensity distributions of a VCSEL subject to modulation at a bias current well above threshold

During the measurements also the mean VCSEL output power was observed. It is equal to the arithmetic mean of the two powers corresponding to the zero and one state. It shows a slight decrease of about $0.3\,dB$ compared to the case of no modulation. This can be explained by the decrease in the differential quantum efficiency (the slope of the P - I characteristics) at higher currents (see Figure 3.13).

3.2.3.2 Bias Current slightly above Threshold

The behavior of the laser diode in this case is quite similar to the one before, although the variation in the spectrum between situations with and without modulation is larger as Figure 3.20 shows. The wavelength shift is a bit larger, about $0.12\,nm$, but also the mean current increases. The change in spectrum is larger because at small currents, as Figure 3.6 shows, already slight current variations lead to large spectral variations. Correspondingly also the change in the intensity distribution is larger. Also the variation in mean power between situations with and without modulation increases to more than $7 - 8\,dB$, depending on the bit rate. In this case the mean power with modulation is higher, but still this can be explained by taking the mean of the powers at the two logical states.

At the investigated data rates there is no difference in the principal nature of the VCSEL output with or
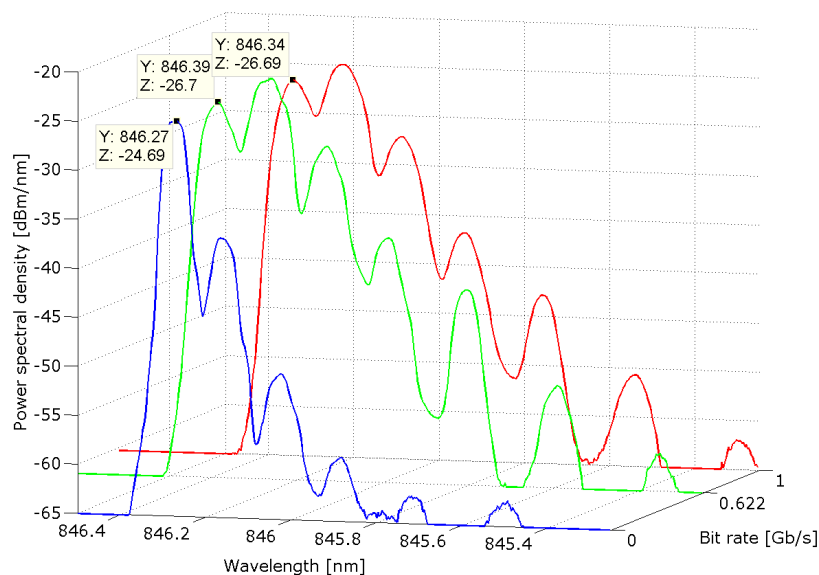
Figure 3.20: Comparison of the output spectra of a VCSEL subject to 01 bit sequence modulation at a bias current slightly above threshold

without modulation and the arguments given in Chapter 4 for static situations will also hold in the dynamic case. This is true at least as long as the laser diode is still able to reach steady state after each rising edge. At very high data rates ($\geq 10\,Gbit/s$) not all supported laser modes are able to start oscillating during the short turn on time. But the opto-electronic waveguide boards are not intended for such high data rates. As already mentioned the principal behavior under modulation is similar for the Avalon VCSEL. This indicates that these statements may hold device independent.

3.3 Temperature Dependence

This section is intended to show that the VCSEL itself does not exhibit any oscillatory behavior concerning the spectrum, intensity distribution or output power over temperature. This means that the effects described in Section 1.2 can not be produced by the laser diode alone, but there must be an external influence that causes such a oscillatory behavior, which is external optical feedback described in Chapter 4.

During this investigation it will be shown that ambient temperature does affect the VCSEL output characteristics, but in a continual way. The total output power reduces with increasing temperature and the spectrum shifts towards longer wavelengths. Accordingly also the intensity distribution changes.

3.3.1 Measurement Setup

In order to measure the dependence of the VCSEL output characteristics on temperature a programmable temperature chamber is used that allows to achieve any desired temperature profiles over time. The corresponding setup is shown in Figure 3.21. Just the optical part of the setup is shown, of course there is also a current source feeding the laser diode, which is not shown for simplicity. Outside the chamber the three different possibilities given in the figure are used to measure either the spectrum, intensity distribution or total output power of the VCSEL (just place the corresponding setup at the chamber opening).

A Avalon VCSEL bonded onto a printed circuit board was used during the measurements, because the package of the ULM laser did not allow adequate stable mounting. The beam moved due to vibrations of
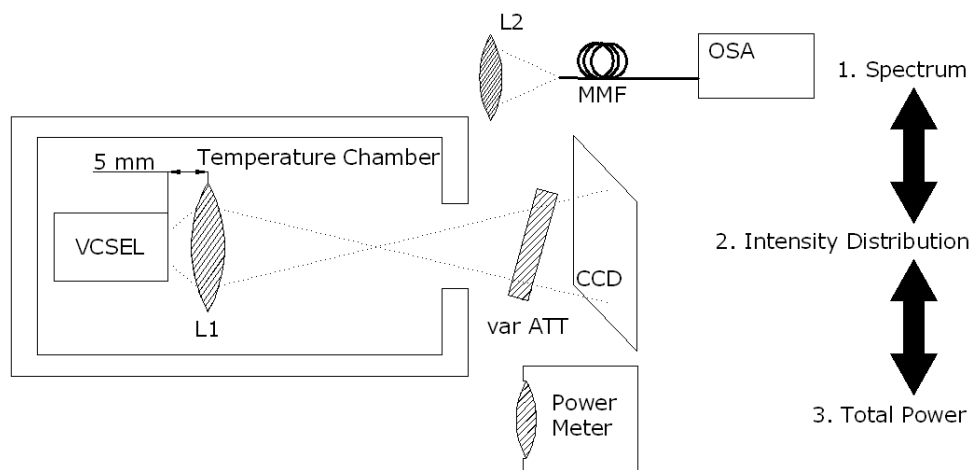
Figure 3.21: Setup to measure the temperature dependence of the VCSEL output characteristics

the temperature chamber, which did not allow constant quality of fiber coupling (this lead to fluctuations in the observed spectra even at constant temperature). The VCSEL was constantly biased at $6\,mA$ during all measurements.

Another difficulty was the thermal deformation of the mechanical attachments. At temperatures higher than $60 - 70°\,C$ screws got loose and the measurements had to be stopped. Unfortunately there were no other possibilities to mount the devices. The thermal deformation also leads to a beam wander which can be seen in the measured intensity distribution (the beam changes its place). This is problematic for the measurement of the spectrum. If the fiber alignment is not changed to compensate for the beam movement, the fiber coupled power decreases very fast with varying temperature. But also if the alignment is adjusted, to keep the fiber coupled power at a maximum, slightest variations in this alignment between fiber tip and the transversal beam profile can lead to changes in the coupling efficiency of different transversal modes and therefore in the spectrum. That is the reason why the spectral measurement is just used to investigate the wavelength shift with temperature and not to deduce any further statements.

3.3.2 VCSEL Output Power

Figure 3.22 shows the result of the measurement with the power meter placed at the opening of the temperature chamber. During this measurement the temperature inside the chamber was increased linearly from $20°\,C$ to $50°\,C$ in 30 minutes and afterwards decreased again (the red curve labeled with temperature in the figure). In this temperature regime the VCSEL output power decreases quite linearly with increasing temperature, the slope equals

$$\tfrac{\partial P}{\partial T} \approx \tfrac{\Delta P}{\Delta T} = \tfrac{0.425 - 0.525}{50 - 20}\,mW/K = -3.33\,mW/K.$$

This is a well known behavior explained by the facts that losses (non radiative recombination, carrier leakage,...) increase with temperature (see [5], [4]).
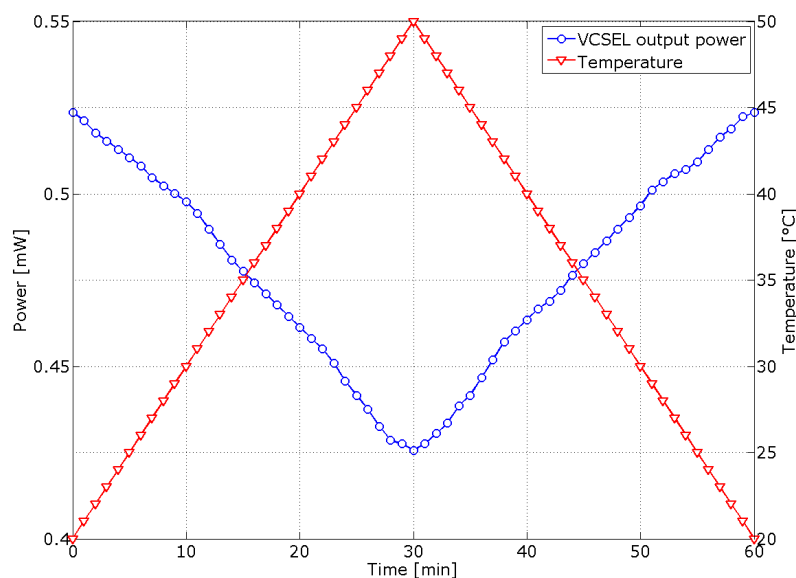
Figure 3.22: Measured VCSEL output power at varying ambient temperature

3.3.3 Spectra and Intensity Distributions at different Temperatures

The problematic of measuring spectra was already discussed in Section 3.3.1. But this problem, with varying fiber coupling efficiencies, does not influence the wavelength of the measured spectra and therefore they can be used to deduce the wavelength shift over temperature. Figure 3.23 shows the dependence of the VCSEL output spectrum on temperature in a spectrogram like illustration. This figure suggests that there is a rather strong change in the spectrum with the temperature, e.g. at $25°\,C$ the two modes with largest wavelength together with the fourth and fifth spectral line (beginning to count at large wavelength) are dominating but at $40°\,C$ the third and fourth are strongest while the others are much weaker. As spectral lines correspond to transversal modes this would also mean a strong change in the far field intensity distribution, which could not be observed. The intensity distribution has the same shape at all temperatures, just the strength is varying according to the decrease in total output power. Therefore the reason for this spectral variations must be a change in fiber coupling efficiency of the different modes. The wavelength shift with temperature equals

$$\frac{\partial \lambda}{\partial T} \approx \frac{\Delta \lambda}{\Delta T} = \frac{847.1 - 844.7}{60 - 20}\,nm/K = 0.06\,nm/K.$$

This value equals the one given in the data sheet.

Far field intensity distributions are given in Figure 3.24 for different ambient temperatures. It has to be mentioned that the variable attenuator was adjusted for weaker attenuation between $25°\,C$ and $40°\,C$, otherwise the intensity would have become too low. The images clearly show that the shape of the distribution stays the same. The position changes because of the mechanical instabilities described above. Images were taken every $0.1°\,C$. There is no oscillatory behavior observable in those images.
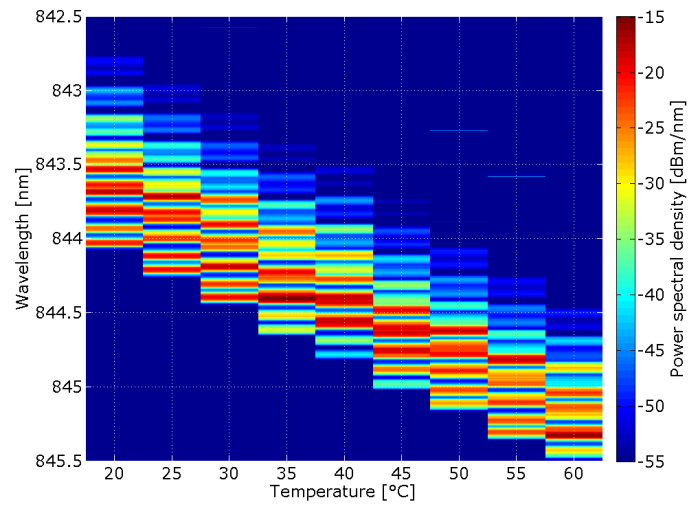
Figure 3.23: "Spectrogram" of the VCSEL output

(a) $20^\circ\,C$

(b) $25^\circ\,C$

(c) $40^\circ\,C$

(d) $60^\circ\,C$
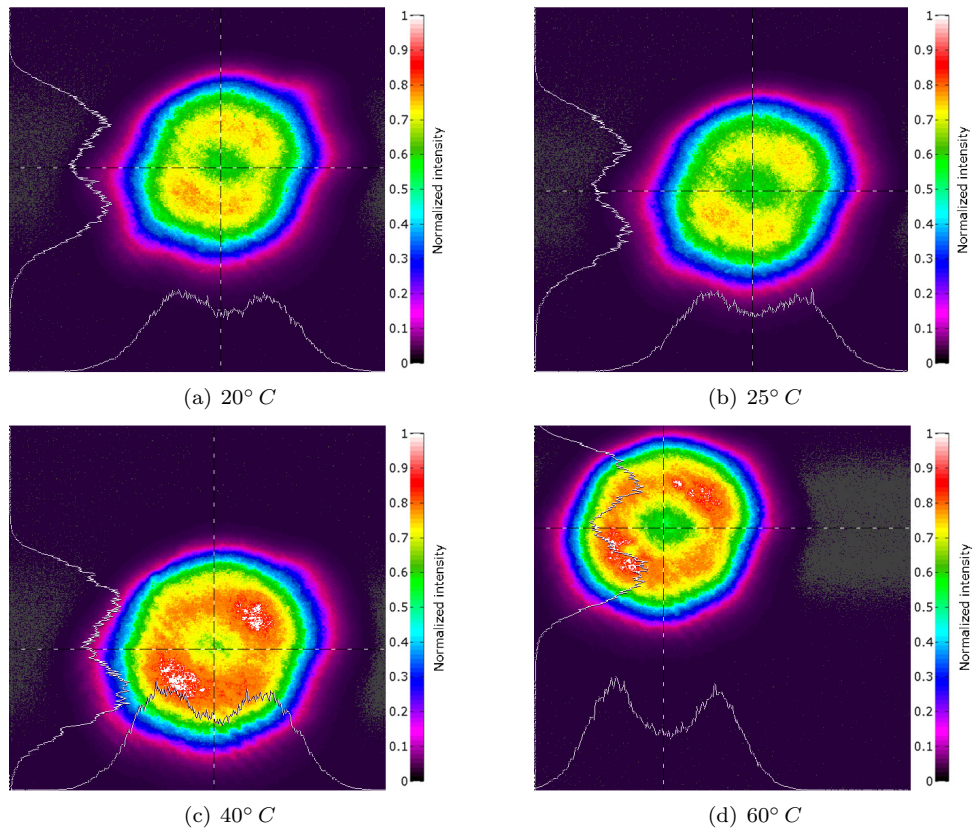
Figure 3.24: Measured far field intensity distributions of a VCSEL at different ambient temperatures

Chapter 4

External Feedback

Chapter 3 has shown that the vertical cavity laser diode alone does not exhibit any oscillatory behavior over temperature. Therefore the oscillations described in Chapter 1, which are to be explained, can not be attributed to the VCSEL as intrinsic behavior but they must be caused by some interaction with the environment.

This chapter is intended to show that external optical feedback, meaning that light from outside the laser cavity is reflected back into the cavity, can be such an interaction. Different citations ([11], [13], [16],...) show that external feedback can cause periodic variations in the laser output, if the feedback phase changes. Different effects on power, modal power distribution and spectral line width have been observed. The basic effects and the theory for the special case of weak external feedback have already described in Chapter 2.

In the opto-electronic waveguide boards, presented in Chapter 1, external feedback may be caused at the beginning of the waveguide, which is just at a distance of $10-20\,\mu m$ to the VCSEL surface. As the Rayleigh distance of the device is about $250\,\mu m$ (see A.2) those reflections would occur in the near field of the laser diode and much more important they would be coherent. Otherwise there may also be reflections from the backside of the waveguide or from some impurity along it, which might cause reflections that are incoherent. It is therefore important to investigate both cases of coherent and incoherent feedback, which will be done in Section 4.3 and 4.2 respectively.

Section 4.2 shows that incoherent feedback does not feature the necessary oscillatory behavior because it is not depending on the feedback phase. On the other hand coherent feedback effects, described in Section 4.3, can cause oscillatory behavior, but they just vary the modal power distribution and not the total VCSEL output power. Therefore another external effect is necessary, which translates those modal power variations into total power variations, some kind of modal filtering effect. Section 4.3.2 shows that the waveguide itself may act as a mode filter, if the transversal alignment between waveguide core and VCSEL is not ideal.

4.1   Overview

Before starting with the details of the different measurements, this section is intended to present an overview about all external feedback measurements carried out. It shall serve as a reference for orientation during the lecture of the rest of the chapter.

Figure 4.1 shows all kind of feedback measurements carried out. They are grouped into coherent and incoherent measurements depending on whether there is a fixed phase relation between feedback light and laser internal light or not.

During the incoherent measurements the strength of the feedback (via a variable attenuator), the feedback phase (via a piezo element that slightly shifted the reflector position) and the feedback alignment was varied. Varying the alignment means changing the part of the surface of the VCSEL that is irradiated by feedback light.
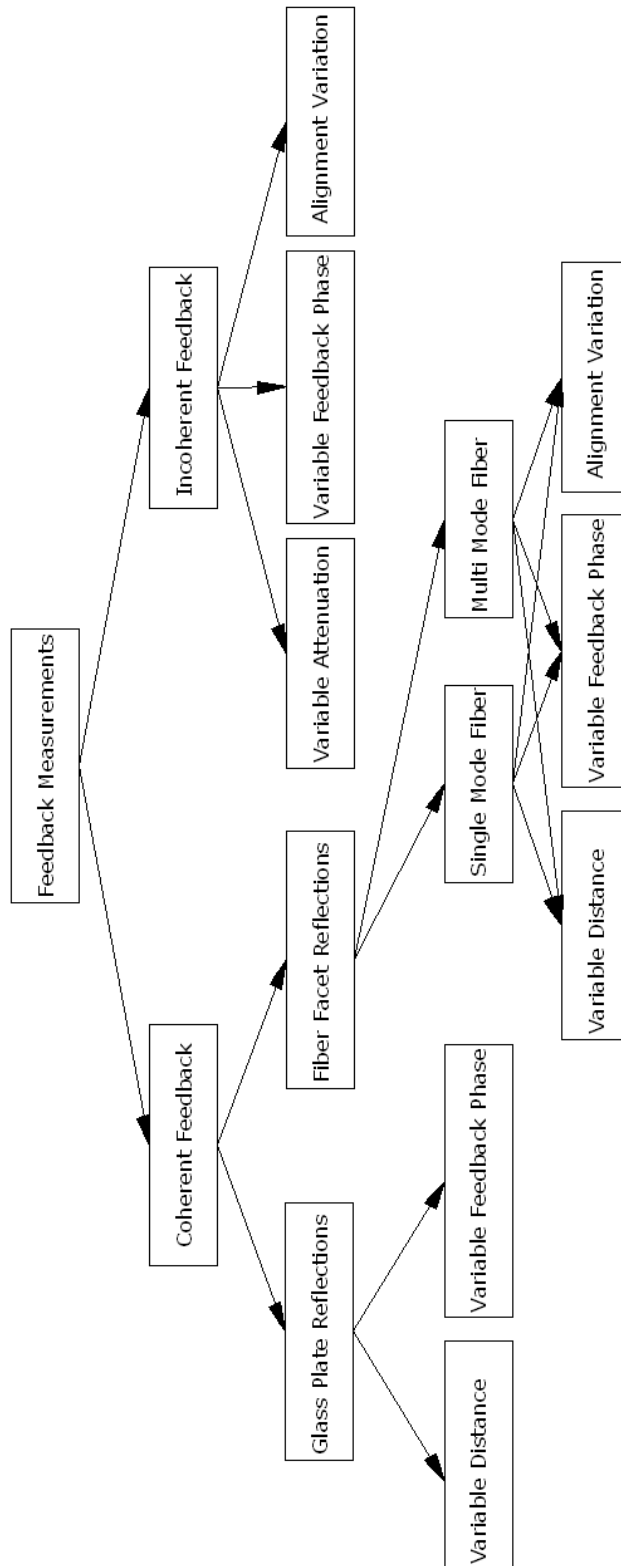
Figure 4.1: Overview about the different external feedback measurements carried out

(a) "Naked" VCSEL   (b) "Embedded" VCSEL   (c) "Waveguide" VCSEL
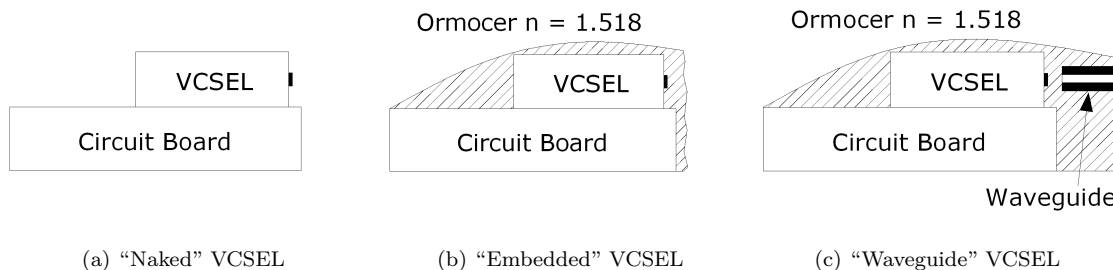
Figure 4.2: Devices under test used during the external feedback measurements

The coherent feedback measurements are further decomposed into ones where the reflections take place at a "infinitely extended" glass plate[1] and others where the feedback light comes from a fiber facet (either a single or a multi mode fiber)[2]. The distance between laser diode and reflector was varied on a large scale compared to the wavelength, influencing the strength of feedback, but also on a sub wavelength scale to change the feedback phase. Also the alignment of the feedback was varied too.

Most measurements were carried out with different devices under test. Those are shown in Figure 4.2 with their corresponding nomenclature that is used during the rest of the chapter. The first device under test (DUT) is the so called naked VCSEL. This is just the laser semiconductor bonded on a printed circuit board without embedding medium. The embedded VCSEL on the other hand is embedded in a ORMOCER® layer. This device under test was created by simply cutting off a waveguide board as close to the VCSEL as possible. The distance from the VCSEL surface to the rough ORMOCER® - air interface is about $50\,\mu m$. Therefore there might be a small part of the waveguide left, but during the measurements no influence was observable. The third device under test is the waveguide VCSEL. In this device a larger part of the waveguide is still left in front of the VCSEL. The distance that the laser beam travels through the polymer is about $150\,\mu m$ and the influence of the waveguide is clearly observable during the measurements. The interface between polymer layer and air is smooth in this case because it is polished (those boards were not self cut but provided in this way).

Figure 4.3 shows some combinations of devices under test and reflectors used during the coherent feedback measurements. The measurements were partly carried out with immersion oil between reflector and laser diode, to better match the situation on the waveguide boards and partly without oil. The oil has the same refractive index as the embedding polymer on the waveguide boards and is intended to emulate this polymer layer. Not only these shown combinations were used for measurements but also others. Still the nomenclature follows always the same rule: first DUT, second type of reflector and third immersion oil in use or not.

4.2   Incoherent Feedback

This section presents the measurement setup used to evaluate the influence of incoherent feedback on the output of a VCSEL diode, the results obtained with this setup, namely spectra and far field intensity distributions and an interpretation of those results. The device under test is a naked VCSEL from ULM Photonics driven under constant bias conditions at $I = 6\,mA$ (if not mentioned differently). The measurements were also carried out with another VCSEL from ULM Photonics of the same type and a VCSEL from Avalon Photonics. The results are comparable for all three lasers and are just presented for the first one.

The influence of the feedback phase and strength is investigated in detail. How the alignment of the feedback path influences the behavior is shown in Appendix B.5.

---

[1]the reflecting surface is large compared to the VCSEL beam width
[2]the reflecting surface is smaller than or equally large as the laser beam width
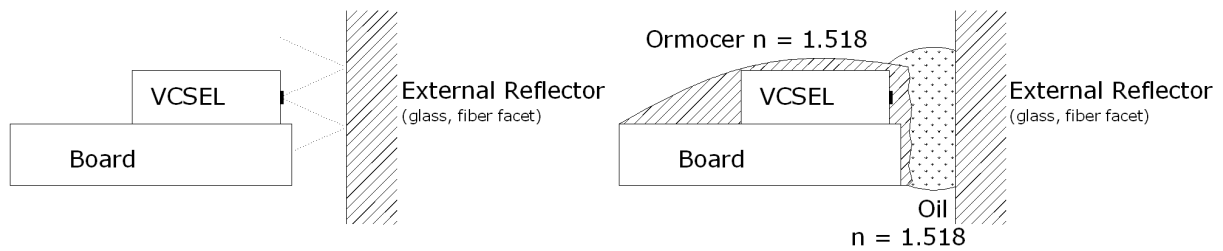
(a) "Naked" VCSEL, glass plate reflector, without immersion oil

(b) "Embedded" VCSEL, glass plate reflector, with immersion oil
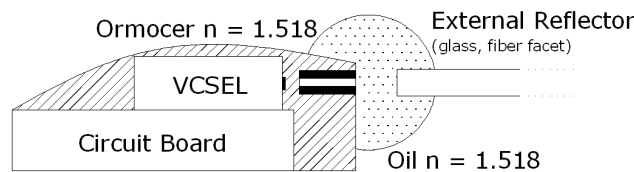
(c) "Waveguide" VCSEL, fiber facet reflector, with immersion oil

Figure 4.3: Devices under test in combination with different reflectors and surrounding media

4.2.1   Measurement Setup

Figure 4.4 shows the measurement setup used. The laser output beam is first collimated with a microscope objective (L3). The first beam splitter splits up the optical paths into the feedback path, where the beam gets focused onto a gold mirror mounted on a piezoelectric element (PZT) and a measurement path.

The feedback path also incorporates a variable attenuator which allows to vary the feedback strength. The PZT enables to shift the position of the mirror in the order of fractions of the wavelength λ so that the feedback phase can be varied. Shifting the position by $\frac{\lambda}{4}$ leads to a 180° phase shift, because the distance is traveled two times. The microscope objective L3 is aligned in such a way that the focus of the laser output beam lies exactly at the external reflector surface. The reflector plain is aligned to be perpendicular to the optical axis in order for the reflected beam to travel the same way back to the VCSEL. Ideally such alignment would lead to identical laser output and reflected beam except for the propagation direction. Therefore it can be assumed that the widths of both beams are identical which is important for the estimation of the feedback power ratio carried out in Appendix A.3.

The measurement path incorporates another beam splitter cube which directs part of the light through a variable attenuator (ATT2) to a CCD camera. The other part is focused via the microscope objective L2 onto a multi mode fiber (MMF) in order to feed the light into a spectrum analyzer (OSA). ATT2 is necessary to reduce the light intensity to values that do not drive the CCD camera into saturation. The lenses, beam
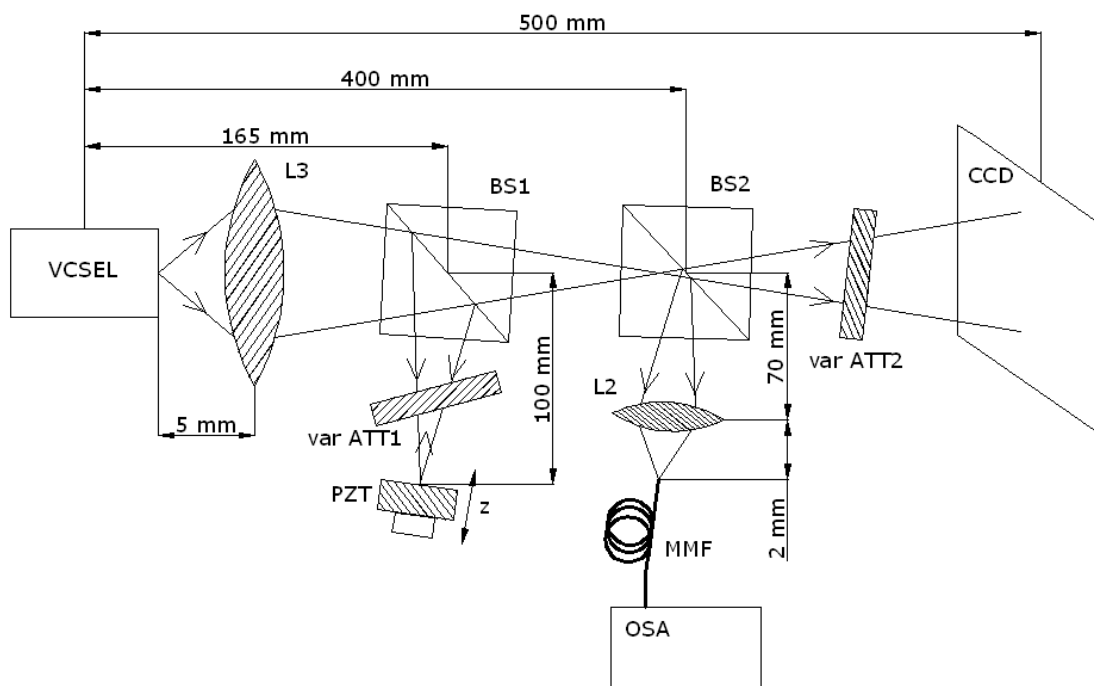
Figure 4.4: Setup used during the incoherent external feedback measurements

splitters, attenuators and measurement instruments are all slightly tilted with respect to the optical axis in order to avoid unwanted feedback from those elements.

The coarse alignment of the measurement setup is carried out with slices of fluorescent paper, which allows to make the beam at $850\,nm$ visible for the human eye. The fine tuning of the feedback path is then carried out with the help of the CCD camera. After the coarse alignment there was already a weak feedback effect observable at the CCD, in that the far field distribution changed when the feedback mirror was screened off. To get optimal alignment of the feedback mirror, in the sense of maximum feedback, the mirror azimuth was slightly tilted in both directions, until no feedback effect was noticeable anymore. The position exactly halfway between these two points was chosen as the optimal feedback alignment position. The same procedure was also carried out for the elevation. In this way a alignment with maximum feedback strength is achieved.

4.2.2 Influence of the Feedback Strength

With the variable attenuator in front of the reflector it is possible to change the strength of external feedback experienced by the laser diode. An estimation of the feedback power ratios achievable in such a way is given in Appendix A.3. The maximum possible feedback power ratio is $-13.5\,dB$, the minimum is $-72.7\,dB$, which already delivers the same results as screening the feedback path completely off.

Figure 4.5 shows how the spectrum changes when varying the feedback strength and keeping the alignment and feedback phase constant[3]. From left to right the external feedback power decreases. The figure shows

---

[3]Note that the scale of the feedback power ratio is not linear. The values in between the ones given on the scale were not
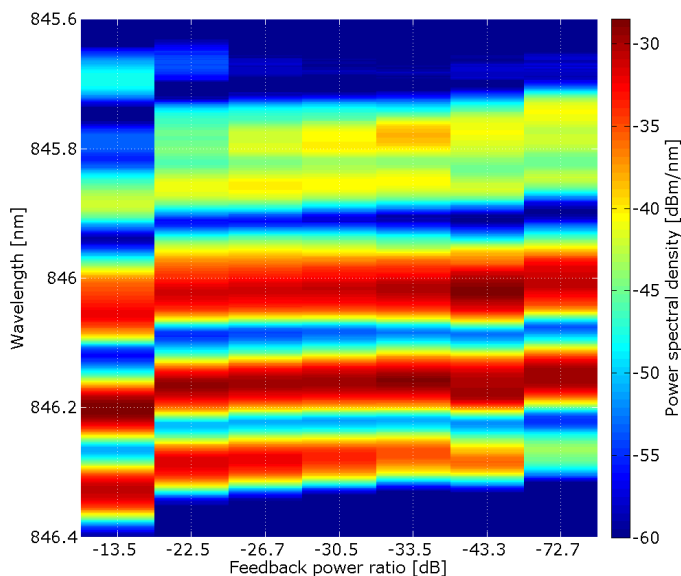
Figure 4.5: Change in VCSEL output spectrum with feedback strength at constant feedback phase

that there is a slight wavelength shift towards shorter wavelengths with decreasing feedback power. The slope of the shift is strongest at large feedback power. An oscillatory behavior is not observable. Figure 4.6 shows a comparison of the two spectra measured at maximum ($FPR = -13.5\,dB$) and minimum ($FPR = -72.7\,dB$) feedback power.

Mainly the lowest order mode (LP01) and the modes around $845.8\,nm$ are influenced by external feedback. An explanation could be that the external feedback path is aligned in such a way that most power couples into these modes. This behavior has also been observed with the Avalon laser diode.

Calculating the total powers in the two situations by integrating numerically over the spectrum delivers a slight increase in VCSEL output power by about 20% if external feedback is present. This increase may explain the wavelength shift, due to a corresponding increase in Joule losses (internal heating).

Corresponding to the spectral changes there are also changes in the far field intensity distribution, which are shown in Figures 4.7. This figure suggests that the mode at largest wavelength is really LP01 because at strong external feedback, when this mode is enhanced, the intensity distribution has a maximum in the center region which is produced by the Gaussian beam profile of LP01. When there is almost no external feedback the second spectral line is dominating which might be identified as LP11, due to the ring structure (see Section 3.1.4 for details, the VCSEL used there is of the same type but not the same exemplar). The feedback strength has a strong influence on the intensity distribution, which may also translate into a total power variation at the output of a waveguide (due to the modal filtering nature of such a device, see Section 4.3.2). The intensity profile changes continually between these two extrema without showing any oscillatory behavior. So the results presented here can not explain the power oscillations described in Chapter 1.

4.2.3   Influence of the Feedback Phase

By applying a voltage to the piezoelectric element it is possible to shift the position of the external reflector ($z_{0r} = 265\,mm$, according to Figure 4.4) in the order of fractions of the wavelength (Δz_r) along the z

---

measured and can not be read out of the figure
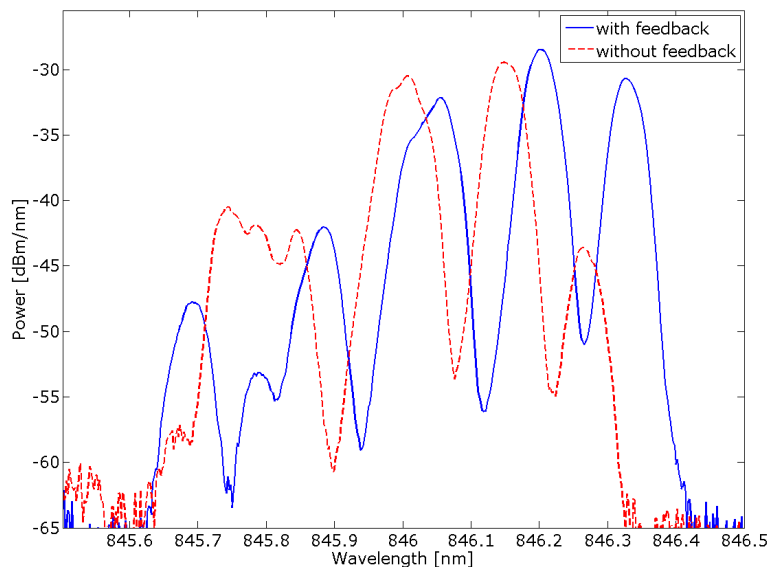
Figure 4.6: Comparison of measured VCSEL output spectra at maximum and minimum feedback power

direction. This shift in position translates directly into a corresponding shift in feedback phase according to

$$\Delta\Phi_r = 2k_{ext}\Delta z_r. \tag{4.1}$$

Varying the position by $\frac{\lambda}{4}$ therefore allows to change the feedback phase by π. This was done during the measurements to find out whether there is an influence of the feedback phase or not. The same measurement was carried out at different feedback strength to see whether some kind of feedback regimes are observable. According to Section 2.2.2 distinct regimes of feedback strength exist in single mode laser devices but those are generally not observable in multi mode devices.

Figure 4.8 shows spectra measured at $FPR = -43.3\,dB$ and two different feedback phases.   The figure clearly shows that the influence of the feedback phase is negligible as expected. As described in Section 2.2.1 this is because the distance to the reflector is larger than the coherence distance of the device. Still there seems to be some degree of coherence left for the spectral line at the largest wavelength, as it is influenced

(a) $FPR = -13.5\,dB$

(b) $FPR = -72.7\,dB$
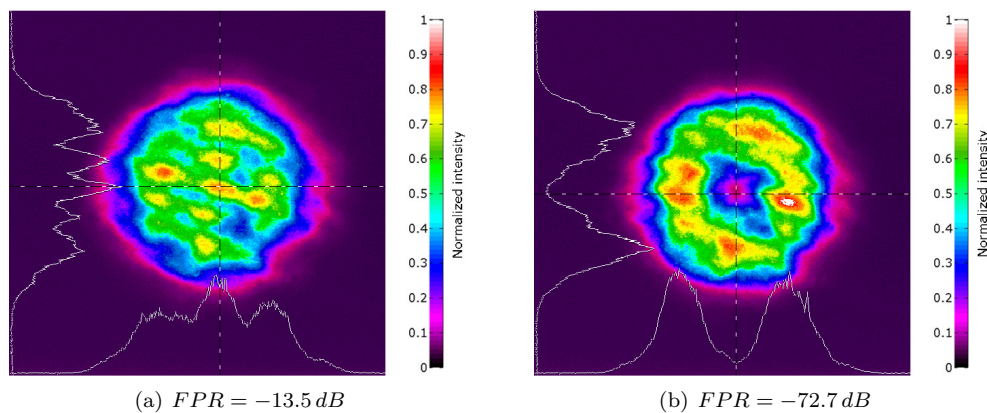
Figure 4.7: Measured far field intensity distributions of a VCSEL subject to incoherent external feedback

41
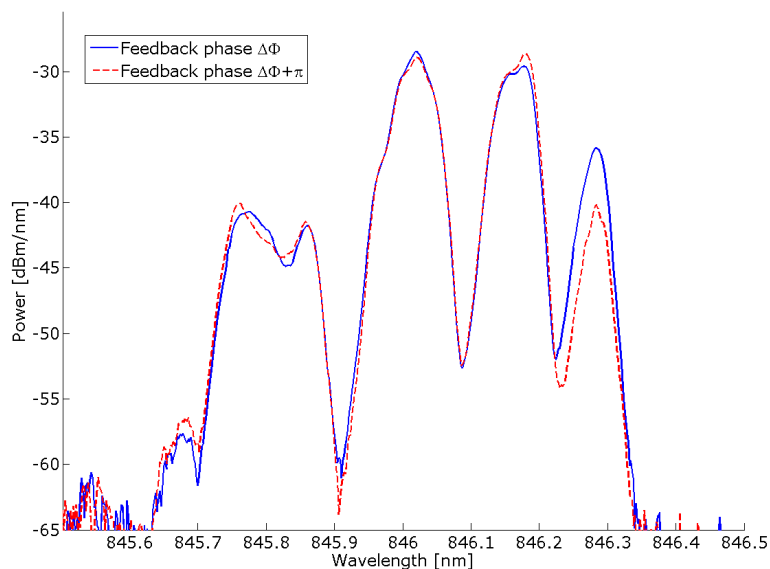
Figure 4.8: Comparison of measured VCSEL output spectra at two different feedback phases

slightly by the phase. The total output power of the VCSEL does not vary with feedback phase. At all other feedback power ratios the influence of the feedback phase is comparable or even weaker than that presented here. Also there are no feedback regimes observable, but this would only be possible if the feedback was coherent. Figure 4.9 shows the corresponding influence on the far field intensity distribution which is hardly visible.

4.2.4 Conclusions

It has been shown that incoherent feedback can strongly influence the spectrum and intensity distribution of the light emitted by the laser diode, if the feedback strength is rather large ($> -30\,dB$). Which modes are being influenced depends on the spatial overlap between the feedback light and the laser internal transversal modes, but also gain competition effects come into play (see Appendix B.5). The influence of the feedback

(a) External feedback phase $\Delta\Phi$
(b) External feedback phase $\Delta\Phi + \pi$
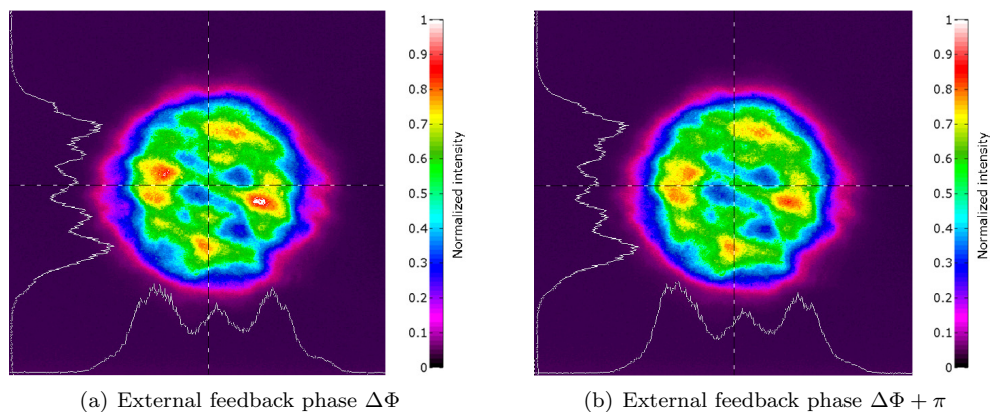
Figure 4.9: Measured far field intensity distributions of a VCSEL subject to incoherent external feedback

phase is negligible and therefore there is no periodic or oscillatory behavior observable in the VCSEL output. So it can be concluded that incoherent feedback can not be used as an explanation for the oscillations over temperature described in Chapter 1.

4.3 Coherent Feedback

The measurements carried out in this section investigate the behavior of a VCSEL diode under feedback from a reflector at a distance smaller than the coherence length of the device. It is a logical step to observe coherent feedback as the last section has shown that external feedback in general has a strong influence on the laser diode output, but incoherent feedback can not explain a periodic behavior.

This section will not use the feedback power ratio anymore to characterize the feedback strength due to three reasons

1. For a meaningful definition of the feedback power ratio it would be necessary to define an area over which the power is calculated. Choosing the total VCSEL diameter as in Appendix A.2 is a somewhat arbitrary definition that just allows a coarse quantification. This is not a problem in the incoherent measurement setup as the area of the emitted and reflected beam are assumed to be equal.

2. Appendix B.4 shows that the efficiency with which the different transversal modes of a beam reflected at a plain surface couple back into the laser cavity is mode dependent. But this also involves a modal dependency of the *FPR*.

3. Quantifying the feedback strength from a fiber facet at some distance would necessitate solving Maxwell's equations for the boundary condition problem at hand.

As there is no space for a variable attenuator between VCSEL and external reflector the only possibility to change the feedback strength is via the distance. That is the reason why this distance is used as the feedback strength quantifying attribute, although it has a different influence onto the individual transversal VCSEL modes (see Appendix B.4) mainly due to different divergences of the modes. Nevertheless Appendix A.2 delivers a rough estimate of the feedback power ratios encountered in Section 4.3.1.

In a first step a glass plate causes the external reflections. Section 4.3.1 shows that feedback from such a "infinitely" extended plain causes strong variations in the VCSEL spectrum and intensity distribution with feedback phase, if the distance to the reflector is small and therefore the reflections are strong. Those variations are periodic in the feedback phase, as explained in Section 2.2.1. If there is a waveguide in front of the VCSEL (see Figure 4.2 (c)), which guides the reflected light back to the laser, the feedback sensitivity is strongly increased. The variations in the VCSEL output do not affect the total output power, which is the reason why a fiber is then used as the external reflector and the output of the fiber is observed. Section 4.3.2 shows that fibers, especially single mode fibers, can translate the variations in the VCSEL intensity distribution into variations in the fiber output power. This can be explained by varying fiber coupled power. The effect is remarkably pronounced if the transversal alignment between the fiber and the VCSEL is not optimal, in the sense that the VCSEL does not irradiate the fiber centrally.

If not mentioned otherwise the measurements are again carried out with the ULM multi mode $850\,nm$ VCSEL already used in previous sections.

4.3.1 Glass Plate Reflections

This section investigates the influence of external reflections from a large[4] glass plate on the output of a VCSEL. It is observed how the laser output spectrum, far field intensity distribution and total power varies with variable feedback phase at different distances z_{0r} between VCSEL and external reflector. Different devices under test are investigated. The VCSEL from ULM Photonics is driven at a constant bias current of $6\,mA$.

---

[4]large compared to the beam width

Before starting with a description of the measurement results, obtained with different devices under test, the measurement setup used is explained. Three different devices under test are used for this measurements

- DUT1: Naked VCSEL, glass plate reflector, without immersion oil

    This DUT is used to investigate the general behavior of a VCSEL subject to coherent external feedback.

- DUT2: Naked VCSEL, glass plate reflector, with immersion oil

    To better match the situation on the waveguide boards immersion oil is used to emulate the ORMOCER® layer that normally covers the boards. Therefore immersion oil with the same refractive index of $n_s = 1.518$ as ORMOCER® is used. Due to a decreasing refractive index step at the external reflector, this situation reduces the feedback strength. This DUT is used to emulate the behavior of possible reflections at the beginning of the waveguide on the opto-electronic boards, where the refractive index step is even much weaker[5], but therefore the distance is smaller.

- DUT3: Waveguide VCSEL, glass plate reflector, with immersion oil

    On the opto-electronic waveguide boards there is the possibility that reflections occur somewhere along or at the end of the waveguide. This DUT is used to emulate such a situation.

4.3.1.1 Measurement Setup

The setup used to measure the influence of coherent reflections is shown in Figure 4.10. As mentioned in
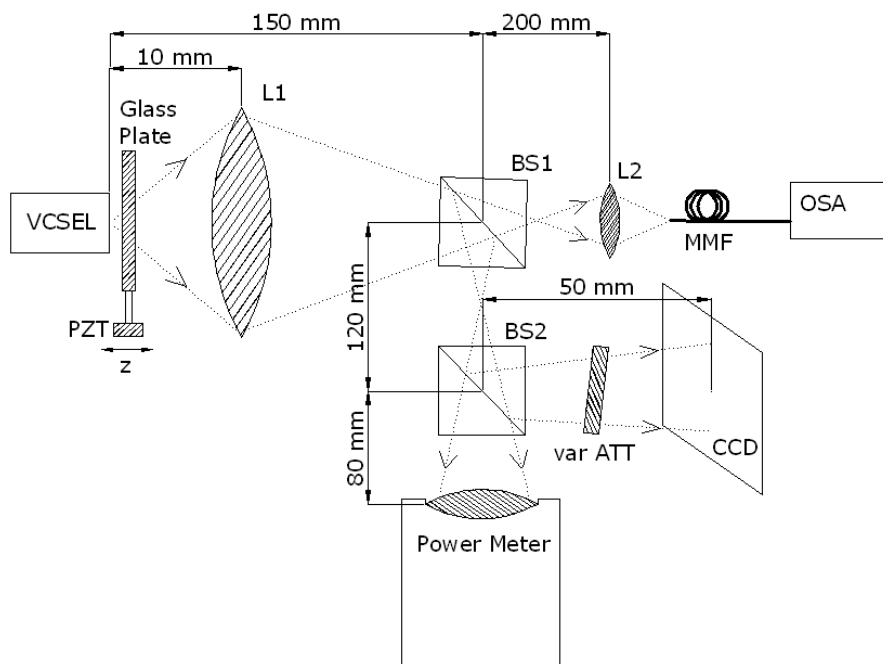

Figure 4.10: Setup used during the coherent external feedback measurements with the glass plate reflector

---

[5]Remember, the difference in refractive index between core and cladding is just 0.004

Section 2.2.1 the typical coherence length of a multi mode VCSEL is in the order of millimeters. But such a large distance to the reflector can not be used in order to keep the feedback strength at reasonably high values. Therefore the distance to the external reflector is just in the order of tens to hundreds of micrometers during the measurements.

The external reflections are caused by the glass plate directly in front of the laser diode. To be able to change the feedback phase the plate is mounted on a piezoelectric element. The phase shift caused by a change in reflector position is given by Equation (4.1). The glass has a refractive index of $n_r = 1.5$ and a thickness of $1.5\,mm$. The reflectivity of the external reflector can be calculated by following equation

$$R_{ext} = \left(\frac{n_r - n_s}{n_r + n_s}\right)^2, \tag{4.2}$$

where n_s is the refractive index of the surrounding medium. To adjust the distance to the VCSEL on a larger scale (tens of micrometers) a mechanical translation stage is used. The distance is visually measured with a stereo microscope. The displacement caused by varying the voltage applied to the PZT is known, because the PZT was gauged before with the help of a Michelson interferometer.

The larger part of the light is passed through the glass plate and collimated by the microscope objective $L1$. Beam splitter cubes are used to split the beam into parts that are gathered by the different measurement instruments, the optical spectrum analyzer, the CCD camera and the power meter.

Device under Test 1: naked VCSEL, glass plate reflector, without immersion oil

As no immersion oil is in use between VCSEL and external reflector the surrounding medium is air, which has a refractive index of $n_s = 1$ and the corresponding external reflectivity is about 4%. The distance between VCSEL and external reflector is varied from $40\,\mu m$ to $260\,\mu m$ and at every distance the influence of the feedback phase on the laser output is observed.

Figure 4.11 shows spectra measured at the two distance extrema. The difference between the red dashed and blue solid spectra is caused by a feedback phase difference of π. For the dashed spectra the phase is adjusted to deliver maximum VCSEL output power (observed with the power meter) and for the solid spectra the power is minimal. But the **maximum power difference with feedback phase** is just about **0.3 dB** at $z_{0r} = 40\,\mu m$. At larger distances it is even smaller. As this difference is rather low and the phase adjustment correspondingly inaccurate it was additionally carried out by taking the change in spectrum into account. Maximum output power is achieved, when the second spectral line (corresponding to LP11, see 3.1.4) is maximized and the power is minimal when this line is minimal too.

Comparing figures (a) and (b) shows that the influence of feedback phase is very strong for small distance to the reflector and correspondingly large feedback strength. All spectral lines are influenced by the external feedback phase. On the other hand at the large distance there is almost no influence observable anymore, the feedback strength is just to weak to appreciably influence the reflectivity of the top DBR according to Equation (2.23).

Far field intensity distributions measured at a reflector distance of $40\,\mu m$ are given in Figure 4.12. Corresponding to the strong variations in the spectrum with feedback phase, also the intensity distribution changes drastically. Looking at (b) allows the statement that the dominating second spectral line in the corresponding spectrum (the dashed one) corresponds to one helical polarity of the LP11 mode, because the intensity distribution shows just one radial maximum ($p = 1$) and there is one zero in the azimuth range $0 \leq \Phi < 180°$ (for details see 3.1.4).

The intensity profile shown in (c) on the other hand is clearly dominated by a Gaussian profile and therefore corresponds to LP01. At this feedback phase the first spectral line is dominating (the spectrum is not shown) which allows to match this line to LP01.

Although the variation in total power is maximum between (a) and (b) the intensity profiles are not so strongly distinct. The distribution shown in (a) is dominated by the second and third spectral lines. It would suggest that the third spectral line corresponds to LP21, as there are two minima in $0 \leq \Phi < 180°$, which is in contradiction to the statement in Section 3.1.4. But the problem is the same as there, the spectral line is too less dominating to allow a reliable statement.
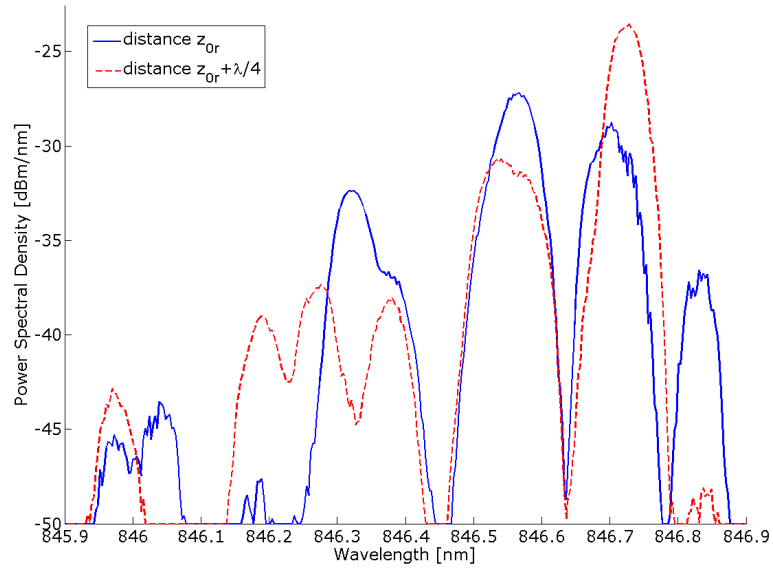
(a) External reflector distance $z_{0r} = 40\,\mu m$
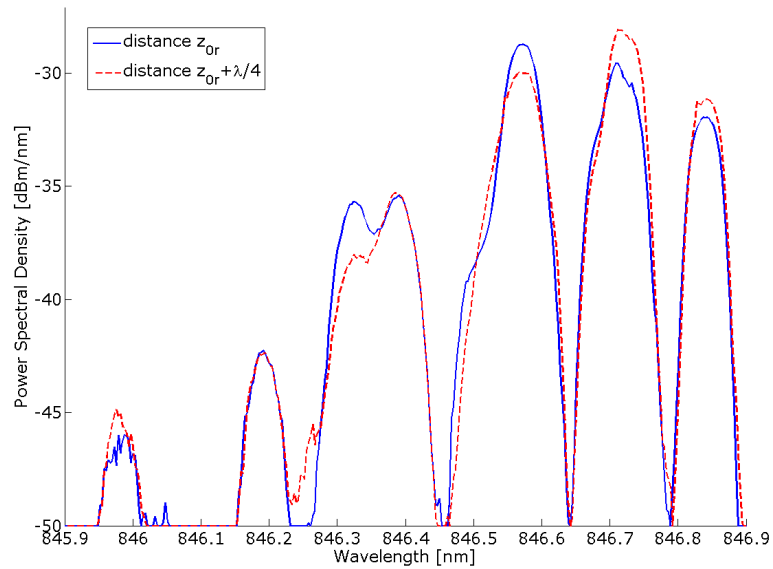
(b) External reflector distance $z_{0r} = 260\,\mu m$

Figure 4.11: Measured spectra of a VCSEL subject to coherent external feedback

(a) Reflector distance z_{0r}

(b) Reflector distance $z_{0r} + \frac{\lambda}{4}$

(c) Reflector distance in between (a) and (b)

Figure 4.12: Measured far field intensity distributions of a VCSEL subject to coherent feedback at a reflector distance of $z_{0r} = 40\mu m$

These observations clearly show that the external feedback phase has a strong influence on the modal power distribution. But the feedback phase is almost the same for all modes, as their wavelength difference is just fractions of nanometers large. The feedback phase difference between the spectral line at about $\lambda_1 = 846.8\,nm$ and the one at $\lambda_2 = 846\,nm$ is, for a reflector distance of $z_{0r} = 40\,\mu m$, just

$$\Phi_{\lambda_2} - \Phi_{\lambda_1} = \frac{2\pi}{\lambda_2} \cdot 2z_{0r} - \frac{2\pi}{\lambda_1} \cdot 2z_{0r} \approx 30° \tag{4.3}$$

This can not explain why one mode is enhanced and the neighboring one is detracted. Gain competition effects, as described in 2.1.2, come into play here and lead to such strong variations in modal power distribution.

With increasing distance the variations in the far field intensity distribution are becoming weaker in accordance to the variations in the spectra (at $z_{0r} = 260\,\mu m$ no feedback phase influence is observable anymore). Figure 4.13 shows far field intensity distributions measured at a reflector distance of $z_{0r} = 140\,\mu m$. These will be needed later for comparison.

Device under Test 2: naked VCSEL, glass plate reflector, with immersion oil

The situation changes drastically when immersion oil is used in between laser diode and the external reflector. The lower refractive index step between the glass plate and the ORMOCER® layer, compared to the last measurement, reduces the external reflectivity to about

$$R_{ext} = \left(\frac{1.5 - 1.518}{1.5 + 1.518}\right)^2 = 0.0035\%.$$

(a) Reflector distance z_{0r} (b) Reflector distance $z_{0r} + \frac{\lambda}{4}$

Figure 4.13: Measured far field intensity distributions of a VCSEL subject to coherent feedback at a reflector distance of $z_{0r} = 140\mu m$

This entails a reduction of the FPR of about $30\,dB$. When using the approximation in Appendix A.2 this means that the feedback power ratio at a distance of $z_{0r} = 40\,\mu m$ is now about $FPR = -54dB$ which is more than $15\,dB$ less than the one at $z_{0r} = 260\,\mu m$ if no oil is in use.
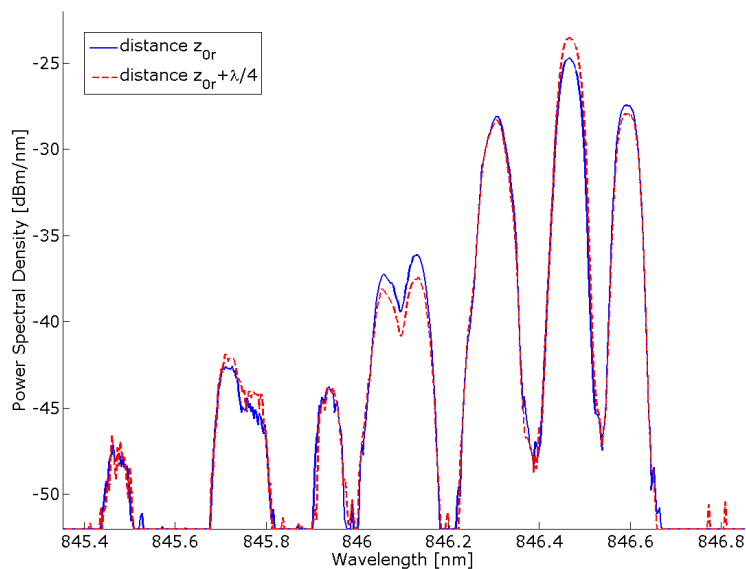
Figure 4.14: Comparison of measured VCSEL output spectra at two different feedback phases and external reflector distance $z_{0r} = 40\,\mu m$

Estimating the feedback power ratio on the waveguide boards in the same way, by assuming reflections at the beginning of the waveguide in a distance of $z_{0r} = 10\,\mu m$ to the VCSEL and a refractive index step of $n_g - n_c = 1.518 - 1.514 = 0.004$ delivers a value of $FPR = -60dB$ which is even less.

According to these observations the measured influence of reflections from a glass plate when using immersion oil is really negligible, as Figure 4.14 shows. The corresponding far field intensity distributions are given in Figure 4.15. The spectra as well as the intensity distributions show that LP11 is slightly increased in the case $z_{0r} + \frac{\lambda}{4}$ compared to z_{0r}.

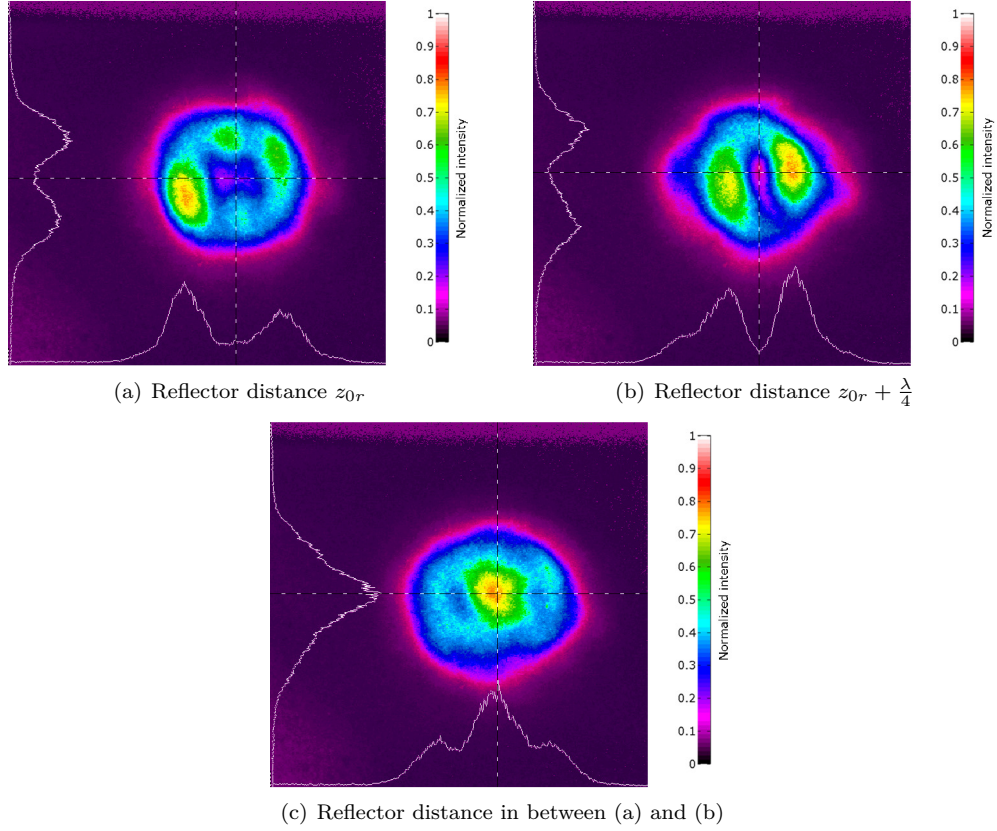(a) Reflector distance z_{0r} (b) Reflector distance $z_{0r} + \frac{\lambda}{4}$
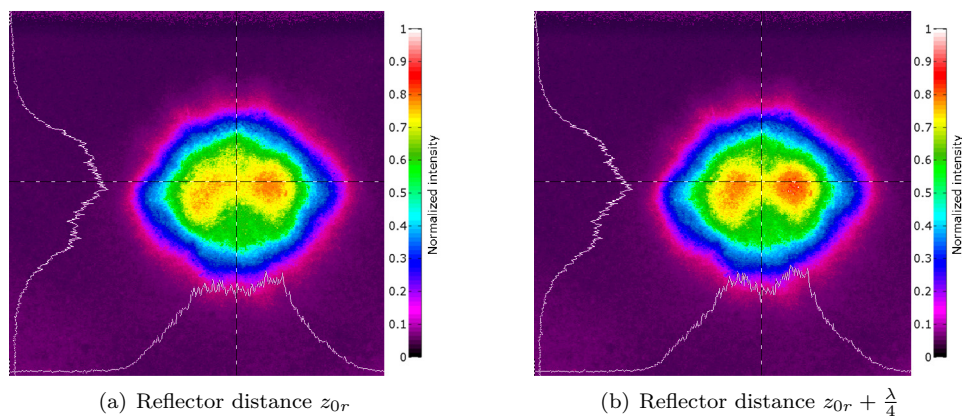
Figure 4.15: Measured far field intensity distributions of a VCSEL subject to coherent feedback at a reflector distance of $z_{0r} = 40 \mu m$

The change in total VCSEL output power is negligible as well. Increasing the distance to the reflector does not show any influence, as the reflections are already too weak. It is not possible to get closer than $40\,\mu m$ to the VCSEL, because then the glass plate hits the bond wire of the laser diode.

Device under Test 3: waveguide VCSEL, glass plate reflector, with immersion oil

These measurements are carried out to find out how a waveguide in front of the VCSEL influences the external feedback sensitivity of the laser diode. The laser in use is a Avalon multi mode VCSEL.

As already mentioned above the waveguide has a length of about $150\,\mu m$, so that is the minimum distance between laser diode and reflector. The measurement is carried out with immersion oil in use because otherwise the beam profile is distorted by the ORMOCER® - air interface, although it is polished. Figure 4.16 shows measured far field intensity distributions at a reflector distance $z_{0r} = 150\,\mu m$ and variable feedback phase. Again the feedback phase is adjusted to achieve maximum and minimum output power although the difference is just fractions of a decibel. Figure 4.17[6] shows the same results for a distance of $z_{0r} = 750\,\mu m$. During this measurement the reflector was a $150\,\mu m$ thin glass plate.

(a) Reflector distance z_{0r} (b) Reflector distance $z_{0r} + \frac{\lambda}{4}$
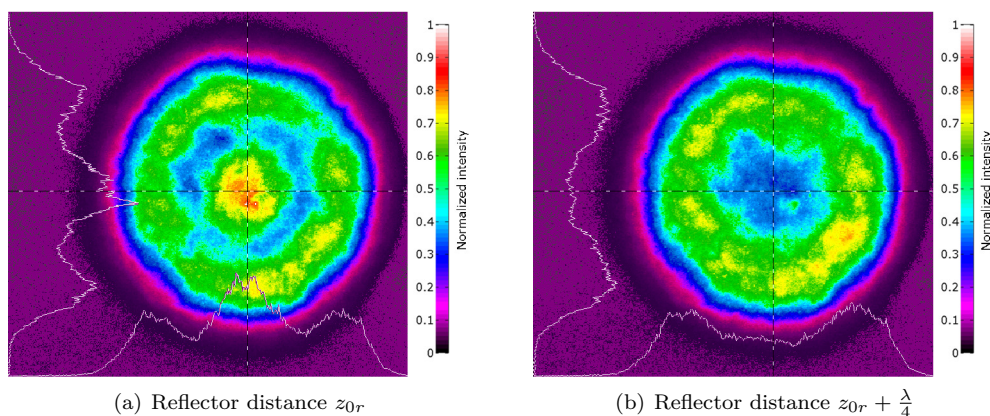
Figure 4.16: Measured far field intensity distributions of a VCSEL with waveguide subject to coherent feedback at a reflector distance of $z_{0r} = 150\,\mu m$

---

[6]The reason why the beam widths of figures 4.16 and 4.17 are so different is that the length of the distance which the light has to travel through the oil is increased

Comparing Figure 4.16 with Figure 4.13 shows that the behavior is quite similar, although immersion oil is in use this time and the laser diode is from Avalon and not from ULM. At the phase corresponding to the smaller VCSEL output power (Figure 4.16 (a)) LP01 is enhanced and at the other phase (Figure 4.16 (b)) the intensity distribution is dominated by LP11.

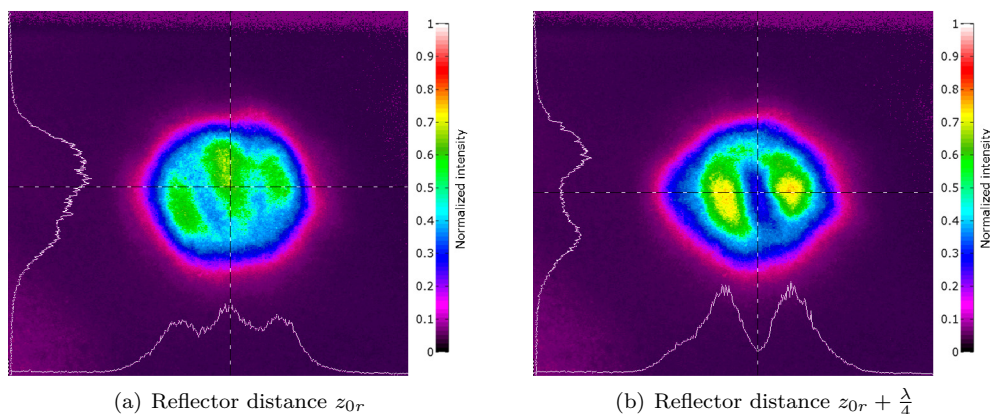(a) Reflector distance z_{0r} (b) Reflector distance $z_{0r} + \frac{\lambda}{4}$
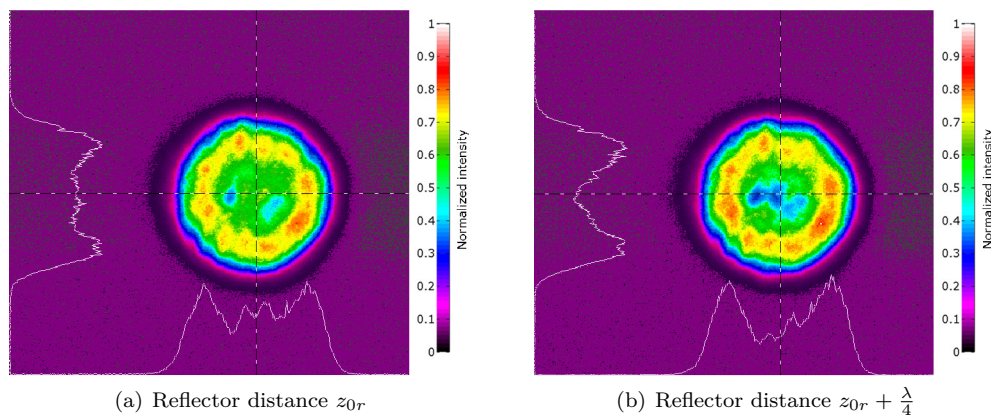
Figure 4.17: Measured far field intensity distributions of a VCSEL with waveguide subject to coherent feedback at a reflector distance of $z_{0r} = 750\,\mu m$

Figure 4.17 shows that even at a distance of $z_{0r} = 750\,\mu m$ the same behavior is still recognizable, although it is weaker. This shows that the waveguide in front of the VCSEL enhances the feedback sensitivity drastically. The explanation is quite straightforward, the waveguide gathers feedback light over a much larger area[7] and guides it back to the laser.

The measurement has also been carried out with the embedded VCSEL. There the influence of the waveguide is not recognizable and no feedback influence is observable.

Also a $2.7\,mm$ thick glass plate has been used for the measurement, showing reduced influence of the feedback phase. This suggests that the dominating feedback source is the backside of the thin glass plate because on this site no immersion oil is used and therefore the reflections are stronger due to a higher refractive index step.

4.3.1.5 Conclusions

Following observations have been made during the measurements with a glass plate reflector at a distance smaller than the coherence distance of the VCSEL.

- If the distance to the external reflector is small, the feedback phase strongly influences the modal power distribution. At distances larger than about $200\,\mu m$ the feedback phase influence gets negligible, in that the far field distribution does not change visibly anymore (such changes will be important for the further argumentation in Section 4.3.2). This corresponds to feedback power ratios smaller than about $-35\,dB$ according to the estimation in Appendix A.2.

- Using immersion oil to emulate the ORMOCER® layer (like it is present on the opto-electronic PCBs) reduces the external reflections so strong that even at a distance of $10\,\mu m$ between VCSEL and reflector the feedback strength would be too low to influence the VCSEL.

- A waveguide in front of the VCSEL can drastically enhance the feedback sensitivity of the device, as the area over which the feedback light is gathered is increased[8]. Also the distance between end of

[7]the diameter of the seven core waveguide is about $70\,\mu m$ compared to $10\,\mu m$ VCSEL diameter

[8]of course only if the waveguide area is larger than the area of the VCSEL, as it is the case for the seven core waveguide in Figure 1.2

the waveguide and external reflector is decisive in estimating the feedback strength and not the total distance to the laser diode because the waveguide guides the light back to the laser diode.

- The strong changes in modal power distribution can not only be assigned to the change in effective modal VCSEL mirror reflectivities (see Equation (2.23)), but are the product of gain competition effects as well.

- The variations are periodic in the feedback phase and therefore in the external reflector distance, with a period of $\frac{\lambda}{2}$.

- There is just negligible influence on the total VCSEL output power, the variation with feedback phase is smaller than $0.3\,dB$, but it is periodic. The power variations in a specific mode are compensated by corresponding opposed power variations in other modes due to gain competition effects.

Until now it is clear that neither incoherent nor coherent feedback alone can explain the observed power oscillations over temperature of the opto-electronic waveguide boards. But in contrast to incoherent feedback coherent reflections at least feature periodic behavior. It is only necessary to translate the modal power variations into total output variations with the help of a modal filtering element. The next section will show that fibers can act as such mode filters.

4.3.2   Fiber Facet Reflections

The measurements described below try to emulate the complete opto-electronic waveguide board with a discrete setup, by replacing the seven core waveguide with a simple standard multi mode (core diameter $50\,\mu m$) or single mode (core diameter $9\,\mu m$) glass fiber. External feedback is given by reflections from the fiber facet, the feedback phase is adjustable by slightly shifting the fiber position along the optical axis and it is even possible to reproduce the tolerances[9] in transversal alignment between the optical axes of the VCSEL and the fiber by transversally (perpendicular to the optical axis) shifting the fiber position.

4.3.2.1   Motivating Idea

The reason for these measurements is to show that fibers really act as modal filters and are therefore able to transform variations in the modal power distribution into variations in the total fiber output power, as already mentioned further above. The explanation for this effect is simply that the fiber coupled power varies with the transversal field distribution irradiating the fiber tip. This idea is visualized in Figure 4.18, the black circle represents the fiber core, the far field distributions are the ones measured in Section 4.3.1 Figure 4.12[10].

  Intuitively this figure allows the statement that more power will couple into the fiber in the situation shown in (b), simply because the intensity irradiating the fiber is higher. For an exact mathematical argumentation it would be necessary to calculate coupling efficiencies between the given laser field and all possible fiber modes at the given wavelength (using a similar formula as given in Appendix B.4 Equation (B.2)) and summing over all modes.

  The figure suggests that this argumentation only holds if the transversal alignment between fiber and laser diode is not optimal, in the sense that the two optical axes do not coincide. The results below will show that this is really the case. If the transversal alignment is optimized there still is a modal filtering effect, but it is in general much weaker than if the alignment is sub optimal. But there also exist alignments, where the VCSEL irradiates the fiber non centrally and nonetheless the dependency on feedback phase completely vanishes.

---

[9]those tolerances are in the order of $15\,\mu m$ according to the manufacturer

[10]note that the fiber is in reality irradiated by near field distributions which have not been measured and look different; but nevertheless the near fields corresponding to the two far fields will be clearly distinct

(a) Far field distribution dominated by LP01   (b) Far field distribution dominated by LP11
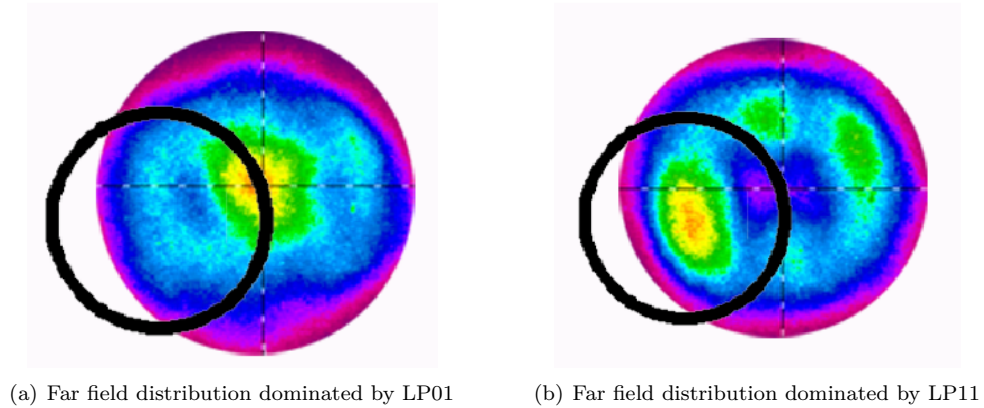
Figure 4.18: Schematic depection of the idea explaining variations in fiber coupled power with changes in the transversal mode distribution

4.3.2.2   Multi Mode Fiber

Measurement Setup

Figure 4.20 shows the measurement setup applied. A multi mode fiber[11] (MMF) is mounted on a piezo-electrically and mechanically adjustable 3D translation stage. The VCSEL beam couples into this fiber and part of the beam is reflected at the fiber facet and couples back into the laser cavity to cause the coherent external feedback. At the other end of the fiber the light is coupled into the same free space measurement setup that was already used in Section 4.3.1. The only function of this part is to feed the light into the three measurement instruments, the OSA, the CCD and the power meter.
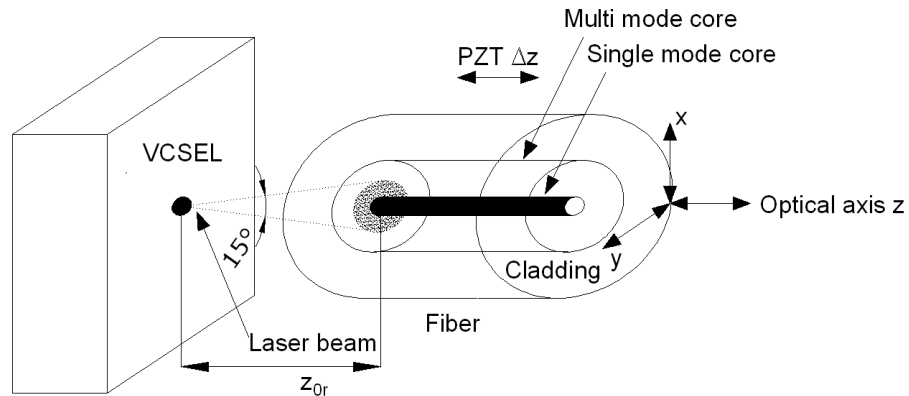
Figure 4.19: Detail of the fiber coupling situation encountered in the single mode and multi mode fiber case

---

[11]a standard datacom fiber with a core diameter of $50\,\mu m$ was used
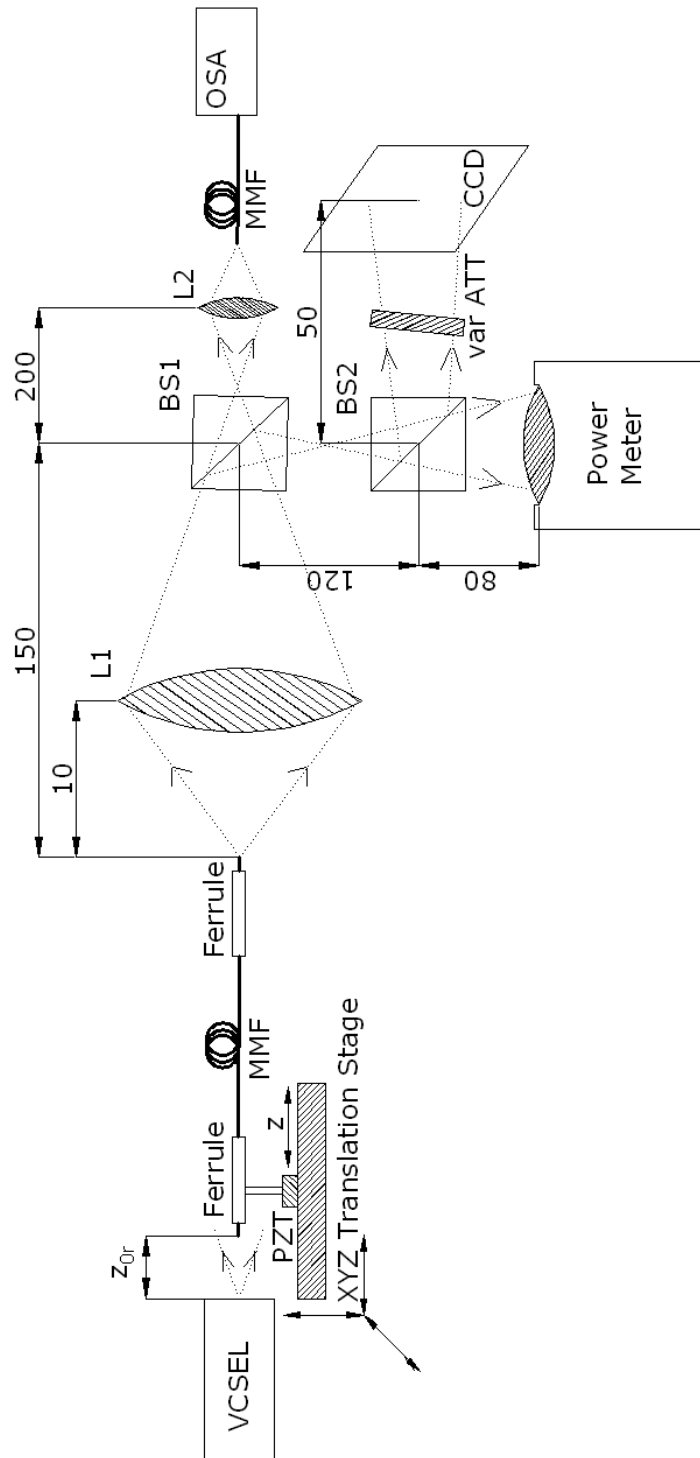
Figure 4.20: Setup used during the coherent external feedback measurements with the multi mode fiber

At the same distance the feedback from the fiber tip is smaller than the one from the glass plate, as the reflecting surface is much smaller. But to compensate for this the fiber allows getting closer to the VCSEL surface because it can be shifted alongside the bond wire.

The translation stage allows varying the distance between laser surface and reflector along the optical axis z on a large scale (compared to the wavelength) mechanically, to change the feedback strength, but also on a sub wavelength scale piezoelectrically to adjust the feedback phase. But it also allows variation of the transversal alignment. The situation is shown in detail in Figure 4.19. The figure shows that the spatial resolution of the single mode fiber is larger than that of the multi mode fiber.

A difficult part in the adjustment of the measurement setup is getting the optical axes of the VCSEL and the fiber as parallel as possible. This is achieved by first maximizing the fiber coupled power at a large distance to the VCSEL ($200\,\mu m$) by accordingly adjusting the transversal fiber alignment. This maximum is achieved when the laser irradiates the fiber centrally. Afterwards the optical axis elevation and azimuth angle are varied (while keeping the fiber tip at the same position) such that the variations in fiber coupled power with feedback phase are maximized. These variations are maximized when the feedback strength is maximized, which is the case when the reflections travel back along the optical axis. This is achieved when the reflecting surface is perpendicular to the optical axis. That this alignment procedure works quite good can be stated because it was just necessary to correct the transversal alignment in the order of fractions of the wavelength to keep the fiber coupled power at a maximum, when the distance was varied by $50\,\mu m$.

The measurements were carried out with two different devices under test.

- DUT1: naked VCSEL, fiber facet reflector, without immersion oil

  This combination is used to investigate the general behavior of external feedback combined with fiber coupling.

- DUT2: naked VCSEL, fiber facet reflector, with immersion oil

  This device under test is again used to better emulate the situation of external feedback from the seven core waveguide in the opto-electronic boards.

The situation with a waveguide in front of the VCSEL is not investigated, as it is already clear that it enhances the feedback sensitivity, which is not different in this case. Measurements with an embedded VCSEL have been carried out but are not reported here because there the distance between reflector and laser is inherently large (as there is a ORMOCER$^{\circledR}$ layer in front of the laser diode) and therefore the feedback is weak. Additionally it is necessary to use immersion oil to smooth the rough ORMOCER$^{\circledR}$ - air interface, which further weakens the reflections so that no external feedback influence is observable.

The measurements described below are carried out at ideal transversal alignment between fiber and VCSEL, meaning that the laser irradiates the fiber centrally.

Device under Test 1: naked VCSEL, fiber facet reflector, without immersion oil

The ultimate figure of merit for these fiber coupling measurements is the variation in fiber output power that is achievable by varying the feedback phase. Therefore Figure 4.21 depicts the maximum power P_{max} achievable at different VCSEL - reflector distances z_{0r} (the line labeled with P_{max}) as well as the minimum power P_{min}, attained by correspondingly adjusting the feedback phase. Also the ratio of these two values in decibel is shown, called the Power ratio PR and given by

$$PR = 10\log_{10}\frac{P_{max}}{P_{min}}. \tag{4.4}$$

The two power curves show expected behavior for distances larger than about $40\,\mu m$, the fiber coupled power decreases, as the intensity irradiating the fiber tip decreases due to the beam divergence. The curve shape below this distance might be somewhat unexpected, as the coupled power decreases with decreasing distance. There is a simple explanation for this behavior shown in Figure 4.22. At small distances the fiber tip hits the bond wire and gets slightly bended away. Therefore the optical axes of fiber and VCSEL do not overlap anymore and the coupled power decreases.

The power ratio curve shows that the maximum power difference attainable is just $0.7\,dB$, reached at a distance of $10\,\mu m$. This corresponds to about 20% power variation, which is much too low to explain the power oscillations observed on the waveguide boards which are about 400%.
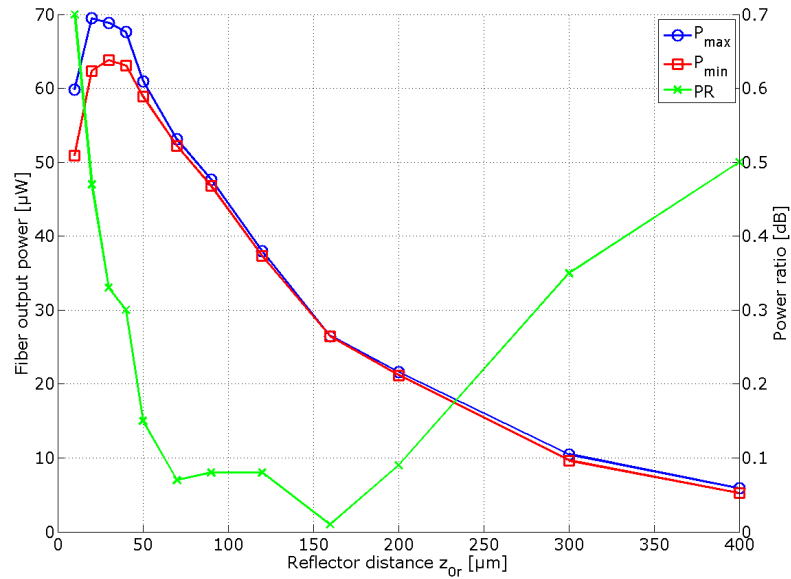
Figure 4.21: Minimum and maximum fiber output power achievable by varying the feedback phase at different laser - reflector distances and corresponding power ratios
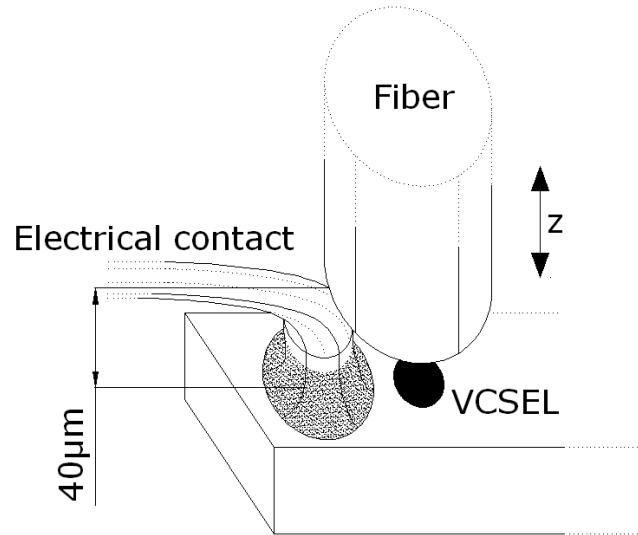
Figure 4.22: Schematic explaining the problems occurring at low distances due to the bond wire

It has to be mentioned that the phase difference between maximum and minimum power is not necessarily $\frac{\lambda}{4}$ anymore as it was the case at the glass plate reflector measurements. The reason for this is that the power difference is not produced by the laser diode itself, but rather by the fiber coupling process. How much power couples into the fiber depends on the transversal intensity distributions irradiating the fiber tip. To

attain a large power difference those must be strongly different which as Figure 4.12 shows must not be the case at a phase difference of $\frac{\lambda}{4}$. Nevertheless the period between two power maxima or minima is still $\frac{\lambda}{2}$.

Figure 4.23: Spectra corresponding to the minimum and maximum fiber coupled power at a reflector distance of $z_{0r} = 10\,\mu m$

Figure 4.23 shows spectra measured at the fiber output at a distance $z_{0r} = 10\,\mu m$ corresponding to P_{min} and P_{max}. The spectrum changes very strong. The two spectral lines at largest wavelengths almost completely vanish in the power minimum. Of course the feedback strength is high at such a small distance (higher than in the glass plate measurement) explaining this pronounced behavior.

The minimum of the power ratio curve at $160\,\mu m$ is also unexpected at first. But it does not mean that the effect that the variation in laser spectrum is also minimal, as Figure 4.24 shows. Rather the power variations in the first spectral line (LP01) are compensated by opposite changes in the second spectral line (LP11).

If the distance becomes larger than about $250\,\mu m$ the influence of feedback phase almost vanishes, although the power ratio increases again. In this case the absolute value of power variation is very small, but also the absolute values of the two powers are already so small that the small variation still corresponds to a large power ratio.

Spectra measured at a distance of $400\,\mu m$ are given in Figure 4.25. Mainly LP01 is influenced by the weak feedback anymore. This is because LP01 has its maximum in the VCSEL central region and there are always reflections that travel exactly back along the optical axis[12]. LP11 is minimal in the central region and therefore not influenced anymore. This also suggests that the modes at about $846.5\,nm$, which are also still influenced by the feedback phase, are modes with a maximum in the center. The total power variation is at large distances dominated by changes in the VCSEL output power and not by fiber coupling effects anymore, because the feedback is to weak to appreciably change the intensity distribution.

The power variation has also been observed for sub optimum transversal alignment. The fiber has been slightly shifted in the two transversal directions by applying a voltage to the piezoelectric elements. But the power variation does not increase, it decreases due to decreasing feedback strength. Obviously the multi mode fiber is too large to allow to spatially resolve the VCSEL beam intensity distribution.

---

[12]reflections from light with a wave vector parallel to the optical axis
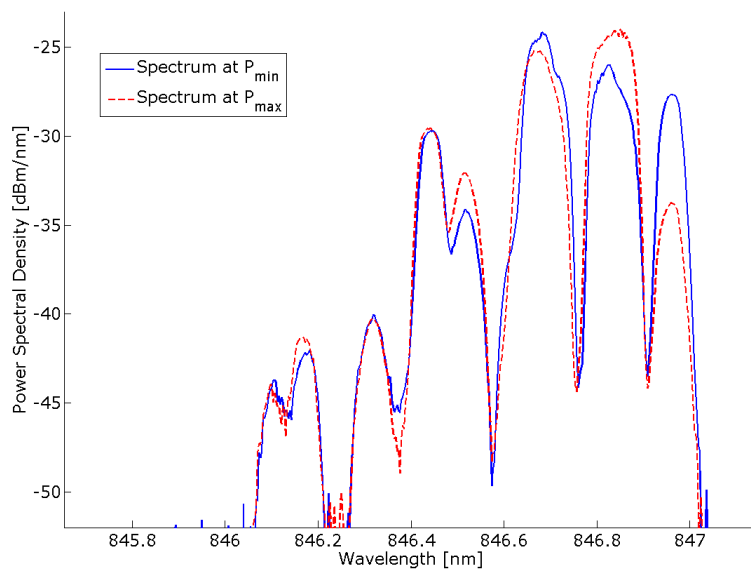
Figure 4.24: Spectra corresponding to the minimum and maximum fiber coupled power at a reflector distance of $z_{0r} = 160\,\mu m$
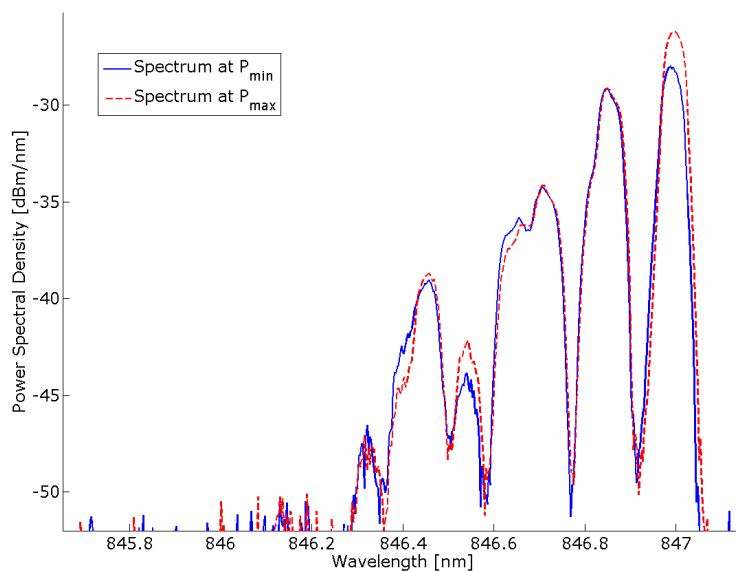
Figure 4.25: Spectra corresponding to the minimum and maximum fiber coupled power at a reflector distance of $z_{0r} = 400\,\mu m$

Device under Test 2: naked VCSEL, fiber facet reflector, with immersion oil

When immersion oil is in use the behavior is similar to that observed with the glass plate reflector. The reflections are too weak to produce a appreciable effect. Figure 4.26 shows again the minimum and max-

imum power attainable by adjusting the feedback phase versus the reflector distance together with the corresponding power ratios.

Figure 4.26: Minimum and maximum fiber output power achievable by varying the feedback phase at different laser - reflector distances and corresponding power ratios when immersion oil is in use

The curves for the two powers show the same behavior as the ones when no immersion oil is in use. The power ratio is close to $0\,dB$ at all distances meaning that there is almost no difference in the minimum and maximum achievable powers. Looking at Figure 4.15 it is clear that this must be the case, as the intensity distribution does almost not change with feedback phase.

The spectra for a reflector distance of $z_{0r} = 10\,\mu m$ are given in Figure 4.27. Of course the variations in spectrum are negligible too. It was not possible to increase the distance to larger values than $200\,\mu m$ as the oil layer then broke down.

4.3.2.3 Single Mode Fiber

As the multi mode fiber does not provide the necessary spatial resolution to resolve extrema in the laser output intensity distribution the next step is to redo the same measurements with a standard datacom single mode fiber[13] (SMF). It will be shown that it is possible to coarsely sense the transversal intensity distribution with such a fiber.

Measurement Setup

As the fiber coupled power must be expected to be much less for a single mode fiber compared to a multi mode fiber at the same distance to the laser because the diameter is just about one fifth, it was chosen to replace the free space measurement setup used above with a fiber based one as shown in Figure 4.28. Also the CCD camera was dropped as it did not reveal any further insights. The fiber coupling part of the setup is kept the same as before just with the multi mode fiber replaced with a single mode fiber. A fiber based power splitter, dimensioned for a wavelength of $850\,nm$, is used to split the power into one part that is fed into the optical spectrum analyzer and another part that irradiates the power meter.

---

[13]This fiber is single mode at its intended datacom wavelength of $1550\,nm$ and not at $850\,nm$. The core diameter is $9\,\mu m$.
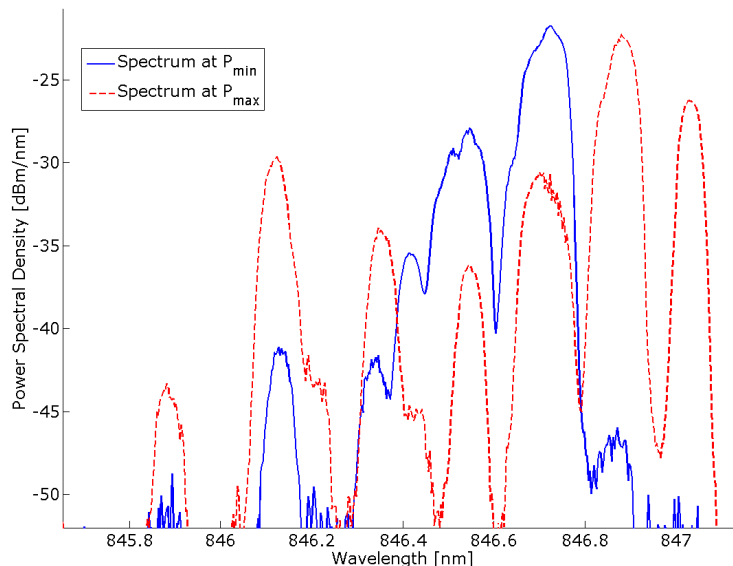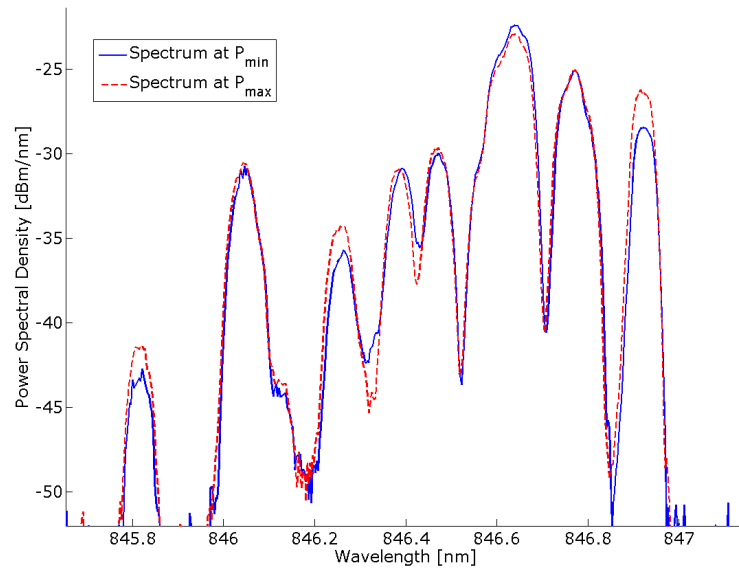
Figure 4.27: Spectra corresponding to the minimum and maximum fiber coupled power at a reflector distance of $z_{0r} = 10\,\mu m$ when immersion oil is in use
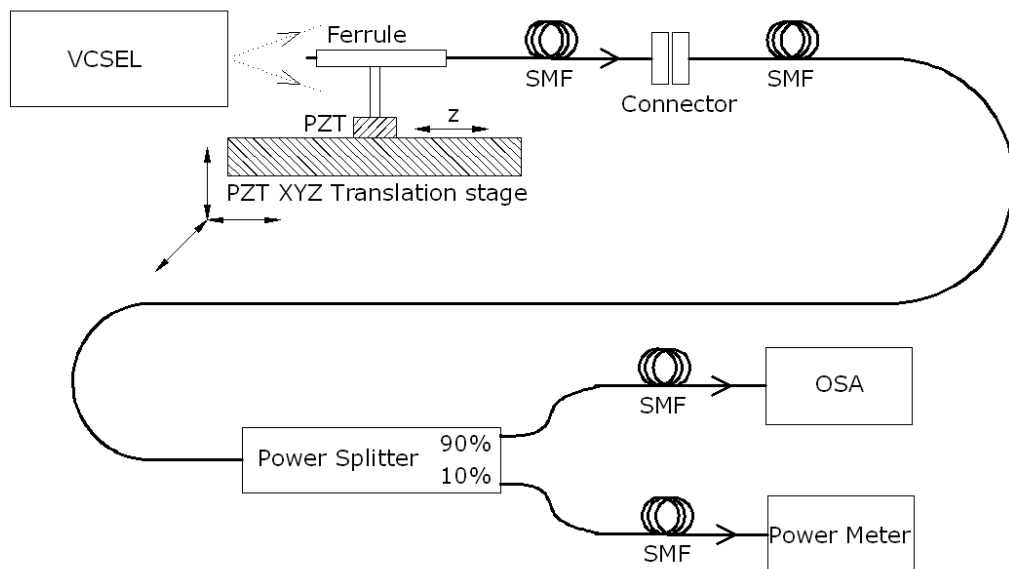
Figure 4.28: Setup used during the coherent external feedback measurements with the single mode fiber

The devices under test used are the same two as in the multi mode fiber case. Measurements are carried out with optimal transversal fiber alignment, in the sense that the fiber coupled power is maximized with

respect to the transversal alignment, but also with variable transversal alignment, to show that a spatial resolution of the beam profile is possible.

Because the location of the intensity maxima of the transversal laser beam profile changes with external feedback phase, this is also the case for the optimal transversal fiber alignment. To omit ambiguities it was chosen to optimize the transversal alignment for the feedback phase that leads to the maximum fiber coupled power. This means that the optimal transversal alignment is achieved by optimizing with respect to the alignment and the feedback phase.

Optimum Transversal Fiber Alignment

Measurement results for device under test 1, the naked VCSEL without immersion oil in use, are given in Figure 4.29. The distance to the laser diode is in this case kept so large that the bond wire is not being
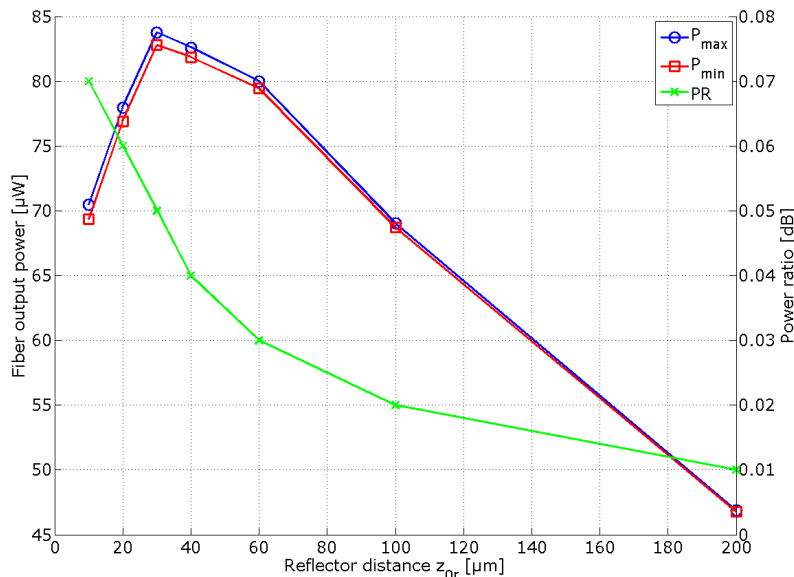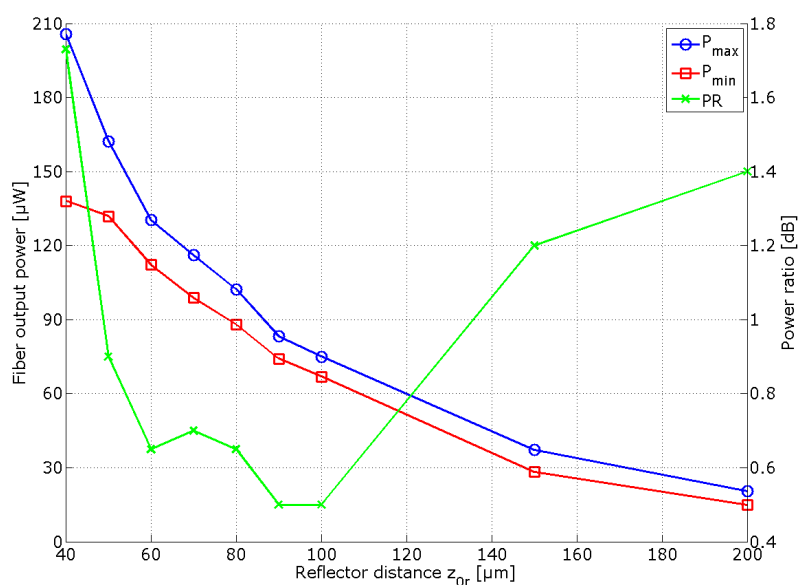

Figure 4.29: Minimum and maximum fiber output power achievable by varying the feedback phase at different laser - reflector distances and corresponding power ratios

hit by the fiber. This is necessary because the bond wire would influence the transversal alignment between fiber and VCSEL and the single mode fiber is very sensitive to such changes. The general behavior of the curves are similar to the multi mode fiber coupling case. The power ratio is large at small distances, shows an intermediate minimum and increases afterwards again, although the absolute value of the power variation with feedback phase is small. The corresponding explanation and spectra are also similar to the multi mode fiber case and not given here. The only difference to the MMF coupling situation is the increase in power ratio, which is now almost $1.8\,dB$ compared to $0.3\,dB$ at the same reflector distance of $z_{0r} = 40\,\mu m$. This shows that a single mode fiber is much more sensitive to variations in the transversal intensity distribution of the beam irradiating it. $1.8\,dB$ corresponds to more than 50% power variation with feedback phase for optimum transversal fiber alignment.

Using immersion oil leads again to a strong decrease in the power variation as Figure 4.30 shows. Still the achievable power ratios are as high as in the multi mode fiber case without immersion oil.

Varying the Transversal Fiber Alignment

The above observations already show that the feedback phase sensitivity is increased with a single mode
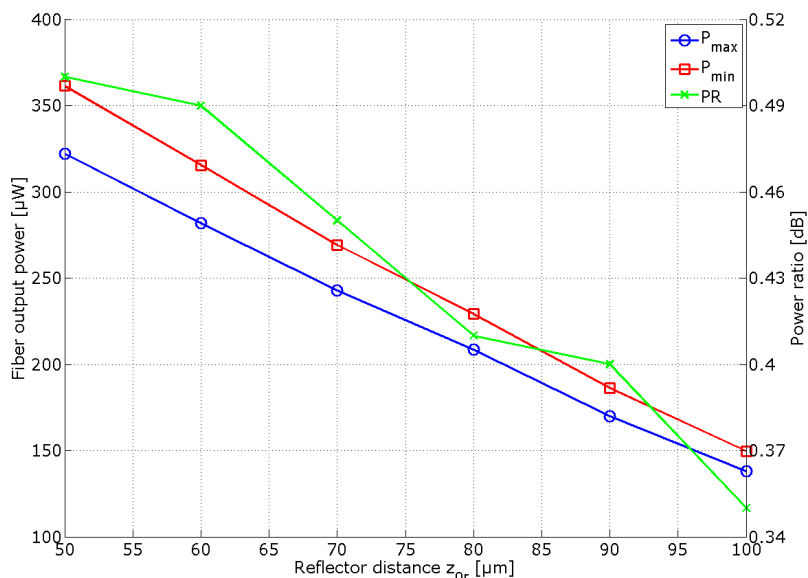
Figure 4.30: Minimum and maximum fiber output power achievable by varying the feedback phase at different laser - reflector distances and corresponding power ratios with immersion oil in use

fiber, but the attainable power ratios are still to weak to explain the strong power oscillations on the optoelectronic waveguide boards. But this is just the case, because the transversal fiber alignment with respect to the laser beam is optimized in the sense that the fiber is irradiated centrally.

Varying the transversal fiber alignment slightly in the order of few micrometers along the x or y axes given in Figure 4.19 allows to coarsely spatially resolve the beam intensity profile. This is shown in Figure 4.31. In this measurement first the transversal alignment is optimized as described above. This leads to the powers measured at $x = 0\,\mu m$. The measurement is carried out at a laser - reflector distance $z_{0r} = 50\,\mu m$. The feedback phase is then kept constant and just the transversal deflection is varied, leading to the red curve with circle markers when the feedback phase is adjusted for maximum power at $x = 0\,\mu m$ and to the blue curve with cross markers at minimum power.

The figure shows that the two transversal intensity distributions corresponding to different feedback phases have a distinct shape. The circle marked line could correspond to a Gaussian shaped intensity distribution dominated by LP01 as shown in Figure 4.12 (c). On the other hand the cross marked line seems to have a ring like shape as it is produced by LP11 or LP21 so it could look like 4.12 (a) or (b).

The figure might suggest that the power variations with feedback phase get weaker with increasing transversal displacement. But the figure is misleading, because the feedback phases that achieve maximum and minimum fiber coupled power also change with the displacement. So the phases adjusted at $x = 0\,\mu m$ do not lead to the power extrema at other displacements.

One might argue that the feedback phase changes with the transversal alignment, because the transversal translation stages are not exactly perpendicular to the optical axis and so they shift the fiber not parallel to the VCSEL surface but in a slightly skew angle θ. Of course this can not be excluded, but there are three reasons that confirm that the observed intensity distributions are not caused or at least dominated by such effects

1. If the feedback phase would change with transversal displacement, there should be some periodic behavior observable, which is not the case.

2. The red circle marked line shows monotonic behavior, which would also not be the case if the feedback
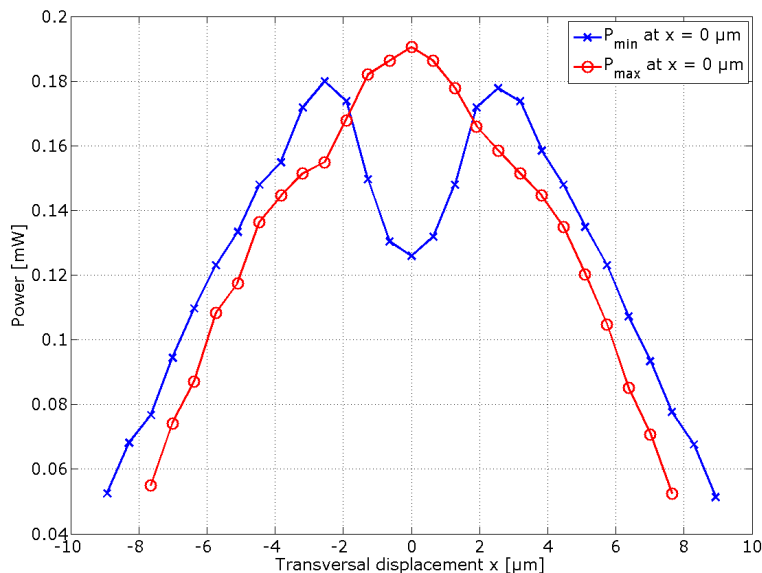
Figure 4.31: Spatially sampled laser beam intensity distribution at the two feedback phases corresponding to maximum and minimum power at $x = 0\,\mu m$

phase changes the intensity distribution

3. The maximum at about $x = 3\,\mu m$ in the blue cross marked line is not an absolute maximum concerning the feedback phase. Changing the phase at this position leads to higher power. This means that the blue curve should further increase with transversal displacement if the feedback phase is changed too.

By trial and error it was tried to find transversal displacements that enhance the power ratio with feedback phase. Table 4.1 gives some observed power ratios with the corresponding displacements.

Table 4.1: Power ratios at different transverse displacements and constant laser - reflector distance $z_{0r} = 50\,\mu m$

Displacement x	Maximum power P_{max}	Minimum power P_{min}	Power ratio PR
1.8 μm	-7.4 dBm	-8.1 dBm	0.7 dB
5 μm	-8.2 dBm	-11.2 dBm	3 dB
10 μm	-29 dBm	-33.1 dBm	4.1 dB

The first row in the table shows that there exists a displacement, where the power does almost not vary with feedback phase. In those cases the fiber is at some location where the intensity distribution does not change very much with the phase. On the other hand the second and third row show that there are as well transversal displacements where the fiber coupled power varies by more than a factor of two when changing the feedback phase. Accordingly this is the case when the intensity distribution illuminating the fiber tip changes strong with the phase. It was not possible to find any simple rule at which displacements the power variation is large. There might be other transversal alignments where the power ratio is even larger.

4.3.2.4 Conclusions

Summarizing the fiber facet reflector measurement results allows to make the following statements.

- Multi mode fibers

  - The core diameter of a multi mode fiber is too large to allow to spatially resolve the transversal laser output beam intensity distribution. Therefore also the fiber coupled power does not strongly vary when the external feedback phase is adjusted to change the transversal intensity distribution.

  - The maximum achievable power ratios are about $0.7\,dB$ at a low distance of about $10\,\mu m$. The power variation with feedback phase does not increase for suboptimal transversal alignment.

  - Using immersion oil in the multi mode fiber case almost completely suppresses the feedback influence.

- Single mode fibers

  - At optimal transversal alignment power ratios of about $PR = 1.8\,dB$ were observed at a rather large distance of $z_{0r} = 40\,\mu m$. At smaller distances larger PRs would surely be possible in analogy to the multi mode fiber case.

  - Using immersion oil does not completely suppress the feedback influence but weakens it to about $PR = 0.5\,dB$.

  - Varying the transversal alignment allows to increase the power variations with feedback phase to more than $PR = 3\,dB$ at $z_{0r} = 50\,\mu m$ distance. Again smaller distances would entail larger values.

  - The single mode fiber allows to coarsely resolve the transversal intensity distribution spatially. Sampling the intensity distributions corresponding to the two phases that produce P_{min} and P_{max} at optimum alignment shows that the maximum power is achieved with a Gaussian like profile dominated by LP01 and P_{min} with a ring shaped profile dominated by LP11 or LP21. This is a expected behavior as LP01 is maximal in the center region and LP11 as well as LP21 is minimal, which maximizes the power variation.

Chapter 5

Conlcusions

5.1 Relating Measurement Results with the Original Problem

During this Diploma thesis it has been shown that external optical feedback can be the source for the waveguide output power oscillations observed over temperature (see Chapter 1).

In a first step the light source, a vertical cavity surface emitting laser diode, was investigated in detail to get better understanding for this complex device. During measurements carried out in Chapter 3 it has been shown that the laser diode does not show any intrinsic oscillatory behaviour wheter over temperature nor over drive current. It has also been observed that different spectral lines in the VCSEL output correspond to different internal cavity transversal modes (mathematically described as Bessel or Laguerre Gaussian modes), therefore variations in the spectrum are connected with corresponding changes in the laser beam intensity distribution. Another important observation was that there is no principal difference in the VCSEL output wheter it is statically driven or modulated. This is cruical for taking over the argumentation carried out in Chapter 4 and established by static measurements to dynamic situations.

Due to corresponding indications in the literature effects caused by external optical feedback were investigated in a next step in Chapter 4. It has to be distinguished between coherent and incoherent feedback, depending on the distance to the external reflector. Section 4.2 showed that incoherent feedback can not be the source for power oscillations, as it does not depend on the feedback phase and therefore is not periodic. Incoherent feedback can drastically change the laser output spectrum and does also have an influence on the output power but the severity of the effects only depends on the feedback strength which can not be expected to vary periodically over temperature on the waveguide boards described in Chapter 1. Therefore the next logical step was to switch to coherent feedback (see Section 4.3), which also showed strong influence on the laser output spectrum and correspondingly the transversal intensity distribution, but not on the total laser output power. This is true at least for transversal multi mode laser devices. In such devices gain competition effects (see Section 2.1.2) equate power variations in the different modes. Effects caused by coherent external feedback are periodic in the feedback phase and therefore would in principal be able to cause oscillatory behavior. But the influence on the total VCSEL output power is negligible.

Therefore it was necessary to find a reason that translates variations in the laser output spectrum into variations of the total power, a modal filtering element. The waveguide coupling portion of the opto-electronic waveguide boards was identified as a possible mode filter as shown in Section 4.3.2 with the help of standard glass fibers. First the situation on the waveguide boards was emulated by using a multi mode fiber, showing that fiber output power oscillations can be as large as 20% but not much more, which is still much less than what was observed in Chapter 1. Using a single mode fiber instead measurements with transversally ideal aligned fibers have produced power variations of up to 50% at a rather large reflector distance of $50\,\mu m$, still too less. But it has also been shown that a single mode fiber is able to spatially resolve the transversal intensity profile of the laser beam coarsly and therefore it was possible to find transversal alignments where the observed power ratios increased to more than $3\,dB$ (see Table 4.1). This is in the same order of magnitude as the power oscillations over temperature of the waveguide boards and the variations can be expected to

increase further with decreasing distance to the laser diode (the distance on the boards is just about $15\,\mu m$).

Summarizing the statements above, it has been shown that the power oscillations over temperature on the opto-electronic waveguide boards can be explained by a combination of external optical feedback together with a modal filtering element translating oscillations in the laser output intensity distribution with feedback phase into variations of the total output power.

5.2 Open Questions

There are mainly three open questions left which could not be answered completely.

- **Where do the reflections come from?**

- **Why does the feedback phase change?**

- **Why do not all boards show this oscillatory behavior?**

To answer the first question four possibilities could be identified.

- Reflections from the end of the waveguide or the photodiode

  Such reflections would occur at a distance of about $10\,cm$, so it is not even sure that they would be coherent anymore which is a necessary prerequisite. On the other hand the measurements with the waveguide VCSEL (see Section 4.3.1) have shown that the feedback sensitivity is strongly enhanced when reflections are guided back to the VCSEL, which could explain the strength of the observed power oscillations. But there is another fact that speaks against this theory. The period of the power oscillations did not change when cutting back the board which would be the case if the reflections occur at the waveguide end, as the length of the external cavity changes (see Equation (2.23)).

- Reflections somewhere along the waveguide

  There is the possibility of a refractive index step along the waveguide due to some impurity or air bubble caused by imperfections in the fabrication process. Due to the increased feedback sensitivity caused by the waveguide already small reflection would suffice. The impurity could be somewhere at the beginning of the waveguide such that it was not cut off during the corresponding measurements described in Chapter 1.

- Reflections from the beginning of the waveguide

  The waveguide is established by slightly increasing the index of refraction with the help of two photon absorption. Of course such a refractive index step always produces reflections which lead to external feedback. Although the distance between laser diode and beginning of the waveguide $z_{0r} \approx 15\,\mu m$ is short according to the manufcturer the feedback power ratio would still be very low, as the refractive index step is just about 0.004. Because measurements with immersion oil between external reflector and laser diode (see Sections 4.3.1 and 4.3.2) did not show appreciable influence on the VCSEL output, it is unprobable that this theory holds, as the feedback power ratio is even smaller in this case compared to the measurements.

- Reflections from an air gap between laser diode and ORMOCER$^{\circledR}$ layer

  This is the most probable possibility, as it would explain the strength of the reflections (due to a large refractive index step and small distance) and also the necessary phase shift by thermal expansion of the air gap. The existence of such a gap can be explained by considering the fabrication process. The viscous ORMOCER$^{\circledR}$ polymer is applied on the printed circuit boards and afterwards thermally cured, a process at which the material is maybe being deformed.

The second question allows mainly three answers, considering the possible sources of reflections

- The wavelength of the laser diode shifts with temperature

  This wavelength shift was measured to equal $\frac{\partial \lambda}{\partial T} = 0.06\,nm/K$ according to Chapter 3. By considering that the period of the oscillations is about $\Delta T = 10\,K$ the necessary external cavity length can be calculated.

$$\phi_{ext} = k_{ext} \cdot 2L_{ext} = \frac{2\pi}{\lambda} n_{ext} 2L_{ext} \tag{5.1}$$

$$|\Delta\phi_{ext}| = |\frac{\partial\phi}{\partial T}\Delta T| = |\frac{\partial\phi}{\partial\lambda}\frac{\partial\lambda}{\partial T}\Delta T| = |\frac{-2\pi}{\lambda^2} n_{ext} 2L_{ext} \frac{\partial\lambda}{\partial T}\Delta T|$$

$$\rightarrow L_{ext} = \frac{\Delta\phi_{ext}\lambda^2}{4\pi\Delta T \frac{\partial\lambda}{\partial T} n_{ext}} \approx 600\,\mu m \tag{5.2}$$

  Clearly this explanation does not fit to the third and fourth possible reflection sources.

- The external cavity phase shift varies due to changes in the material refractive index

  Equation 5.1 for the external cavity phase shift holds here as well. As I do not know how strong the refractive index of ORMOCER® changes with temperature no estimation for the necessary external cavity length can be given. But most likely it would also necessitate a rather long cavity as in Equation 5.2 which is not consistent with the third and fourth reflector possibilities.

- Thermal expansion of the material changes the external cavity length

  The thermal expansion coefficient of ORMOCER® is quite large, it amounts about $50-250 \cdot 10^{-6}\,/K$. A change in external cavity length with temperature due to thermal expansion can explain the necessary phase shift for all external reflector possibilities.

The last thing to discuss is the third question, "Why do not all boards show the oscillatory behavior?". One answer to this question could be the sensitivity of the power variations to the transversal alignment. With the single mode fiber it has been observed in Section 4.3.2 that the strength of power variations with feedback phase strongly depends on the transversal alignment between fiber and laser. How pronounced such behavior exists in the case of the seven core waveguide can of course not be answered with the measurements above. It would be necessary either to redo the measurements of varying transversal alignment with the seven core waveguide[1] or try to find it out with simulations of the structure.

On the other hand if really some impurity along the waveguide is the source of the external reflections it would be self explaining why the effects do not occur on all boards.

5.3 Possible Countermeasures

The external feedback problem can not be solved in a trivial way. In standard fiber data com links similar difficulties with external feedback exist although there mainly the noise enhancement introduced by reflections is bothering ([22]). These problems are not solved as well. Nevertheless some hints shall be given for further development.

- Use one single large waveguide core

  As the measurements with the multi mode fiber have shown (see Section 4.3.2.2) a fiber with a large core diameter is much less sensitive to external feedback. The observed power ratios are in the order of $0.7\,dB$ which corresponds to about 20% power variation with feedback phase independent of the transversal alignment between fiber and laser optical axis.

---

[1]this would have been done if such a structure with polished surface had been available

- Optimize the fabrication process

  Above it is shown that reflections from some air gap between laser diode and the ORMOCER® layer is the most probable explanation for external feedback. The feedback problem would vanish if it is possible to avoid such an air gap.

- Usa a single mode laser

  A single mode laser does not change its transversal intensity distribution with feedback phase and therefore no phase dependency of waveguide coupling would exist. Still the feedback would lead to small power variations due to interference effects between reflected and emitted light inside the laser cavity but those are negligible compared to the variations introduced by coupling effects (compare Sections 4.3.1 and 4.3.2). As Appendix B.5 shows it would be necessary to use a device with a high side mode suppression ratio such that no second mode can be excited. Of course the problem with single mode lasers is their lower output power.

- Optimize the transversal alignment

  Sections 4.3.2.2 and 4.3.2.3 have shown that the power variations are much lower for optimal transversal alignment and can even vanish at special alignments. If it would be possible to control the transversal alignment with higher accuracy feedback effects could be minimized.

Appendix A

Measurement Setups

A.1 Device Characterization

Vertical Cavity Surface Emitting Lasers:
ULM Photonics multi mode VCSEL 850-05-TN-U46FOP
Avalon Photonics multi mode VCSEL AP-A72-0101-0000

Power Meter:
ANRITSU MA912B
Indicator: ANRITSU ML910B

Pyroelectric Array Camera (PAC): Spiricon Pyrcom III

Charge Coupled Device (CCD) Camera: Spiricon STC-700-1550

Current Source: Thorlabs LDC200C

Multi Meter: Fluke 175

Optical Spectrum Analyzer (OSA): Yokogawa AQ 6319

Optical Oscilloscope (OSCI): LeCroy waveexpert 100H

Beam Splitters: Non polarizing beam splitter cubes
BS1:
Attenuation transmitted beam $A_{BS1t} = 3.7$dB
Attenuation redirected beam $A_{BS1r} = 4.3$dB
BS2:
Attenuation transmitted beam $A_{BS2t} = 3.9$dB
Attenuation redirected beam $A_{BS2r} = 3.3$dB

Variable Attenuator: Circular variable neutral-density filter (vacuum deposited alloy on a polished glass substrate)

Table A.1: Attenuation of the variable attenuator

Angle [°]:	5	40	70	90	95	100	110	120	130	160	355
A_{ATT}[dB]:	0.4	0.7	1.1	2.2	3.7	4.9	7	8.9	10.4	15.3	30

Microscope Objectives:
L1: 20x/0.5 NA, Attenuation $A_{L1} = 2dB$
L2: 40x/0.65 NA, Attenuation $A_{L2} = 2dB$
L3: 10x/0.25 NA, Attenuation $A_{L3} = 2dB$

Pattern Generator: Agilent Technologies N4906B

A.2 Estimation of the Feedback Power Ratio for the Coherent Measurement Setup

Although in Section 4.3 the distance to the reflector is used to characterize the feedback strength, this Appendix shall provide a rough estimate of the feedback power ratios corresponding to these distances for the glass plate reflector setup.

A.2.1 Idealized Model

The strength of the reflections shall be estimated with a simple worst case model. This model will provide an upper bound to the situation in reality, it is schematically depicted in Figure A.1. The Rayleigh distance
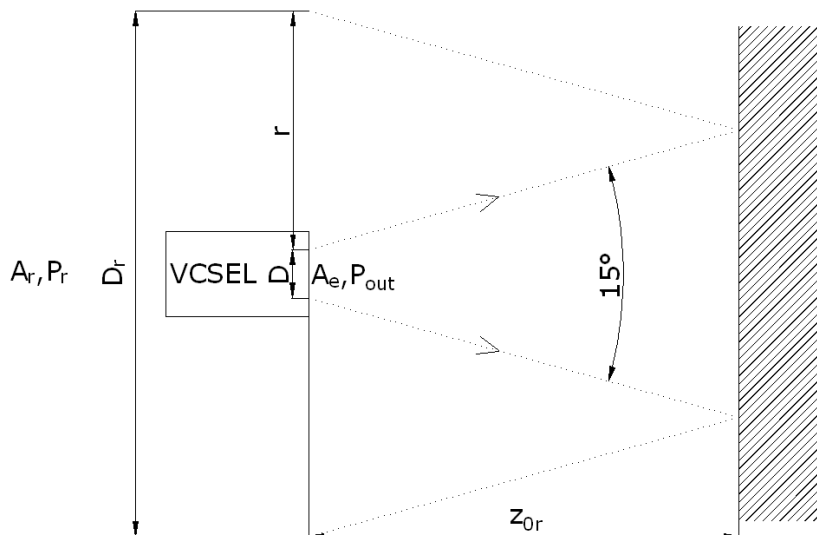
Figure A.1: Idealized model to upper bound the strength of reflections from collimating lenses

of the laser can be upper bounded with diameter D of the VCSEL as

$$d_R = \frac{2 \cdot D^2}{\lambda} \approx 250 \mu m. \tag{A.1}$$

This is an upper bound because the real diameter of the emitting surface will be smaller than the VCSEL total diameter $D \approx 10\,\mu m$. Because the distance to the reflector glass plate is smaller than the Rayleigh distance the reflections take place in the near field of the laser. Nevertheless the far field beam divergence will be used because it allows the calculation with a ray model. The full width beam divergence is about $25°$ according to Figure 3.7 at a drive current of $6\,mA$. But modes with low mode order like LP01 do have

lower divergence, so to stick with the worst case estimation a divergence of 15° will be used. This reduction is also necessary because the divergence in the near field is generally smaller than the far field value (see [3]). According to this simple model the diameter of the reflected beam at the VCSEL surface D_r can be calculated to equal

$$D_r = D + 2 \cdot \overbrace{\tan(7.5°) \cdot \underbrace{2 \cdot z_{0r}}_{\text{round trip distance}}}^{r}.$$

Energy conservation states that the power of the beam must not change, as there are no losses, which allows the calculation of the intensity of the reflected beam I_r, knowing the emitting surface $(A_e = (D/2)^2 \pi)$ and the surface of the reflected beam at the VCSEL $(A_r = (D_r/2)^2 \pi)$ and assuming a mirror reflectivity of 100%

$$P_r = P_{out} = I_r A_r = I_{out} A_e \rightarrow I_r = \frac{P_{out}}{A_r}.$$

Because the mirror reflectivity is not 100% but just

$$R = \left(\frac{n-1}{n+1}\right) = 0.04$$

the above value for the reflected power must be corrected by this factor (it has been assumed that the surrounding medium is air and the refractive index of the glass plate equals $n = 1.5$).

$$P_r = \frac{P_{out}}{A_r} \cdot R$$

Assuming that all the reflected intensity that lies inside the area of the emitting surface couples back into the laser cavity (which is again an upper bound, see B.4) the feedback power ratio can be calculated to be

$$FPR = 10 \log_{10} \left(\frac{I_r A_e}{P_{out} \cdot R}\right) = 10 \log_{10} \left(\frac{A_e}{A_r} \cdot R\right). \tag{A.2}$$

The following table lists the estimated feedback power ratios together with the corresponding distances. In

Table A.2: Estimated FPRs for the glass plate reflector measurements

Distance $z_{0r} [\mu m]$:	40	60	80	100	120	140	180	220	260
FPR[dB]:	-23.8	-26.4	-28.3	-29.9	-31.3	-33.4	-34.4	-36.0	-37.3

most of the applied measurement setups microscope objectives are used to collimate the laser beam or to focus it at some point. Of course part of the light is reflected at those obstacles and part of this light couples back into the laser cavity. In order to produce genuine measurement results it is necessary to guarantee that those reflections are so weak that their influence on the laser can be neglected. This can also be estimated with the above model. The divergence of the reflected beam is for sure larger than that of one reflected at a plain surface (because the lenses used are convex) and therefore the above model also delivers an upper bound for those reflections. Clearly as there is hardly a feedback influence observable at a distance of $260 \, \mu m$ the reflections from the objectives, which are at a distance of more than $1 \, mm$ are negligible.

Only the reflections from the lenses directly after the VCSEL are important because it is very unlikely that reflections from other surfaces will hit the VCSEL. Those surfaces were always slightly tilted with respect to the optical axis to guarantee this.

A.3 Estimation of the Feedback Power Ratio for the Incoherent Measurement Setup

For the characterization of the feedback strength in the literature the feedback power ratio is used, which is defined as the logarithm of the ratio between the optical power returned to the facet of the laser substrate divided by the power emitted from that facet (the areas over which the power is calculated are the same, see Equation (2.22)).

The incoherent measurement setup (see Figure 4.4) is aligned in such a way that the focus of the laser beam lies as close as possible to the external reflector plain. The reflector plain is aligned perpendicular to the optical axis. Therefore, if the alignment is good, the reflected beam travels exactly the same way back to the laser diode and gets focused onto it. In this ideal case the area of the reflected beam at the VCSEL surface would be the same as that of the laser output beam. The only losses that the beam experiences are the attenuations of the different devices along the optical axis (the values of those attenuations are given in Section A.1). In general the alignment won't be perfect and the area of the reflected beam at the laser surface will be different from that of the output beam. This will lead to additional losses, but those can't be evaluated. Therefore the feedback power ratio is calculated without taking them into account.

The power of the back reflected light can be calculated by considering the attenuation of the components along the path traveled by the beam according to

$$P_{refl} = P_{out} - 2 \cdot A_{L1} - 2 \cdot A_{BS1r} - 2 \cdot A_{ATT} + R_{ext}$$

where R_{ext} is the reflectivity of the gold coated mirror. This reflectivity is about 97.5% which corresponds $-0.1\,dB$. The feedback power ratio can now easily be calculated to equal

$$R = 2 \cdot A_{L1} + 2 \cdot A_{BS1r} + 2 \cdot A_{ATT} - R_{ext}.$$

For the above given values of the attenuation of the components this amounts to feedback power ratios of

Table A.3: Estimated FPRs for the incoherent measurement setup

$A_{ATT}[dB]$:	0.4	0.7	1.1	2.2	3.7	4.9	7	8.9	10.4	15.3	30
$FPR[dB]$:	-13.5	-14.1	-14.9	-17.1	-20.1	-22.5	-26.7	-30.5	-33.5	-43.3	-72.7

Still this is not the light power which couples back into the laser cavity. If we assume perfect coupling between the reflected field and the field inside the laser, still the power would have to be decreased by typically 24 dB, which corresponds to a reflectivity of the VCSEL top distributed Bragg reflector of 99.6%.

Appendix B

Additional Measurements and Simulations

B.1 Evaluation of the VCSEL Beam Divergence

This appendix shows how the beam divergence of the laser diode has been obtained from the far field distribution measured with the pyroelectric array camera (see 3.1.3).

An example of a measured far field intensity distribution at a drive current slightly above threshold at $I = 1.3\,mA$ is given in Figure B.1 (a). The distribution has a Gaussian like shape. A Gaussian fit to the measured intensity distribution is shown in Figure B.1 (b). The mean is given by the center of mass of the measured distribution and the variance is calculated by minimizing the mean square error between the fit and the measured profile.

Contour plots of the two distributions are shown in Figure B.2. The agreement between the Gaussian fit and the measured intensity profile is very good. This allows the conclusion that the dominating transversal mode at this drive current is the LP01 mode. The plots allow easy evaluation of the $\frac{1}{e^2}$ beam width and with it according to (3.1) the angle of beam divergence. The result is shown in Figure 3.7. At higher drive currents more transversal modes are stimulated and it is not easily possible to find a fit for the measured intensity distribution. But again it is possible to estimate the beam divergence from the corresponding contour plots.
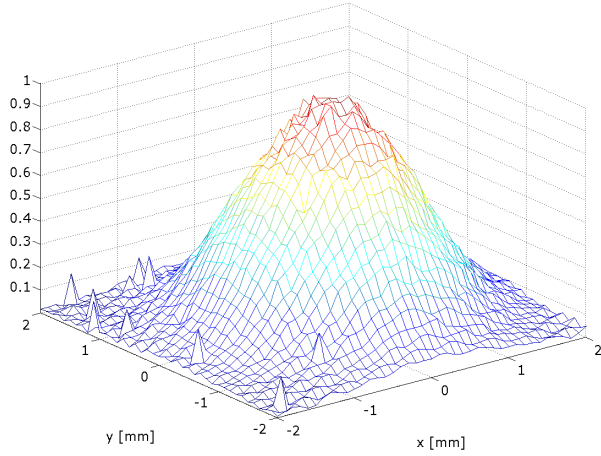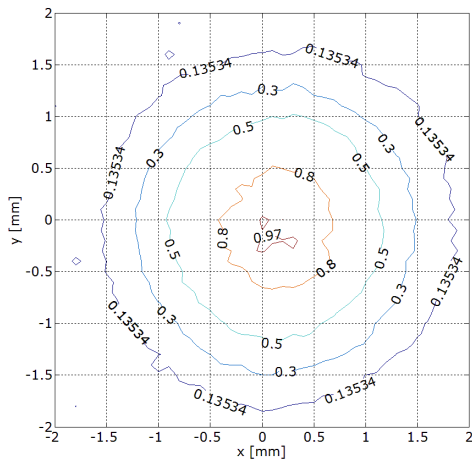
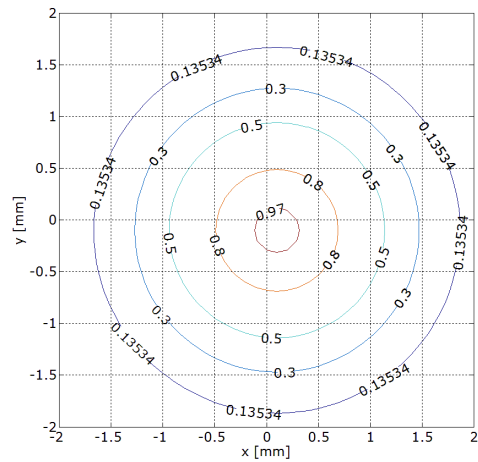(a) Measured intensity distribution
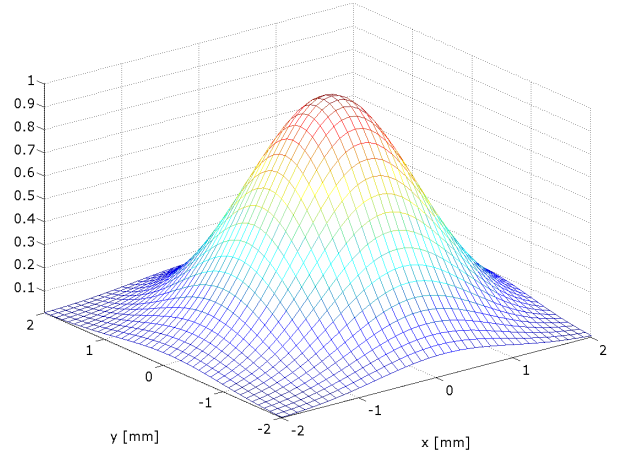
(b) Gaussian fit

Figure B.1: Measured normalized far field intensity distribution and Gaussian fit

(a) Measured intensity distribution

(b) Gaussian fit

Figure B.2: Contour plots of the measured far field intensity distribution and Gaussian fit

B.2 VISTAS Parameter Extraction and Simulation Results

The "VCSEL Integrated Spatio Temporal Advanced Simulator" (VISTAS) is a freely available software tool [23], developed by Marc Jungo at ETH Zürich during his dissertation [6], that allows the simulation of VCSELs.

VISTAS is a 2D, multi mode, time-domain VCSEL model. It accounts dynamically for the spatial interactions between the optical field and carrier distributions in the active layer. It is capable of effects as spatial hole burning (SHB), gain (mode) competition or carrier diffusion losses.

There exist three versions of the program namely VISTAS basic, advanced and expert. The basic version implements the 2D spatially dependent photon, phase and carrier rate equations. The advanced version additionally includes noise and some external cavity effects and expert adds features like thermal effects and electrical parasitics.

The number of parameters grows drastically from version to version. Those parameters range from geometrical over material to parameters necessary for modeling the current flow. Most of the parameters can only be known by the manufacturer of the device, some necessitate electrical simulation of the device with a SPICE like tool, for others typical values can be obtained from literature (knowing the material composition) and just few are accessible experimentally.

To keep the number of parameters low it was chosen to use VISTAS basic as a starting point. More information about the software tool can be found in [6] and [20]. Some hints on parameter extraction may be found in [21] and [6].

B.2.1 Necessary parameters

The device that is being simulated is the ULM multi mode VCSEL that is also used in chapters 3 and 4. A lot of geometrical and other parameters are kindly provided by ULM Photonics. Those parameters are given in the following list.

- Top and bottom mirror reflectivities

- Effective cavity length

- Single quantum well thickness

- Number of quantum wells

- Thickness of the separate confinement structure

- Oxide aperture radius

- Oxide thickness

- Internal losses

Other parameters that are also required can be found in literature.

- Current injection efficiency

  $\eta_i \approx 0.9$, typical value according to literature [5].

- Transparency carrier density

  $N_{tr} = 2.4 \cdot 10^{18} \, /cm^3$, according to literature for $GaAs/Al_{0.2}Ga_{0.8}As$ 8nm quantum wells, which is the standard material composition for 850nm emission wavelength [8].

- Logarithmic gain coefficient

  This value is necessary to model the dependency of the material gain g on carrier density according to

  $g = g_0 \ln \frac{N}{N_{tr}}$

  where g_0 is the logarithmic gain coefficient. $g_0 = 2400\,/cm$ according to literature for $GaAs/Al_{0.2}Ga_{0.8}As$ [8].

- Carrier lifetime

  Can be calculated from the transparency current density

  $j_{tr} = \frac{N_{tr}e \cdot d_{qw}n_{qw}}{\eta_i \tau_n} \rightarrow \tau_n = \frac{N_{tr}e \cdot d_{qw}n_{qw}}{\eta_i j_{tr}}$

  where j_{tr} is given from ULM. This delivers a value which fits well to the literature values of about 2.0 - $4.0\,ns$ [4].

- Core equivalent refractive index

  $n_g = 3.6$, according to literature for GaAs [4].

- Cladding equivalent refractive index

  This value is chosen to reproduce the divergence of $5.5°$ at a drive current of $1.3\,mA$. The divergence is only influenced by the oxide aperture radius and the refractive index step between core and cladding, so the cladding index is the only value left to choose. The value that is being used is $n_c = 3.575$.

- Optical confinement factor

  This value equals the ratio of the active volume and the photon volume. It is necessary to account for this difference in the rate equations.

  $\Gamma = \frac{V_a}{V_p} = \Gamma_z \cdot \Gamma_t = 2\frac{n_{qw}d_{qw}}{L_{eff}} \cdot \Gamma_t \approx 0.02.$

  The confinement factor can be split into a longitudinal and a transversal part, where the longitudinal part depends on the active layer thickness and the effective cavity length. The factor 2 comes from the enhancement factor (see 2.1.3). The transversal part depends on the mode of interest, but is in most cases simply set to 0.9 [4].

- Current spreading coefficient r_s

  This coefficient can not be found in literature because it strongly depends on the design of the VCSEL. The current flow in the VCSEL is modeled as constant inside the oxide aperture and exponentially decreasing outside. The current spreading coefficient describes the slope of the exponential function. It can only be evaluated by a simulation of the electronic behavior of the device with a device simulator like SPICE. It is not even clear if the device is designed such that this modeling makes sense. According to [6] the value is typically somewhere in between $0.1 - 2.0\,\mu m$.

- Ambipolar diffusion coefficient D_N

  There is no single value in literature for this coefficient, it varies between 1 and $20\,cm^2/s$ for the same material composition [5], [4], [6].

The last two coefficients leave some freedom for fitting to the actual VCSEL behavior. Both influence the threshold current as well as the differential quantum efficiency and can therefore be used to match these values.

B.2.2 Parameter modification

Applying the values given above and running simulations in VISTAS produces P-I characteristics with too low threshold current ($\approx 0.9\,mA$) and also too low differential quantum efficiency (≈ 0.19). Therefore I investigated those values with simple formulas that are just approximately valid for multi mode devices, but can be used to find out which parameters influence the VCSEL behavior.

The differential quantum efficiency is given by

$\eta_d = \eta_o \cdot \eta_i$

$\eta_o = F_t \frac{\alpha_m}{\alpha_i + \alpha_m} = 0.23862$, optical efficiency

$\alpha_m = \frac{1}{2L_{eff}} \ln \frac{1}{R_t R_b}$, mirror losses

$F_t = \frac{1-R_t}{1-R_t+\sqrt{R_t/R_b}(1-R_b)}$, fraction of power coupled out with the top mirror.

This already shows that the current injection efficiency would need to be larger than one to achieve the desired differential quantum efficiency of 0.255, according to 3.1.1, which is not possible. It was therefore chosen to vary some parameters in order to reproduce the measured behavior. Looking at the formula for the threshold current shows, that varying the mirror reflectivities allows to match both the differential quantum efficiency and the threshold current, by changing α_m.

$I_{th} = \frac{eV_a B N_{tr}^2}{\eta_i} e^{2\frac{(\alpha_i+\alpha_m)}{\Gamma g_0}}$

with B, the bimolecular recombination coefficient ($\approx 10^{-10} cm^3/s$ according to [8]). Setting $I_{th} = 1.28mA$ and allows to calculate the mirror losses α_m. The equations for the mirror losses and the differential quantum efficiency can be combined to deliver values for the top and bottom mirror reflectivities.

When running simulations with parameters obtained by this procedure and varying D_N and r_s still it is not possible to reach the desired values of I_{th} and η_d. Both values are a bit too small and therefore it was first chosen to increase the mirror losses further, which increases the threshold current and then to change the values of R_b and R_t in such a way that more power couples out the top mirror, which increases the differential quantum efficiency. Varying then the values of the ambipolar diffusion coefficient and the current spreading coefficient allows to achieve the desired behavior. Increasing the spreading coefficient leads to a less confined current and therefore to an increase of the threshold current.

Figure B.3 shows the input-output characteristics obtained in that way, which matches the measured one in terms of the threshold current and the differential quantum efficiency. VISTAS basic only produces physically correct results for low drive currents, like the ones shown in the figure. At larger currents the simulated differential quantum efficiency increases, which contradicts physics. The main reason maybe that thermal effects are not included in this version. Taking the same values for simulations in VISTAS advanced or expert (while leaving the additional values like they are given in the distributed program version) produces non fitting results with too high threshold current and too low differential quantum efficiency. This suggests that the values given by ULM Photonics for the top and bottom mirror reflectivities (which had to be adjusted for VISTAS basic) deliver better results in those more complex VCSEL models.

Another problem of simulations with the parameters from above is that the power distribution to the different transversal modes does not fit to the measured spectra. The reason for this is that modal dependent parameters like the internal losses or the optical confinement factor have been taken as equal for all modes. Varying these parameters allows to achieve almost arbitrary modal power distributions.

These observations show that it is necessary to know the exact geometry and material composition of the device to be able to calculate all modal dependent parameters. Just with these parameters at hand a useful simulation is possible.
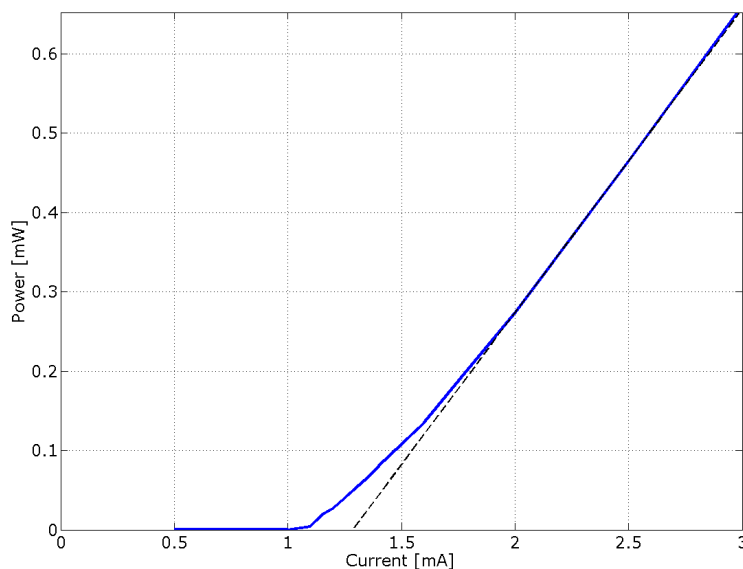
Figure B.3: Simulated VCSEL output power - current characteristics

B.3   Measurement of Polarization Resolved Spectra

This section is intended to show that there is indeed a splitting of the spectral line corresponding to a specific transversal mode due to lifting of the polarization caused mode degeneracy. Different polarizations have slightly different wavelength due to anisotropies in the device crystal.

B.3.1   Measurement Setup

In order just to pass one polarization state to the measurement instruments it is necessary to use a polarizer in the measurement setup as shown in Figure B.4. The VCSEL (850-05-TN-U46FOP) is driven at a constant bias current of $2.5\,mA$. The polarizer passes light of a specific polarization orientation. The VCSEL in general emits light in two orthogonal polarization orientations. These orientations correspond to crystallographic orientations (see [5]). By matching the orientation of the polarizer (rotating it) with one of the orientations of the VCSEL it is possible to filter out that orientation. The measurement setup also incorporates a fiber power splitter which allows to feed part of the light into a optical spectrum analyzer and a smaller part into a power meter. The power meter is used to observe power variations with polarizer orientation. When the polarizer is rotated such that a vertical polarization orientation is preferred the according polarizer angle is $0°$. The angle is further counted clock wisely. To really see the splitting of the spectral lines it is necessary to adjust the optical spectrum analyzer for maximum wavelength resolution ($10\,pm$ in this case). It is difficult to find the two orthogonal polarization states, as the total power observed with the power meter does almost not change with the polarizer angle. Therefore it was chosen to measure the spectrum at two orthogonal polarizer orientations, where the change in the spectrum is rather large. Clearly it can not be guaranteed that these orientations correspond to the VCSEL polarization orientations.

B.3.2   Measurement Results

Figure B.5 shows the VCSEL output spectrum measured at two orthogonal polarizer orientations compared with the one measured without polarizer. At least for the second spectral line (at about $845.85\,nm$) it
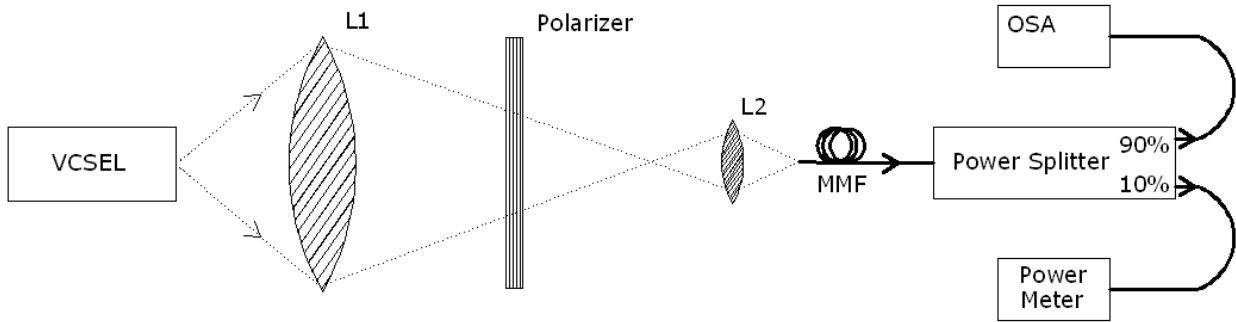
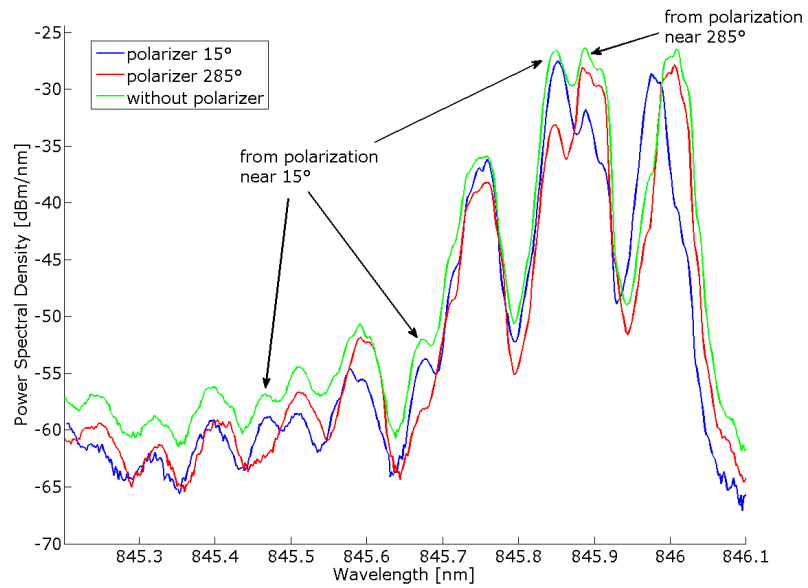Figure B.4: Setup to measure the polarization resolved spectra

Figure B.5: Polarization resolved VCSEL spectra compared to the spectrum without polarizer

is possible to see that the line splitting in the spectrum measured without polarizer comes from the two orthogonal polarization orientations.

B.4 Modal Coupling Efficiencies

In Section 4.3 it is observed that feedback tends to influence only lowest order modes (those at largest wavelengths) with increasing distance to the reflector. To explain this observation the efficiency with which the reflected light couples back into the different transversal modes inside the laser cavity shall be calculated. This efficiency is modal dependent, meaning that different transversal modes experience different efficiencies. The calculated values are valid for the ULM multi mode VCSEL 850-05-TN-U46FOP.

The model that is used for this calculation is quite the same as the one shown in Figure A.1 but of course now it is not possible to calculate with a simple ray model. It is necessary to use the full expressions for the mode field distributions. The calculation is carried out assuming Laguerre Gaussian modes (see Section 2.1.2) because they provide a closed form expression for the electric field at arbitrary distance to the VCSEL. Calculating with Bessel modes would necessitate using numerical methods (Rayleigh-Sommerfeld diffraction integrals) to calculate the electric field at some distance which is time and memory consuming (the method would be included in VISTAS advanced, but the memory of the computer used for the simulations was too less for the calculation).

The field distribution in cylindrical coordinates at arbitrary distances z to the VCSEL is given by the following expression.

$$E_{lp}(r, \phi, z) = E_0 \cdot \Big(\frac{\sqrt{2}r}{w(z)}\Big)^l \cdot L_{p-1}^l\Big(\frac{2r^2}{w^2(z)}\Big) \cdot \frac{w_0(l,p)}{w(z)} \cdot e^{\frac{-r^2}{w^2(z)}} \cdot e^{jl\phi} \cdot e^{\frac{jkr^2}{2R(z)}} \cdot e^{jkz} \cdot e^{-j(2(p-1)+l+1)\xi(z)} \quad \text{(B.1)}$$

Laguerre Gaussian modes are derived from the Gaussian beam (details on Gaussian beams may be found in [3]). Therefore the parameters used are also the same and given as follows.

- l, p describe the azimuthal and radial mode order

- $w(z) = \sqrt{w_0^2 \cdot (1 + (\frac{z}{z_0})^2)}$ describes the mode field radius

- $w_0(l, p)$ is the radius of the beam waist of the mode under investigation

- $R(z) = z \cdot (1 + (\frac{z_0}{z})^2)$ describes the curvature of the beam wave front

- $\xi(z) = \arctan \frac{z}{z_0}$ is the so called Gouy phase, which describes the fast change in phase at the beam waist

- $z_0(l, p) = \frac{\pi w_0^2(l,p)}{\lambda}$ is the confocal parameter and describes the length of the section where the beam is best collimated

There is one unknown parameter in these equations and that is $w_0(l, p)$. This parameter is obtained by matching the Laguerre Gaussian modes best to the Bessel modes provided by VISTAS, where best is to be understood in the sens of minimizing the mean squared error (MMSE) between the two. The only two parameters that VISTAS requires to calculate the laser internal modes are the diameter of the oxide aperture (which is provided by ULM for the VCSEL under investigation) and the refractive index step, which is chosen to reproduce the measured divergence of the LP01 mode (see B.2). The result of this matching procedure is shown in Figure B.6 for some modes. Knowing the beam waist radius it is possible to calculate the field distribution at an arbitrary distance z. The distance of interest is the round trip distance to the reflector. The modal coupling efficiencies from reflected mode (l, p) to VCSEL mode (s, t) can be calculated with the following overlap integral

$$\eta_{(lp)\to(st)} = \frac{\Big|\int_0^{2\pi} \int_0^\infty E_{lp}(r, \phi, z) \cdot E_{st}^*(r, \phi, 0) r dr d\phi\Big|^2}{\int_0^{2\pi} \int_0^\infty |E_{lp}(r, \phi, z)|^2 r dr d\phi \cdot \int_0^{2\pi} \int_0^\infty |E_{st}(r, \phi, 0)|^2 r dr d\phi}. \quad \text{(B.2)}$$

It is only necessary to calculate the overlap integral between a specific reflected mode (l, p) and the same mode (l, p) inside the laser cavity. This is because all transversal modes have slightly different wavelength.
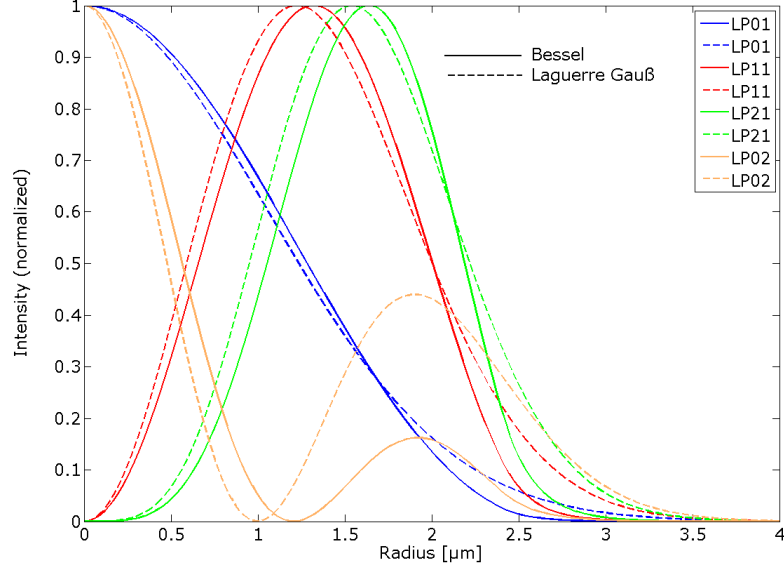
Figure B.6: Radial intensity distribution of Bessel and MMSE matched Laguerre Gaussian modes

Therefore that part of light that couples from one mode into another mode is not able to oscillate inside the laser cavity, because the resonance condition (Equation 2.14) is not fulfilled.

Figures B.7 show the result of the numerical calculation of the coupling efficiencies versus the distance to the reflector (the one way distance) for different transversal modes. As expected the coupling efficiency tendential decreases with the distance due to the beam divergence. The figure shows that the coupling efficiency also tends to decrease with the mode order. This can simple be explained by an increased divergence of that modes. Also the number of zeros in the modal coupling efficiency seems to correlate with the radial mode number p. For modes with $p > 1$ there is at least one intermediate distance ($< \infty$) where the coupling efficiency is zero.

For low mode order the calculation above can also be carried out analytically. In the following this will be done for the LP01 mode (with $E_0 = 1$) in order to show the correctness of the numerical results obtained above.

$$E_{01} = \frac{w_0}{w(z)} \cdot e^{\frac{-r^2}{w^2(z)}} \cdot e^{\frac{jkr^2}{2R(z)}} \cdot e^{jkz} \cdot e^{-j\xi(z)} \tag{B.3}$$

$$\int_0^{2\pi} \int_0^{\infty} E_{01}(r,\phi,z) \cdot E_{01}^*(r,\phi,0) r dr d\phi =$$

$$= \int_0^{2\pi} \int_0^{\infty} \frac{w_0}{w(z)} e^{\frac{-r^2}{w^2(z)}} e^{\frac{jkr^2}{2R(z)}} e^{jkz} e^{-j\xi(z)} \cdot \frac{w_0}{w(0)} e^{\frac{-r^2}{w^2(0)}} e^{\frac{-jkr^2}{2R(0)}} e^{-jk0} e^{j\xi(0)} r dr d\phi =$$

$$= 2\pi \int_0^{\infty} \frac{w_0}{w(z)} e^{\frac{-r^2}{w^2(z)}} e^{\frac{jkr^2}{2R(z)}} e^{jkz} e^{-j\xi(z)} \cdot e^{\frac{-r^2}{w_0^2}} r dr = 2\pi \frac{w_0}{w(z)} e^{jkz} e^{-j\xi(z)} \int_0^{\infty} e^{-r^2 \left(\frac{1}{w^2(z)} + \frac{1}{w_0^2} - j\frac{k}{2R(z)}\right)} r dr =$$

$$= 2\pi \frac{w_0}{w(z)} e^{jkz} e^{-j\xi(z)} \frac{1}{2} \frac{1}{\frac{1}{w^2(z)} + \frac{1}{w_0^2} - j\frac{k}{2R(z)}}$$

$$\rightarrow \left| \int_0^{2\pi} \int_0^{\infty} E_{01}(r,\phi,z) \cdot E_{01}(r,\phi,0) r dr d\phi \right|^2 = \pi^2 \frac{w_0^2}{w^2(z)} \frac{1}{\left| \frac{1}{w^2(z)} + \frac{1}{w_0^2} - j\frac{k}{2R(z)} \right|^2}$$
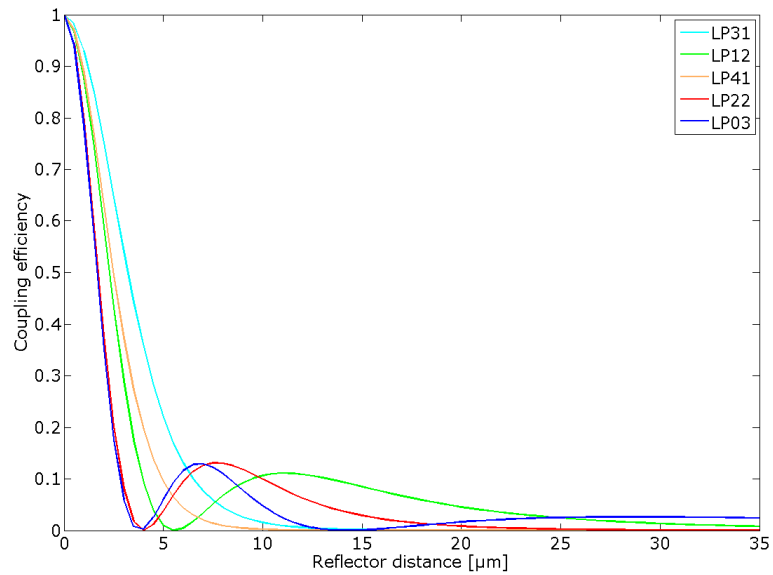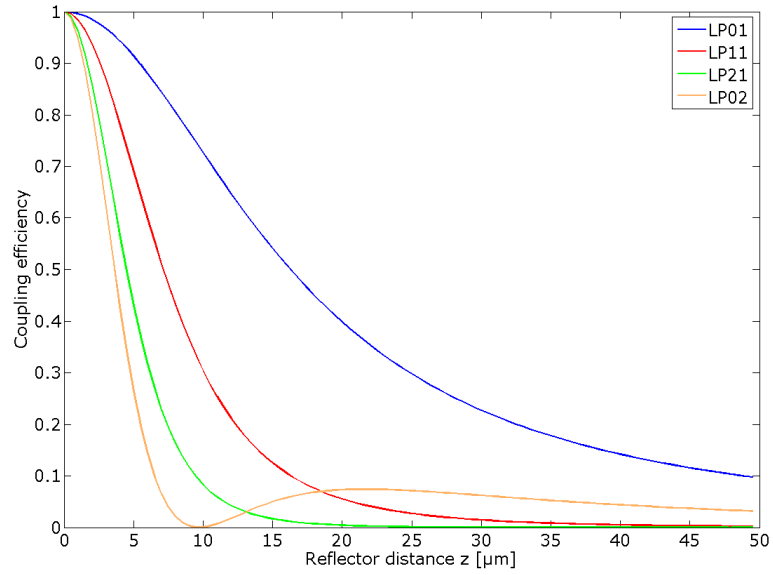
Figure B.7: Calculated coupling efficiencies of different transversal modes

Setting in this equation $z = 0$ directly allows to calculate the normalization constants needed for the denominator of the formula for the modal coupling efficiency. The coupling efficiency then equals

$$\eta_{(01)\to(01)} = \frac{4}{w_0^2 w^2(z)} \cdot \frac{1}{\left| \frac{1}{w^2(z)} + \frac{1}{w_0^2} - j\frac{k}{2R(z)} \right|^2}. \tag{B.4}$$

Next LP11 will be calculated.

$$E_{11} = \frac{\sqrt{2}r}{w(z)}\frac{w_0}{w(z)} \cdot e^{\frac{-r^2}{w^2(z)}} \cdot e^{\frac{jkr^2}{2R(z)}} \cdot e^{jkz} \cdot e^{-j2\xi(z)}e^{j\Phi} \tag{B.5}$$

$$\int_0^{2\pi}\int_0^\infty E_{11}(r,\phi,z) \cdot E_{11}^*(r,\phi,0)rdrd\phi =$$
$$= \int_0^{2\pi}\int_0^\infty \frac{\sqrt{2}r}{w(z)}\frac{w_0}{w(z)}e^{\frac{-r^2}{w^2(z)}}e^{\frac{jkr^2}{2R(z)}}e^{jkz}e^{-j2\xi(z)}e^{j\Phi} \cdot \frac{\sqrt{2}r}{w(0)}\frac{w_0}{w(0)}e^{\frac{-r^2}{w^2(0)}}e^{\frac{-jkr^2}{2R(0)}}e^{-jk0}e^{j2\xi(0)}e^{-j\Phi}rdrd\phi =$$
$$= \frac{4\pi}{w^2(z)}\int_0^\infty r^3 e^{-r^2(\frac{1}{w^2(z)}+\frac{1}{w_0^2}-j\frac{k}{2R(z)})}dr = \frac{2\pi}{w^2(z)(\frac{1}{w^2(z)}+\frac{1}{w_0^2}-j\frac{k}{2R(z)})^2}$$

$$\to \left| \int_0^{2\pi}\int_0^\infty E_{11}(r,\phi,z) \cdot E_{11}(r,\phi,0)rdrd\phi \right|^2 = \frac{4\pi^2}{w^4(z)}\frac{1}{\left| \left(\frac{1}{w^2(z)}+\frac{1}{w_0^2}-j\frac{k}{2R(z)}\right)^2 \right|^2}$$

The normalization constants can be evaluated to be equal to

$$|E_{11}(r,\Phi,z)|^2 = |E_{11}(r,\Phi,0)|^2 = \frac{\pi w_0^2}{2}.$$

This then delivers the coupling efficiency

$$\eta_{(11)\to(11)} = \frac{16}{w_0^4|w^2(z)|^2} \cdot \frac{1}{\left| \left(\frac{1}{w^2(z)}+\frac{1}{w_0^2}-j\frac{k}{2R(z)}\right)^2 \right|^2}. \tag{B.6}$$

Figure B.8 shows the numerical and analytical solution. As can be seen, there is no visible difference between the two.

B.5 Varying the Alignment of the Feedback Path in the Incoherent Measurement Setup

By varying the elevation or azimuth of the feedback mirror slightly (see Figure 4.4), so that the reflected beam does not irradiate the VCSEL surface centrally but just part of it, it is possible to change the modal power distribution. To see this clearly, the measurement was carried out at a bias current of $I = 1.5\,mA$, just slightly above threshold, where the VCSEL operates originally in single mode operation. The measured spectra when varying the feedback reflector elevation are shown in Figure B.9. When the feedback path is aligned for maximum feedback[1], meaning that the VCSEL is irradiated centrally, the modal power distribution just changes slightly, compared to the case of no feedback, in that the power of the only radiating mode is slightly increased. This behavior is expected, as the laser internal light and the feedback light add up on a power basis. When varying the elevation of the mirror by $\pm10°$ or more the feedback light does not

---

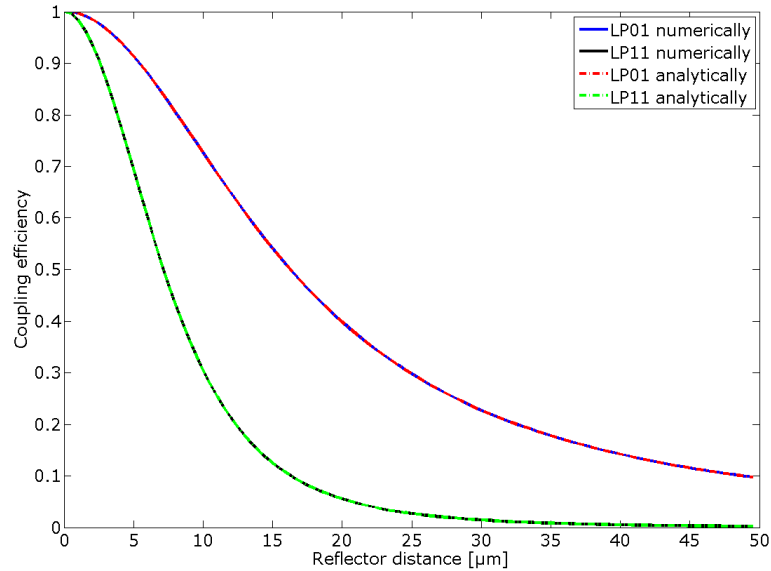[1] This situation is called "Elevation $0°$"

Figure B.8: Comparison of the analytically and numerically calculated coupling efficiencies of the LP01 and LP11 mode
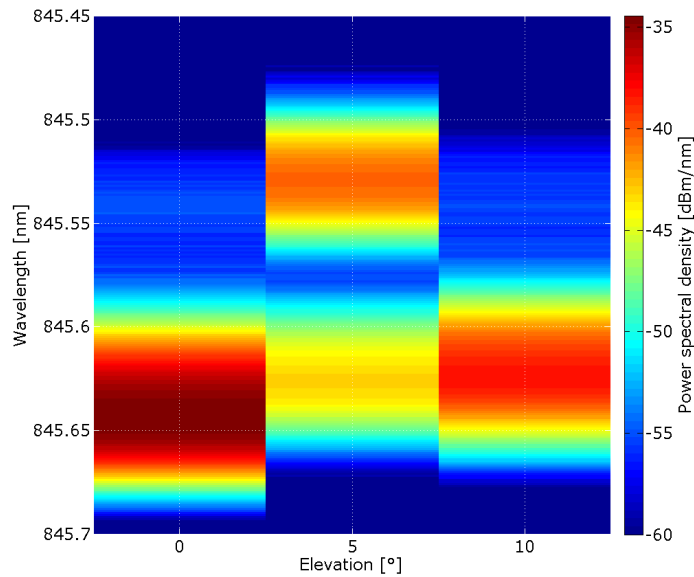

Figure B.9: Change in VCSEL output spectrum with feedback alignment at constant feedback phase

irradiate the VCSEL surface anymore and there is no feedback influence observable. But by choosing a elevation in between 0° and 10° it is possible to change the modal power distribution drastically. At 5° the feedback light enhances a second mode (LP11) so strong that it is dominating the VCSEL spectrum. In this situation clearly the effect of gain competition is observable, the second mode consumes gain which weakens the original one.

(a) Elevation 0°

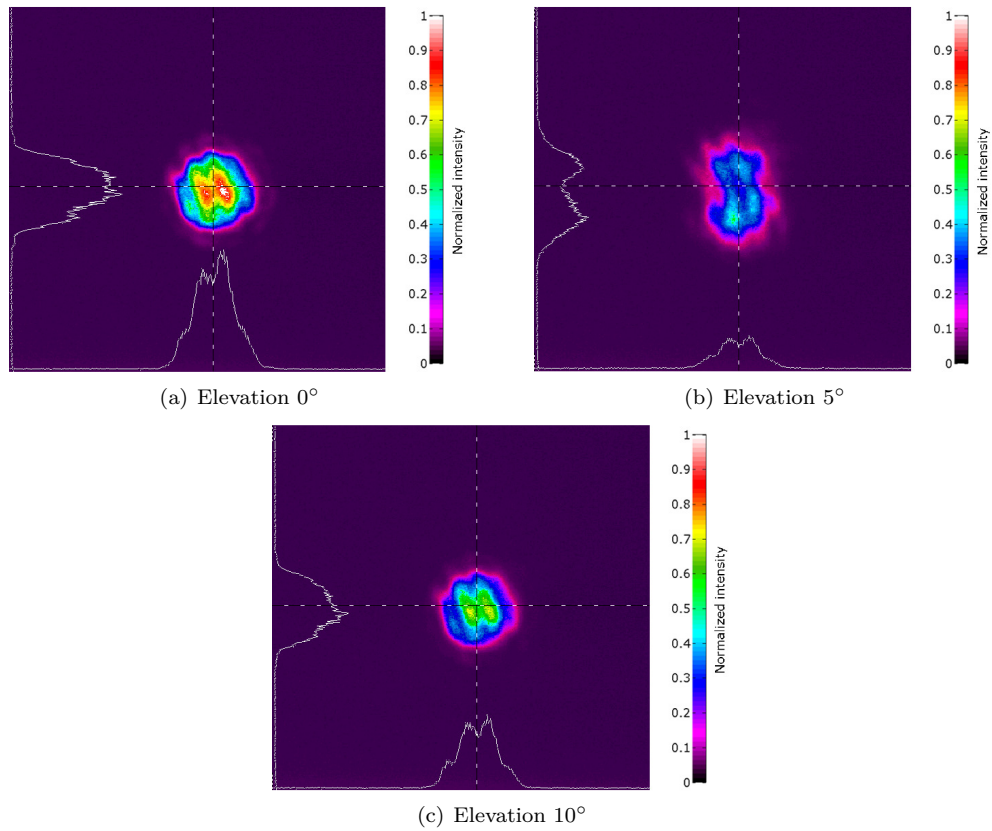(b) Elevation 5°

(c) Elevation 10°

Figure B.10: Measured far field intensity distributions of a VCSEL subject to incoherent external feedback with varying alignment

Figure B.10 shows far field intensity distributions corresponding to the described situations. As can be seen, the feedback light at 5° elevation enhances just that helical polarity that has a large overlap with the irradiated area. The same behavior is also observable when varying the azimuth instead of the elevation, but in this case the other helical polarity is enhanced.

Bibliography

[1] Uhlig S., Fröhlich L., Chen M., Arndt-Staufenbiel N., Lang G., Schröder H., Houbertz R., Popall M., Robertsson M., *"Polymer Optical Interconnects - A Scalable Large-Area Panel Processing Approach"*, IEEE Transactions on Advanced Packaging Vol. 29 No. 1, 2006

[2] Schmidt V., Kuna L., Satzinger V., Houbertz R., Jakopic G., Leising G., *"Application of two-photon 3D lithography for the fabrication of embedded ORMOCER$^®$ waveguides"*, Proceedings of SPIE Vol. 6476, 2007

[3] Reider Georg A., *"Photonik - eine Einführung in die Grundlagen"*, Springer, 2005

[4] Li H., Iga K., *"Vertical-Cavity Surface-Emitting Laser Devices"*, Springer, 2003

[5] Wilmsen C., Temkin H., Coldren L. A., *"Vertical-Cavity Surface-Emitting Lasers"*, Cambridge studies in modern optics, 1999

[6] Jungo M. X., *"Spatiotemporal VCSEL Model for Advanced Simulations of Optical Links"*, Series in Quantum Electronics Vol. 30, 2003

[7] Mederer F., *"Optische Datenübertragung mit Vertikal-Laserdioden im Wellenlängenbereich von 650 bis 1550 nm"*, Cuvillier Verlag Göttingen, 2004

[8] Coldren L. A., Corzine S. W., *"Diode Lasers and Photonic Integrated Circuits"*, Wiley, 1995

[9] Hecht E., *"Optik"*, Oldenbourg, 2005

[10] Paschotta R., *"Encyclopedia of Laser Physics and Technology"*, Wiley, 2008

[11] Tkach R. W., Chraplyvy A. R., *"Regimes of Feedback Effects in $1.5\,\mu m$ Distributed Feedback Lasers"*, IEEE Journal of Lightwave Technology Vol. LT-4 No. 11, 1986

[12] Osmundsen J. H., Gade N., *"Influence of Optical Feedback on Laser Frequency Spectrum and Threshold Conditions"*, IEEE Journal of Quantum Electronics Vol. QE-19 No. 3, 1983

[13] Lang R., Kobayashi K., *"External Optical Feedback Effects on Semiconductor Injection Laser Properties"*, IEEE Journal of Quantum Electronics Vol. QE-16 No. 3, 1980

[14] Goldberg L., Taylor H. F., Dandridge A., Weller J. F., Miles R. O., *"Spectral Characteristics of Semiconductor Lasers with Optical Feedback"*, IEEE Transactions on Microwave Theory and Techniques Vol. MTT-30 No. 4, 1982

[15] Law J. Y., Agrawal G. P., *"Effects of Optical Feedback on Static and Dynamic Characteristics of Vertical-Cavity Surface-Emitting Lasers"*, IEEE Journal of Selected Topics in Quantum Electronics Vol. 3 No. 2, 1997

[16] Chung Y. C., Lee Y. H., *"Spectral Characteristics of Vertical-Cavity Surface-Emitting Lasers with External Optical Feedback"*, IEEE Photonics Technology Letters Vol.3 No. 7, 1991

[17] Chilla J. L. A., Benware B., Watson M.E., Stanko P., Rocca J.J., Wilmsen C., Feld S., Leibenguth R., *"Coherence of VCSEL's for Holographic Interconnects"*, IEEE Photonics Technology Letters Vol. 7 No. 5, 1995

[18] Jansen van Doorn A. K., Woerdman J. P.,*"Effect of transverse anisotropy on VCSEL spectra"*, IET Electronics Letters 30, 1994

[19] Bruenstein M., Papen G. C., *"Extraction of VCSEL Rate-Equation Parameters for Low-Bias System Simulation"*, IEEE Journal of selected topics in Quantum Electronics Vol. 5 No. 3, 1999

[20] Jungo M. X., Ernie D., Bächtold W., *"VISTAS: A Comprehensive System-Oriented Spatiotemporal VCSEL Model"*, IEEE Journal of selected topics in Quantum Electronics Vol. 9 No. 3, 2003

[21] Sialm G., Lenz D., Erni D., Bona G. L., *"Comparison of Simulation and Measurement of Dynamic Fiber-Coupling Effects for High-Speed Multimode VCSELs"*, IEEE Journal of Lightwave Technology Vol. 23, No. 7, 2005

[22] Langley L. N., Shore K. A., *"Effect of optical feedback on the noise properties of vertical cavity surface emitting lasers"*, IEE Proceedings Optoelectronics, Vol. 144 No. 1, 1997

[23] Jungo M., *"VCSEL Integrated Spatio-Temporal Advanced Simulator"*, http://sourceforge.net/projects/vistas/ [Internet August 2009]